DEPARTMENT OF COMMERCE
LEWIS L. STRAUSS, Secretary

WEATHER BUREAU
F. W. REICHELDERFER, Chief

MONTHLY WEATHER REVIEW

JAMES E. CASKEY, JR., Editor

Volume 86
Number 12

DECEMBER 1958

Closed February 15, 1959
Issued March 15, 1959

ON THE NUMERICAL INTEGRATION OF THE PRIMITIVE EQUATIONS OF MOTION FOR BAROCLINIC FLOW IN A CLOSED REGION

J. SMAGORINSKY

General Circulation Research Section, U.S. Weather Bureau, Washington, D.C.

[Manuscript received November 5, 1958; revised January 7, 1959]

ABSTRACT

This paper considers the problem of numerically integrating the primitive equations corresponding to a 2-level model of the atmosphere bounded by two zonal walls on a spherical earth. Inertio-gravitational motions of the external type are filtered *a priori;* for such a constraint it is possible to define a stream function corresponding to the vertically integrated motions. A system of integration is developed for initial conditions which specify the shear wind vector, the specific volume, and the vorticity of the vertically integrated flow. Methods for reducing truncation error and for increasing the rate of convergence of the elliptic part are discussed.

The question of boundary conditions is discussed at length. It is shown that the usual central difference methods yield independent solutions at alternate points, thus providing a source of computational instability to which the primitive equations are particularly sensitive. The solutions may be made compatible by suitable computational boundary conditions which can be deduced as sufficient conditions for insuring that the numerical solutions possess exact integrals. The application of these considerations to viscous flow is also discussed.

1. INTRODUCTION

The object of this paper is to discuss some of the problems of employing the primitive equations as a framework in which to study large-scale atmospheric processes. These problems are to a large extent connected with the deduction of a stable and rational means for numerically integrating the primitive equations. It has been common experience that the application of the primitive equations to large-scale motions has suffered from the delicate balance between the Coriolis and pressure-gradient forces resulting in relatively small accelerations and horizontal divergence. Therefore, attempts to integrate the primitive equations numerically can be successful only if the problem stated in numerical form is properly compatible with the system of continuous (differential) equations. Slight incompatibilities (e.g., incorrect boundary conditions) in systems which are not sensitive in this manner, e.g., those admitting only gravitational motions or only Rossby wave solutions, apparently do not produce a very rapid degeneracy.

The particular system of equations, and the domain of integration to be discussed, has been designed in essence to form the hydrodynamic framework for numerical studies of the dynamics of the general circulation. However, those physical considerations which do not directly or crucially bear on the present objective of establishing a stable mathematical and hydrodynamic framework will be omitted here. At the time of the preparation of this manuscript, stable numerical integrations had been performed over periods in excess of 50 atmosphere days within the context of the system and methods to be described. The physical considerations directly bearing on the construction of this general circulation model, together with the results of the integrations, will form the subject of a later report.

2. NON-LINEAR BAROCLINIC FLOWS

a. DIFFERENTIAL EQUATIONS

The equations of motion in spherical coordinates with height as the vertical coordinate are (see for instance Haurwitz [6]):

$$\frac{r}{m}\ddot{\lambda}+2(\dot{\lambda}+\Omega)\left(\frac{\dot{r}}{m}-r\alpha\dot{\theta}\right)=-\frac{m}{r\rho}\frac{\partial p}{\partial\lambda}+F_\lambda \tag{1a}$$

$$r\ddot{\theta}+2\dot{r}\dot{\theta}+\frac{r\alpha}{m}\dot{\lambda}(\dot{\lambda}+2\Omega)=-\frac{1}{r\rho}\frac{\partial p}{\partial\theta}+F_\theta \tag{1b}$$

$$\ddot{r}-r(\dot{\theta})^2-\frac{r}{m^2}\dot{\lambda}(\dot{\lambda}+2\Omega)=-\frac{1}{\rho}\frac{\partial p}{\partial r}-g+F_r \tag{1c}$$

in which λ is the longitude, positive eastward; θ is the latitude; r is the radial distance from the center of the earth; $m\equiv\sec\theta$; $\alpha\equiv\sin\theta$; Ω is the angular velocity of the earth's rotation; ρ is the density; p is the pressure; g is the acceleration of gravity; $\mathbf{F}=\mathbf{i}F_\lambda+\mathbf{j}F_\theta$ is the horizontal component of the frictional force vector, F_r its vertical component, and $\mathbf{i}$ and $\mathbf{j}$ are the unit vectors in the λ and θ directions; and $\dot{(\ )}\equiv d(\ )/dt$ is the time change on a material particle. The effect of the ellipsoidal shape of the earth in balancing the centrifugal accelerations has already been taken into account.

The kinetic energy equation for *non-hydrostatic* motions is obtained by multiplying (1a), (1b), and (1c) by $r\dot{\lambda}/m$, $r\dot{\theta}$, and $\dot{r}$, respectively, and adding the resulting equations:

$$\frac{1}{2}\frac{d}{dt}\left[\left(\frac{r\dot{\lambda}}{m}\right)^2+(r\dot{\theta})^2+(\dot{r})^2\right]=-\frac{1}{\rho}\left(\dot{\lambda}\frac{\partial p}{\partial\lambda}+\dot{\theta}\frac{\partial p}{\partial\theta}+\dot{r}\frac{\partial p}{\partial r}\right)$$
$$-g\dot{r}+\frac{r\dot{\lambda}}{m}F_\lambda+r\dot{\theta}F_\theta+\dot{r}F_r. \tag{2a}$$

If we constrain the motions to be quasi-static, then (1c) becomes

$$0=-\frac{1}{\rho}\frac{\partial p}{\partial r}-g \tag{2b}$$

In this case, the individual change of kinetic energy of the horizontal motions calculated from (1a) and (1b) no longer *only* depends on the work done by the pressure gradient and external forces. A correct kinetic energy equation consistent with the quasi-static approximation can be derived if:

(i) the terms $2(\dot{\lambda}+\Omega)\dot{r}/m$ and $2\dot{r}\dot{\theta}$ are dropped from (1a) and (1b) respectively, and

(ii) where r appears undifferentiated in (1a) and (1b), it is replaced by a, the mean radius of the earth.

The kinetic energy equation for quasi-static motions then becomes

$$\frac{a^2}{2}\frac{d}{dt}\left[\left(\frac{\dot{\lambda}}{m}\right)^2+(\dot{\theta})^2\right]=-\frac{1}{\rho}\left(\dot{\lambda}\frac{\partial p}{\partial\lambda}+\dot{\theta}\frac{\partial p}{\partial\theta}\right)+a\left(\frac{\dot{\lambda}}{m}F_\lambda+\dot{\theta}F_\theta\right). \tag{2c}$$

Furthermore, the quasi-static assumption permits us to transform the resulting horizontal equations of motion and the hydrostatic equation to a coordinate system in which p is the vertical coordinate (Eliassen [2]):

$$\frac{a}{m}\ddot{\lambda}-2a\alpha(\dot{\lambda}+\Omega)\dot{\theta}=-\frac{m}{a}\frac{\partial\phi}{\partial\lambda}+F_\lambda \tag{3}$$

$$a\ddot{\theta}+\frac{a\alpha}{m}(\dot{\lambda}+2\Omega)\dot{\lambda}=-\frac{1}{a}\frac{\partial\phi}{\partial\theta}+F_\theta \tag{4}$$

$$0=\frac{\partial\phi}{\partial p}+\frac{1}{\rho} \tag{5}$$

where $\phi\equiv g(r-a)$ is the geopotential and

$$\dot{(\ )}\equiv\left[\frac{\partial}{\partial t}+\dot{\lambda}\frac{\partial}{\partial\lambda}+\dot{\theta}\frac{\partial}{\partial\theta}+\omega\frac{\partial}{\partial p}\right](\ );\ \omega\equiv\frac{dp}{dt}.$$

Differentiations with respect to t, λ, and θ are now in a constant pressure surface.

The continuity equation is

$$\mathcal{D}+\frac{\partial\omega}{\partial p}=0 \tag{6}$$

where

$$\mathcal{D}\equiv\frac{\partial\dot{\lambda}}{\partial\lambda}+m\frac{\partial}{\partial\theta}\left(\frac{\dot{\theta}}{m}\right). \tag{7}$$

The thermodynamic energy equation is

$$\left.\begin{aligned}(\ln\dot{\Theta})&=\frac{1}{c_pT}\dot{q}\\ \ln\Theta&=\text{const}+(1-\kappa)\ln p+\ln\left(\frac{1}{\rho}\right)\end{aligned}\right\} \tag{8}$$

where

and Θ is the potential temperature; T is the temperature; $(1-\kappa)=c_v/c_p$ is the ratio of the specific heat of air at constant volume to that at constant pressure; $\dot{q}$ is the non-adiabatic heat added or removed per unit mass per unit time.

Anticipating our ultimate needs for the numerical integration, we will conformally map the sphere onto a Mercator projection. We denote the map coordinates by x and y, positive in the easterly and northerly directions, respectively. For this projection the map scale factor is $m=\sec\theta$, so that

$$\left.\begin{aligned}dx&=a\,d\lambda\\ dy&=a\,m\,d\theta\end{aligned}\right\} \tag{9}$$

and

$$\left.\begin{aligned}x&=a\lambda\\ y&=a\ln\tan\left(\frac{\theta}{2}+\frac{\pi}{4}\right).\end{aligned}\right\} \tag{10}$$

It will be convenient to deal with the *map velocity* components:

$$\left.\begin{aligned}\mathbf{V}&=\mathbf{i}u+\mathbf{j}v\\ u&\equiv\dot{x}=a\dot{\lambda}\\ v&\equiv\dot{y}=a\,m\dot{\theta}\end{aligned}\right\} \tag{11}$$

where the earth velocity is $\mathbf{V}/m$. The following scalar and vector transformations will be useful:

$$\left.\begin{aligned}\nabla\beta&=\mathbf{i}\frac{m}{a}\frac{\partial\beta}{\partial\lambda}+\mathbf{j}\frac{1}{a}\frac{\partial\beta}{\partial\theta}=m\left(\mathbf{i}\frac{\partial\beta}{\partial x}+\mathbf{j}\frac{\partial\beta}{\partial y}\right)\\ \nabla^2\beta&=\frac{m^2}{a^2}\frac{\partial^2\beta}{\partial\lambda^2}+\frac{m}{a^2}\frac{\partial}{\partial\theta}\left(\frac{1}{m}\frac{\partial\beta}{\partial\theta}\right)=m^2\left(\frac{\partial^2\beta}{\partial x^2}+\frac{\partial^2\beta}{\partial y^2}\right)\\ \nabla\cdot\mathbf{B}&=\frac{m}{a}\left(\frac{\partial B_\lambda}{\partial\lambda}+\frac{\partial B_\theta/m}{\partial\theta}\right)=m\frac{\partial B_x}{\partial x}+m^2\frac{\partial B_y/m}{\partial y}\\ \text{curl }\mathbf{B}&=\frac{m}{a}\left(\frac{\partial B_\theta}{\partial\lambda}-\frac{\partial B_\lambda/m}{\partial\theta}\right)=m\frac{\partial B_y}{\partial x}-m^2\frac{\partial B_x/m}{\partial y}.\end{aligned}\right\} \tag{12}$$

Here $\nabla\cdot\mathbf{B}$ has been defined as a 2-dimensional operator in the x–y plane and curl $\mathbf{B}$ is a scalar which has been defined as the vertical component of the usual $\nabla\times\mathbf{B}$ vector.

Equations (3), (4), and (7) become upon being mapped:

$$\dot{u}-2\alpha\left(\frac{u}{a}+\Omega\right)v=-m^2\frac{\partial\phi}{\partial x}+mF_x \tag{13}$$

$$m\left(\frac{\dot{v}}{m}\right)+\alpha\left(\frac{u}{a}+2\Omega\right)u=-m^2\frac{\partial\phi}{\partial y}+mF_y \tag{14}$$

$$\mathcal{D}=\nabla\cdot\left(\frac{\mathbf{V}}{m}\right)\equiv\frac{\partial u}{\partial x}+m^2\frac{\partial v/m^2}{\partial y} \tag{15}$$

where

$$\dot{(\ )}=\left[\frac{\partial}{\partial t}+u\frac{\partial}{\partial x}+v\frac{\partial}{\partial y}+\omega\frac{\partial}{\partial p}\right](\ ). \tag{16}$$

We now construct a 2-level model in the fashion of Eliassen [4]. The atmosphere is divided in the vertical into 4 equal pressure intervals $\Delta p/2$, such that $\Delta p\equiv p_{k+1}-p_{k-1}$ and $k=0, 1, 2, 3, 4$. We take $\Delta p=500$ mb.

The upper boundary condition must be

$$\omega\equiv 0 \text{ at } k=0. \tag{17}$$

We exclude external gravitational propagation by requiring that $\omega\equiv 0$ at the lower boundary which is taken to coincide with the pressure coordinate surface $p_4=1000$ mb. Therefore, applying (6) at $k=1, 3$, we have that

$$\left.\begin{aligned}-\mathcal{D}_1=\mathcal{D}_3&=\frac{\omega_2}{\Delta p}\\ \text{and}\qquad\qquad\\ \omega_1=\omega_3&=\frac{\omega_2}{2}=-\frac{\Delta p}{2}\mathcal{D}_1\end{aligned}\right\} \tag{18}$$

in which ω_1 and ω_3 have been linearly interpolated from the neighboring levels.

Applying the equations of motion (13) and (14) at $k=1, 3$, we have

$$\left.\begin{aligned}\frac{\partial\mathbf{V}_k}{\partial t}&=m\mathbf{G}_k-m\nabla\phi_k\\ \mathbf{G}_k&=-\mathbf{I}_k+\mathbf{F}_k\end{aligned}\right\} \tag{19}$$

where

$$m\mathbf{I}\equiv\mathbf{i}\left[u\frac{\partial u}{\partial x}+mv\frac{\partial u/m}{\partial y}+\omega\frac{\partial u}{\partial p}-\alpha v\left(\frac{u}{a}+2\Omega\right)\right]$$
$$+\mathbf{j}\left[u\frac{\partial v}{\partial x}+mv\frac{\partial v/m}{\partial y}+\omega\frac{\partial v}{\partial p}+\alpha u\left(\frac{u}{a}+2\Omega\right)\right]. \tag{20}$$

It will be useful at this point to adopt the notation

$$\bar{(\ )}\equiv(\ )_1+(\ )_3;\ \hat{(\ )}\equiv(\ )_1-(\ )_3. \tag{21}$$

The vertical momentum transport in (20) is calculated by evaluating the vertical wind shear non-centrally, and applying the continuity equation (18):

$$\left(\omega\frac{\partial\mathbf{V}}{\partial p}\right)_1=\left(\omega\frac{\partial\mathbf{V}}{\partial p}\right)_3=\frac{\hat{\mathcal{D}}\hat{\mathbf{V}}}{4}. \tag{22}$$

The viscosity will be discussed in Section 2b.

The thermodynamic energy equation (8) is applied at $k=2$. The horizontal wind in (16) is evaluated by the arithmetic mean

$$2\mathbf{V}_2=\mathbf{V}_1+\mathbf{V}_3=\bar{\mathbf{V}}.$$

Hence (8) becomes, upon applying the hydrostatic and gas equations,

$$\frac{\partial\hat{\phi}}{\partial t}=-\left(\frac{\bar{u}}{2}\frac{\partial}{\partial x}+\frac{\bar{v}}{2}\frac{\partial}{\partial y}\right)\hat{\phi}-\gamma^2\hat{\mathcal{D}}+\frac{R}{c_p}Q \tag{23}$$

in which $2\gamma^2\equiv(\Delta p)^2\,(\partial\phi/\partial p)\,(\partial\ \ln\theta/\partial p)\approx\hat{\phi}\,\hat{\theta}/\theta_2$ is taken as a constant and $Q\equiv\dot{q}\Delta p/p_2$. We shall not specify the nature of the external heat source, Q, since it is not germane to the present discussion.

Upon substituting (22) into (20) then the system (19) and (23) provides 5 scalar equations in 6 unknowns: u_k, v_k, ϕ_k. The sixth equation is provided by the requirement that the mean motions remain nondivergent. Forming $\partial\bar{\mathcal{D}}/\partial t$ from (19) according to (15) and setting it to zero we have

$$\nabla^2\bar{\phi}=\nabla\cdot\bar{\mathbf{G}} \tag{24}$$

which is the "divergence" equation corresponding to the vertically integrated flow. We shall refer to this system as System I.

Alternatively we may define a stream function ψ for the vertically integrated flow:

$$\left.\begin{aligned}\bar{u}&=-m^2\frac{\partial\psi}{\partial y}\\ \bar{v}&=m^2\frac{\partial\psi}{\partial x}.\end{aligned}\right\} \tag{25}$$

Hence the stream function tendency $\psi^*\equiv\partial\psi/\partial t$ in the equations of motion (19) gives:

$$\frac{\partial\bar{u}}{\partial t}=-m^2\frac{\partial\psi^*}{\partial y}=m\bar{G}_x-m^2\frac{\partial\bar{\phi}}{\partial x} \tag{26}$$

$$\frac{\partial\bar{v}}{\partial t}=m^2\frac{\partial\psi^*}{\partial x}=m\bar{G}_y-m^2\frac{\partial\bar{\phi}}{\partial y}. \tag{27}$$

Taking the curl of (26) and (27) yields

$$\nabla^2\psi^*=\text{curl}\,\bar{\mathbf{G}}. \tag{28}$$

This of course is the vorticity equation governing the vertically integrated flow. If we now form the equations of motion for the shear wind $\hat{\mathbf{V}}$ from (19)

$$\frac{\partial\hat{\mathbf{V}}}{\partial t}=m\hat{\mathbf{G}}-m\nabla\hat{\phi} \tag{29}$$

then equations (23), (28), and (29), which will be referred to as System II, constitute 4 scalar equations in the 4 unknowns ψ^*, $\hat{u}$, $\hat{v}$, $\hat{\phi}$. $\hat{\phi}$ is proportional to the specific volume. Because the history of the vertically integrated flow in this system is carried in ψ, $\bar{\phi}$ never is calculated explicitly.

Hence the constraint of filtering the external gravitational

solutions, which dictates the elliptic balance condition (24) in System I or (28) in System II, yields a system of equations which is a combined marching-jury problem. Without this constraint, the primitive equations are completely hyperbolic and constitute a pure marching problem.

b. PHYSICAL LATERAL BOUNDARY CONDITIONS AND THE VISCOSITY

We take as the domain of integration a zonal strip bounded by two latitudinal walls at $y=0$ and $y=Y$. The walls are taken to be perfectly smooth. In the x direction we assume cyclic continuity so that all dependent variables and their derivatives are continuous. At the walls we must impose the kinematic boundary condition

$$v_h=0 \text{ at } y=0, Y \text{ for all } t \tag{30}$$

which by (25) and (27) requires the boundaries to be a streamline at each level for all t, giving the corollary physical boundary conditions

$$\psi,\ \psi^* \text{ independent of } x \text{ on } y=0,\ Y. \tag{31}$$

It will suffice for our present purposes to postulate only a lateral viscosity of the Navier-Stokes type. Physically it is desirable that the form of this viscosity be such that the walls do not affect the total zonal angular momentum nor the total energy (through the kinetic energy). This smoothness condition will provide us with a second physical boundary condition. Such a form is

$$\mathbf{F}=Km^3\left\{\mathbf{i}\left[\frac{\partial}{\partial x}\left(\frac{1}{m^2}\frac{\partial u}{\partial x}\right)+\frac{\partial}{\partial y}\left(\frac{1}{m^2}\frac{\partial u}{\partial y}\right)\right]+\mathbf{j}\left[\frac{\partial}{\partial x}\left(\frac{1}{m^2}\frac{\partial v}{\partial x}\right)+\frac{\partial}{\partial y}\left(\frac{1}{m^2}\frac{\partial v}{\partial y}\right)\right]\right\} \tag{32}$$

where K is assumed constant. We will now demonstrate that this form does indeed possess the above properties.

The change of the total relative zonal angular momentum per unit mass is

$$\frac{\partial}{\partial t}\iint\left(\frac{a^2}{m^2}\dot{\lambda}\right)\frac{ad\lambda}{m}\,ad\theta\equiv\frac{\partial}{\partial t}\int_0^Y\oint au\,\frac{dxdy}{m^4}. \tag{33}$$

Hence the contribution from $\mathbf{F}$ can be calculated from (19) and (32) to be

$$a\int_0^Y\oint\frac{F_x}{m^3}\,dxdy=aK\int_0^Y\oint\left[\frac{\partial}{\partial x}\left(\frac{1}{m^2}\frac{\partial u}{\partial x}\right)+\frac{\partial}{\partial y}\left(\frac{1}{m^2}\frac{\partial u}{\partial y}\right)\right]dxdy. \tag{34}$$

The first term on the right side must vanish due to the cyclic continuity condition, leaving

$$aK\oint\left[\frac{1}{m^2}\frac{\partial u}{\partial y}\right]_{y=0}^{y=Y}dx. \tag{35}$$

The change of total kinetic energy is

$$\frac{\partial}{\partial t}\iint\frac{a^2}{2}\left[\left(\frac{\dot{\lambda}}{m}\right)^2+(\dot{\theta})^2\right]\frac{ad\lambda}{m}\,ad\theta=\frac{\partial}{\partial t}\int_0^Y\oint\frac{1}{2}(u^2+v^2)\,\frac{dxdy}{m^4} \tag{36}$$

so that the contribution of $\mathbf{F}$ is

$$\int_0^Y\oint(uF_x+vF_y)\,\frac{dxdy}{m^3}=-K\int_0^Y\oint\left[\left(\frac{\partial u}{\partial x}\right)^2+\left(\frac{\partial u}{\partial y}\right)^2+\left(\frac{\partial v}{\partial x}\right)^2+\left(\frac{\partial v}{\partial y}\right)^2\right]\frac{dxdy}{m^2}+K\int_0^Y\oint\left[\frac{\partial}{\partial x}\left(\frac{u}{m^2}\frac{\partial u}{\partial x}+\frac{v}{m^2}\frac{\partial v}{\partial x}\right)+\frac{\partial}{\partial y}\left(\frac{u}{m^2}\frac{\partial u}{\partial y}+\frac{v}{m^2}\frac{\partial v}{\partial y}\right)\right]dxdy \tag{37}$$

where we have integrated by parts. The first term on the right side represents the energy dissipation within the atmosphere and is negative definite. The second integral becomes, upon applying the cyclic continuity condition and the kinematic boundary condition (30),

$$K\oint\left[\frac{u}{m^2}\frac{\partial u}{\partial y}\right]_{y=0}^{y=Y}dx. \tag{38}$$

Upon comparing (38) and (35), we observe that to prevent lateral boundary influence on both the total angular momentum and total kinetic energy we must impose the physical boundary condition

$$K\left(\frac{1}{m^2}\frac{\partial u}{\partial y}\right)=0 \text{ on } y=0,\ Y, \tag{39}$$

i.e., the lateral stress must vanish on each boundary individually.

c. INITIAL CONDITIONS AND TIME INTEGRATION

It will be shown in the discussion which follows that a sufficient set of initial conditions are:

$$\hat{u},\ \hat{v},\ \hat{\phi},\ \bar{\zeta}, \text{ given everywhere} \tag{40}$$

where the vertical component of relative vorticity is

$$\zeta=\text{curl}\left(\frac{\mathbf{V}}{m}\right)=\frac{\partial v}{\partial x}-m^2\frac{\partial u/m^2}{\partial y}. \tag{41}$$

From (25), the vertically integrated vorticity may be written as

$$\bar{\zeta}=\nabla^2\psi. \tag{42}$$

By virtue of the two physical boundary conditions (30) and (39) we have the corollary condition

$$\bar{\zeta}=\frac{2\alpha}{a}\,\bar{u}=-\frac{2\alpha m^2}{a}\frac{\partial\psi}{\partial y} \text{ on } y=0,\ Y. \tag{43}$$

Hence (42) and (43) constitute a Neumann boundary value problem. ψ may thus be determined everywhere to within an arbitrary constant. System (42) and (43) may be transformed into a Dirichlet problem since ψ must be a constant on $y=0, Y$. Taking $\psi=0$ on $y=0$, then inte-

grating (42), we have

$$\left.\begin{aligned}\psi(Y)=-\frac{Y}{L}\left(\frac{a}{2\alpha}\oint\frac{\bar{\zeta}}{m^2}\,dx\right)_{y=0}\\ +\frac{1}{L}\int_0^Y\left[\int_0^y\left(\oint\frac{\bar{\zeta}}{m^2}\,dx\right)dy\right]dy\\ L\equiv\oint dx.\end{aligned}\right\}\quad(44)$$

$\bar{u}$ and $\bar{v}$ may therefore be calculated on the interior. Note that since ψ must be independent of x on $y=0, Y$, then $\int_0^Y(\bar{u}/m^2)dy$ must be independent of x; i.e., zonally symmetric. Furthermore,cyclic continuity requires that $\oint\bar{v}\,dx=0$. Equation (42) need only be solved initially since the ellipticity condition (24) or alternatively (28) solved at each time insures that $\overline{\mathcal{D}}$ remain zero.

With $\bar{u}$ and $\bar{v}$ thus obtained everywhere and $\hat{u}$ and $\hat{v}$ having been prescribed everywhere initially, one can calculate the wind components at each level from the identities (21). The completion of the set of initial data necessary to integrate timewise will depend on whether we employ System I or II.

For System I it is necessary to solve (24), subject to an appropriate boundary condition. This is provided by requiring that (30) be satisfied for all time in (27), resulting in the corollary condition

$$\frac{\partial\bar{\phi}}{\partial y}=\frac{\overline{G}_y}{m}\qquad\text{on } y=0, Y.\quad(45)$$

Hence (24) and (45) constitute a Neumann boundary value problem for which $\overline{G}_y$ and $\nabla\cdot\overline{\mathbf{G}}$ must be known on the boundaries. With $\bar{\phi}$ found as a solution of (24) and $\hat{\phi}$ having been given initially, ϕ_k may be calculated from (21), so that the six dependent variables u_k, v_k, ϕ_k are known initially. V_k and $\hat{\phi}$ may then be calculated at the next time from (19) and (23). The new V_k fields are then used to invert (24) giving $\bar{\phi}$ and hence ϕ_k at the new time. Thus all of the initial dependent variables have been reconstructed. System I is in essence the one proposed by Eliassen [4].

To proceed by means of System II, we need first to determine the corollary boundary conditions for (28). These are obtained by integrating (26) over the entire region and then applying the cyclic continuity condition:

$$\psi^*(Y)-\psi^*(0)=-\frac{1}{L}\int_0^Y\oint\frac{\overline{G}_x}{m}\,dxdy.\quad(46)$$

Since ψ^* is independent of x on $y=0, Y$, we set the arbitrary datum

$$\psi^*(0)=0\quad(47)$$

so that

$$\psi^*(Y)=-\frac{1}{L}\int_0^Y\oint\frac{\overline{G}_x}{m}\,dxdy.\quad(48)$$

Since the initial ψ has been set to zero on $y=0$, then ψ must remain zero on $y=0$ for all time.

Therefore, System II requires the solution of a Dirichlet boundary value problem. The field ψ^* together with the initial ψ then permits us to calculate $\overline{\mathsf{V}}$ at the next time. Equation (29), which depends on $\hat{\phi}$ but not on $\bar{\phi}$, gives us the new $\hat{\mathsf{V}}$. As before $\overline{\mathsf{V}}$ and $\hat{\mathsf{V}}$ together yield V_k. Finally (23) gives the new $\hat{\phi}$. The data have therefore been reconstructed.

It will be useful at this point to digress for the purpose of discussing some of the computational stability characteristics of the system of equations with which we are dealing.

3. COMPUTATIONAL STABILITY

The Courant-Friedrichs-Lewy (CFL) stability criterion is for the most part governed by the speed of the internal gravitational waves relative to the mesh (Eliassen [4]):

$$\left(\frac{|\overline{\mathsf{V}}|_{\max}}{2}+\gamma\right)\sqrt{2}\leq\frac{\Delta s}{\Delta t}\quad(49)$$

where Δs is the horizontal grid distance on the earth, and Δt the time increment. Suppose we take $\Delta\lambda$ to be 5° longitude, then at the equator $\Delta s=555$ km. If we take the zonal channel to be 17 grid lengths wide, with $y=0$ at the equator, then $y=Y$ corresponds to 64.4° latitude. Therefore Δs has its smallest value, 240 km., at the north boundary. For an average value of the static stability, $\gamma=60$ m. sec.$^{-1}$. Then for $\Delta t=20$ min. the criterion is fulfilled when

$$\frac{|\overline{\mathsf{V}}|_{\max}}{2}\leq 80\text{m. sec.}^{-1}$$

Hence one would presume that if (49) were satisfied, the numerical integration should remain stable under the customary techniques of centered differences. The experience of a number of research workers in the past 6 or 7 years has been that attempts at numerical integration of very simple physical systems (such as non-viscous barotropic flows) in the framework of the primitive equations, have resulted in spurious inertio-gravitational oscillations which obscured the meteorologically significant motions even when the CFL criterion was satisfied. Investigations by the Princeton group (Charney [1]) disclose that one cause can be an incorrectly specified initial velocity field. In the present case this corresponds to $\overline{\mathsf{V}}$ which is never specified independently but is derived from the initially specified vertically integrated vorticity, $\bar{\zeta}$, through equation (42). Another possibility offered by Charney for the apparently spurious oscillations is computational instability due to incorrect boundary conditions. It is this latter source of instability that will be dwelt upon here. The nature of the instability will be demonstrated in less rigorous fashion than is normally possible by an analysis of the amplification of small-scale motions.

As a matter of convenience we shall refer to instability

resulting from incorrect boundary conditions as *computational instability of the second kind* (in contrast to the CFL instability which may be considered as that of the *first kind*). As it turns out this instability is already possible in the linear zonally symmetric equations corresponding to the model described in the previous section. This is rather fortunate since such a simple system lends itself to a rather clear-cut analysis.

Let us consider zonally symmetric perturbations on a vertically integrated flow which is at rest. At first we will deal with non-viscous, thermally inactive motions.

Assuming for the present that α and m may be replaced by their average values, then equation (23) becomes

$$\frac{\partial\hat{\phi}}{\partial t}=-\gamma^2\frac{\partial\hat{v}}{\partial y} \tag{50}$$

and the equations of motion for the shear flow (29) become

$$\frac{\partial\hat{u}}{\partial t}=2\alpha\Omega\hat{v} \tag{51}$$

$$\frac{\partial\hat{v}}{\partial t}=-2\alpha\Omega\hat{u}-m^2\frac{\partial\hat{\phi}}{\partial y}. \tag{52}$$

We take the domain as before to lie between two latitudinal walls so that the physical boundary condition is

$$\hat{v}=0 \text{ on } y=0, Y \text{ for all } t. \tag{53}$$

The initial conditions are $\hat{\phi}$, $\hat{u}$, $\hat{v}$, given everywhere, the latter subject to (53). Also, to satisfy (52) and (53), $2\alpha\Omega\hat{u}+m^2\partial\hat{\phi}/\partial y\equiv 0$ on the boundaries initially as well as in the interior of time. Hence the time-dependent equations (50–52) constitute a complete set and we have a pure marching problem.

We form the difference analogues of the three first-order equations (50–52), employing central differences over intervals Δt and Δy where $t=\tau\Delta t$ and $y=j\Delta y$, $0\leq j\leq(J-1)$.

$$\frac{\hat{\phi}_j^{\tau+1}-\hat{\phi}_j^{\tau-1}}{2\Delta t}=-\frac{\gamma^2}{2\Delta y}(\hat{v}_{j+1}^{\tau}-\hat{v}_{j-1}^{\tau}) \tag{54}$$

$$\frac{\hat{u}_j^{\tau+1}-\hat{u}_j^{\tau-1}}{2\Delta t}=f\hat{v}_j^{\tau} \tag{55}$$

$$\frac{\hat{v}_j^{\tau+1}-\hat{v}_j^{\tau-1}}{2\Delta t}=-f\hat{u}_j^{\tau}-\frac{m^2}{2\Delta y}(\hat{\phi}_{j+1}^{\tau}-\hat{\phi}_{j-1}^{\tau}). \tag{56}$$

It will be instructive to form a single differential equation in $\hat{v}$ from (50–52)

$$\frac{\partial^2\hat{v}}{\partial t^2}=-f^2\hat{v}+\Gamma^2\frac{\partial^2\hat{v}}{\partial y^2} \tag{57}$$

where $f\equiv 2\alpha\Omega$, $\Gamma\equiv m\gamma$. Then differencing (57) centrally, we have

$$\frac{\hat{v}_j^{\tau+1}-2\hat{v}_j^{\tau}+\hat{v}_j^{\tau-1}}{(\Delta t)^2}=-f^2\hat{v}_j^{\tau}+\frac{\Gamma^2}{(\Delta y)^2}(\hat{v}_{j+1}^{\tau}-2\hat{v}_j^{\tau}+\hat{v}_{j-1}^{\tau}). \tag{58}$$

TABLE 1.—*Compatibility of three dependent variables* $\hat{v}$, $\hat{u}$, *and* $\hat{\phi}$.

		Is physical boundary condition satisfied at—	
		$j=0$	$j=(J-1)$
Even J	Solutions for $\hat{v}$, $\hat{u}$ at odd j and $\hat{\phi}$ at even j	No	Yes
	Solutions for $\hat{v}$, $\hat{u}$ at even j and $\hat{\phi}$ at odd j	Yes	No
Odd J	Solutions for $\hat{v}$, $\hat{u}$ at odd j and $\hat{\phi}$ at even j	No	No
	Solutions for $\hat{v}$, $\hat{u}$ at even j and $\hat{\phi}$ at odd j	Yes	Yes

If we use (56) initially to obtain $\hat{v}_j^1$ as a function of $\hat{v}_j^{-1}$ in terms of the initial conditions, $\hat{\phi}_j^0$, $\hat{u}_j^0$, $\hat{v}_j^0$, given everywhere, then (58) may be solved as a marching problem with no difficulty in satisfying (53) at both boundaries $j=0, (J-1)$. This process will proceed stably provided the CFL condition is met. However, if we form the difference equation in $\hat{v}$ from the first-order difference equations (54–56)

$$\frac{\hat{v}_j^{\tau+2}-2\hat{v}_j^{\tau}+\hat{v}_j^{\tau-2}}{(2\Delta t)^2}=-f^2\hat{v}_j^{\tau}+\frac{\Gamma^2}{(2\Delta y)^2}(\hat{v}_{j+2}^{\tau}-2\hat{v}_j^{\tau}+\hat{v}_{j-2}^{\tau}) \tag{59}$$

we find it exactly in the form of (58) except that (59) applies to double time and space intervals. Therefore, the ratio $\Delta t/\Delta y$ is preserved and the CFL criterion remains the same. We now note that in (59) $\hat{v}$ is linked only at alternate values of j as well as of τ.* Consider the case when J is odd. Then (59) applied at even j satisfies (53) at both boundaries. On the other hand, application of (59) at odd j cannot directly satisfy (53) at either boundary since the finite difference equivalent of $\partial\hat{v}/\partial y$ is required. Alternatively, consider the case of even J. Now the application of (59) at even j will satisfy the physical boundary condition at $j=0$ but not at $j=(J-1)$, whereas solutions at odd j will not satisfy (53) at $j=0$ but will at $j=(J-1)$. Therefore, neither solution is compatible with the physical conditions at both boundaries. That is, solutions at even j require $\partial\hat{v}/\partial y$ at $j=(J-1)$, and solutions at odd j require $\partial\hat{v}/\partial y$ at $j=0$. Returning to the system of first-order equations (54–56), we can also see the consequences on $\hat{u}$ and $\hat{\phi}$ for even and odd J. The compatibility of the three dependent variables is summarized in table 1.

It is clear that corollary boundary conditions can be deduced from the system of differential equations (50–52) and the physical condition (53). From (51) we see that $\partial\hat{u}/\partial t=0$; differentiating (52) timewise yields $\partial^2\hat{\phi}/\partial t\partial y=0$; differentiating (50) with respect to y yields $\partial^2\hat{v}/\partial y^2=0$. These, however, do not provide the conditions for $\partial\hat{v}/\partial y$.

The condition on $\partial\hat{v}/\partial y$ must be such as to yield compatible solutions at adjacent points and hence must depend not only on the differential equations and the physical boundary conditions, but also on their form when differencing is performed and on the method of differencing. We will refer to such conditions as *computational boundary conditions.*

*During the preparation of this manuscript the writer's attention was drawn to a paper by Platzman [7] which also points out this property of central differencing techniques.

Heuristically it appears reasonable that numerical integration between the boundaries of the difference analogue of the quantity for which a computational boundary condition is required must correspond exactly to the integral of its continuous form.

Let this quantity be denoted in general by $\partial\chi/\partial y$, where χ is known on $y=0,Y$ as a physical condition or as a corollary. Therefore the integral of $\partial\chi/\partial y$:

$$\int_0^Y \frac{\partial\chi}{\partial y}\,dy=\chi(Y)-\chi(0) \tag{60}$$

is exact and known. The finite difference sum over *all* points equivalent to the left side of (60) is

$$\left[\frac{1}{2}\left(\frac{\partial\chi}{\partial y}\right)_0+\sum_{j=1}^{J-2}\left(\frac{\partial\chi}{\partial y}\right)_j+\frac{1}{2}\left(\frac{\partial\chi}{\partial y}\right)_{J-1}\right]\Delta y. \tag{61}$$

In the case of central differences

$$\left(\frac{\partial\chi}{\partial y}\right)_j=\frac{\chi_{j+1}-\chi_{j-1}}{2\Delta y}. \tag{62}$$

Substituting (62) in (61) and equating to the right side of (60)

$$\frac{1}{4}[(\chi_1-\chi_{-1})+(\chi_J-\chi_{J-2})]+\frac{1}{2}\sum_{j=1}^{J-2}(\chi_{j+1}-\chi_{j-1})=\chi_{J-1}-\chi_0. \tag{63}$$

Upon carrying out the indicated summation we have

$$(\chi_J-2\chi_{J-1}+\chi_{J-2})=(\chi_1-2\chi_0+\chi_{-1}) \tag{64}$$

which is the difference analogue of the condition that $\partial^2\chi/\partial y^2$ be equal at the boundaries. A *sufficient* condition to satisfy (64) is that the left and right sides vanish individually so that

$$\left.\begin{aligned}\left(\frac{\partial\chi}{\partial y}\right)_0&=\frac{1}{2\Delta y}(\chi_1-\chi_{-1})=\frac{1}{\Delta y}(\chi_1-\chi_0)\\ \left(\frac{\partial\chi}{\partial y}\right)_{J-1}&=\frac{1}{2\Delta y}(\chi_J-\chi_{J-2})=\frac{1}{\Delta y}(\chi_{J-1}-\chi_{J-2}).\end{aligned}\right\} \tag{65}$$

Equations (65) are the required computational boundary conditions. They are equivalent to the requirement that $\partial\chi/\partial y$ be calculated at the boundaries by means of one-sided differences over a single grid interval. This result is intuitively acceptable and might have been arrived at without the *a priori* requirement that the exact integral condition be satisfied. It is of interest that Phillips, in a recent successful integration of the barotropic primitive equations for a fluid with a free surface in a hemispheric domain bounded by an equatorial wall, applied anti-symmetry conditions on the wind component normal to the boundary.* This may be deduced as a consequence of (64). The exact integral condition has provided a sufficient condition for deriving the computational boundary conditions. The sufficiency has only been established empirically; i. e. through extended period integrations. It is not as yet clear what the *necessary and sufficient* conditions must be.

It is to be emphasized that the computational boundary conditions will depend on the form of the differential equations which are differenced and the difference technique; for instance, whether derivations of products are carried out before differencing. In particular (58) does not require any computational boundary conditions at all. The case of system (54–56), as we have seen, requires $\partial\hat{v}/\partial y$. Applying the physical condition (53) to (65) we have

$$\left.\begin{aligned}\left(\frac{\partial\hat{v}}{\partial y}\right)_0&=\frac{\hat{v}_1}{\Delta y}\\ \left(\frac{\partial\hat{v}}{\partial y}\right)_{J-1}&=-\frac{\hat{v}_{J-2}}{\Delta y}\end{aligned}\right\} \tag{66}$$

and the problem for zonally-symmetric linear motion is completely stated for numerical integration.

Let us now proceed to a somewhat more complex case—that of viscous flow with external heating RQ/c_p, which will assume a given function of y.

We will now consider the effect of a lateral viscosity and heating in the linear zonally symmetric system. The system of equations is then

$$\frac{\partial\hat{\phi}}{\partial t}=-\gamma^2\frac{\partial\hat{v}}{\partial y}+\frac{R}{c_p}Q \tag{67}$$

$$\frac{\partial\hat{u}}{\partial t}=f\hat{v}+m^2K\frac{\partial^2\hat{u}}{\partial y^2} \tag{68}$$

$$\frac{\partial\hat{v}}{\partial t}=-f\hat{u}-m^2\frac{\partial\hat{\phi}}{\partial y}+m^2K\frac{\partial^2\hat{v}}{\partial y^2}. \tag{69}$$

From the considerations of the non-symmetric system in Section 2, we have two physical boundary conditions

$$\hat{v}=0 \text{ on } y=0,\ Y \tag{70}$$

$$\frac{\partial\hat{u}}{\partial y}=0 \text{ on } y=0,\ Y. \tag{71}$$

The initial conditions are the same as before: $\hat{\phi}$, $\hat{u}$, $\hat{v}$ given everywhere subject to (70), and we still have a pure marching problem. On the boundaries $\partial\hat{v}/\partial t$ is known from (70), and $\partial\hat{\phi}/\partial t$ in (67) is known if $\partial\hat{v}/\partial y$ is calculated from the computational boundary condition (66), as before. For $\partial\hat{u}/\partial t$ in (68) we need an additional computational condition on $\partial^2\hat{u}/\partial y^2$. This is obtained by taking $\partial\hat{u}/\partial y$ for χ in (65) and applying (71), then the exact integral condition yields:

$$\left.\begin{aligned}\left(\frac{\partial^2\hat{u}}{\partial y^2}\right)_0&=\frac{1}{\Delta y}\left(\frac{\partial\hat{u}}{\partial y}\right)_1=\frac{1}{2(\Delta y)^2}(\hat{u}_2-\hat{u}_0)\\ \left(\frac{\partial^2\hat{u}}{\partial y^2}\right)_{J-1}&=-\frac{1}{\Delta y}\left(\frac{\partial\hat{u}}{\partial y}\right)_{J-2}=-\frac{1}{2(\Delta y)^2}(\hat{u}_{J-1}-\hat{u}_{J-3}).\end{aligned}\right\} \tag{72}$$

It should be pointed out that central time and space

*These results are as yet unpublished, but a reference to this condition is given in an earlier paper by Phillips [6].

differences applied to (68) and (69) will, due to the viscosity, give rise to equations of the form

$$\hat{u}_j^{\tau+1}-\hat{u}_j^{\tau-1}=\ldots-\left(\frac{m^2K4\Delta t}{(\Delta y)^2}\right)\hat{u}_j^{\tau}. \tag{73}$$

Hence a spurious computational solution is introduced that is unstable when the coefficient $K>0$, which it is in this case. One means for avoiding it is to evaluate $\hat{u}_j$ on the right side at $(\tau-1)$. We may refer to this as *computational instability of the third kind*, which is thoroughly discussed by Eliassen [3] and Richtmyer [8].

4. NON-LINEAR BAROCLINIC FLOWS (CONTINUED)

a. COMPUTATIONAL BOUNDARY CONDITIONS

We may now proceed to complete the discussion of the numerical integration of the fully non-linear, zonally asymmetric system described in Section 2.

It is appropriate at this time to compare the merits of Systems I and II. Perhaps the most important consideration is their relative stability under numerical integration. The purpose of the elliptic equations is to insure that $\partial\overline{\mathcal{D}}/\partial t\equiv 0$. System II does this directly by regenerating the stream function. Hence by definition, truncation and round-off errors cannot introduce divergence into the $\overline{\nabla}$ field computed from it. On the other hand, by working through $\bar{\phi}$ in System I, there is no way of avoiding degeneracy (i.e., the introduction of spurious $\overline{\mathcal{D}}\neq 0$) due to truncation and round-off except through periodic rebalancing by means of (42), assuming $\bar{\zeta}$ to be essentially correct. One further advantage in favor of System II is that the numerical solution of Dirichlet problems by relaxation methods seems to converge more rapidly than that for Neumann problems. This may be due only to the fact that we have far greater experience with Dirichlet problems. Nevertheless, it is an important economical consideration where extended-period calculations are contemplated. Therefore, we will confine ourselves to consideration of System II.

It is desirable that the form of the continuous equations to be differenced be such that time changes of zonal angular momentum and temperature possess exact integrals over the entire area. That is, we wish to avoid spurious sources of angular momentum and heating due to truncation error in the non-linear terms. It is clear that the potential and kinetic energy integrals will not be exact. Furthermore one should avoid terms of the form (73) from appearing in non-viscous terms if there is a possibility of computational instability of the third kind. Thus applying (18) to (23), and (18) and (22) to (20), we have

$$\frac{\partial\hat{\phi}}{dt}=-\frac{\partial}{\partial x}\left(\frac{\hat{\phi}\overline{u}}{2}\right)-m^2\frac{\partial}{\partial y}\left(\frac{\hat{\phi}\overline{v}}{2m^2}\right)-\gamma^2\hat{\mathcal{D}}+\frac{R}{c_p}Q \tag{74}$$

$$\left.\begin{aligned}
\mathsf{I}_1&=\mathrm{i}\left[\frac{\partial u_1^2}{\partial x}+m^4\frac{\partial}{\partial y}\left(\frac{u_1v_1}{m^4}\right)-\frac{\hat{\mathcal{D}}\overline{u}}{4}-2\Omega\alpha v_1\right]\\
&+\mathrm{j}\left[\frac{\partial u_1v_1}{\partial x}+m^3\frac{\partial}{\partial y}\left(\frac{v_1^2}{m^3}\right)-\frac{\hat{\mathcal{D}}\overline{v}}{4}+\alpha\left(2\Omega+\frac{v_1}{a}\right)u_1\right]\\
\mathsf{I}_3&=\mathrm{i}\left[\frac{\partial u_3^2}{\partial x}+m^4\frac{\partial}{\partial y}\left(\frac{u_3v_3}{m^4}\right)+\frac{\hat{\mathcal{D}}\overline{u}}{4}-2\Omega\alpha v_3\right]\\
&+\mathrm{j}\left[\frac{\partial u_3v_3}{\partial x}+m^3\frac{\partial}{\partial y}\left(\frac{v_3^2}{m^3}\right)+\frac{\hat{\mathcal{D}}\overline{v}}{4}+\alpha\left(2\Omega+\frac{u_3}{a}\right)u_3\right].
\end{aligned}\right\} \tag{75}$$

It is clear that because of the cyclic continuity condition in x, computational boundary conditions may be necessary only on the zonal boundaries. We have seen in Section 2c that the boundary value problem to construct the initial ψ field everywhere is completely stated for numerical integration, without need for a computational boundary condition. This is also true for the initial $\overline{\nabla}$ field.

In the time integration of the geopotential thickness, $\hat{\phi}$, in (74), we need $\hat{\mathcal{D}}$ on the boundaries, and also $m^2\partial(\hat{\phi}\overline{v}/2m^2)/\partial y$. Note that the latter would not have been necessary had we used the form in (23) since $\overline{v}$ vanishes on the boundary. Applying (65) we have

$$\left.\begin{aligned}
(\hat{\mathcal{D}})_{i,0}&=\left(\frac{\partial\hat{u}}{\partial x}\right)_{i,0}+\frac{m_0^2}{m_1^2\Delta}(\hat{v})_{i,1}\\
(\hat{\mathcal{D}})_{i,J-1}&=\left(\frac{\partial\hat{u}}{\partial x}\right)_{i,J-1}-\frac{m_{J-1}^2}{m_{J-2}^2\Delta}(\hat{v})_{i,J-2}
\end{aligned}\right\} \tag{76}$$

and

$$\left.\begin{aligned}
\left[m^2\frac{\partial}{\partial y}\left(\frac{\hat{\phi}\overline{v}}{2m^2}\right)\right]_{i,0}&=\frac{m_0^2}{2m_1^2\Delta}(\hat{\phi}\overline{v})_{i,1}\\
\left[m^2\frac{\partial}{\partial y}\left(\frac{\hat{\phi}\overline{v}}{2m^2}\right)\right]_{i,J-1}&=-\frac{m_{J-1}^2}{2m_{J-2}^2\Delta}(\hat{\phi}\overline{v})_{1,J-2}
\end{aligned}\right\} \tag{77}$$

where we have taken $\Delta\equiv\Delta x=\Delta y$.

To calculate inertial terms, I, on the boundary from (75) we need in addition:

$$\left.\begin{aligned}
\left[m^4\frac{\partial}{\partial y}\left(\frac{uv}{m^4}\right)\right]_{i,0}&=\frac{m_0^4}{m_1^4\Delta}(uv)_{i,1}\\
\left[m^4\frac{\partial}{\partial y}\left(\frac{uv}{m^4}\right)\right]_{i,J-1}&=-\frac{m^4{}_{J-1}}{m^4{}_{J-2}\Delta}(uv)_{i,J-2}
\end{aligned}\right\} \tag{78}$$

$$\left.\begin{aligned}
\left[m^3\frac{\partial}{\partial y}\left(\frac{v^2}{m^3}\right)\right]_{i,0}&=\frac{m_0^3}{m_1^3\Delta}(v^2)_{i,1}\\
\left[m^3\frac{\partial}{\partial y}\left(\frac{v^2}{m^3}\right)\right]_{i,J-1}&=-\frac{m^3{}_{J-1}}{m^3{}_{J-2}\Delta}(v^2)_{i,J-2}
\end{aligned}\right\} \tag{79}$$

The frictional force (32) requires

$$\left.\begin{aligned}
\left[m^3\frac{\partial}{\partial y}\left(\frac{1}{m^2}\frac{\partial u}{\partial y}\right)\right]_{i,0}&=\frac{m_0^3}{m_1^2 2\Delta^2}(u_{i,2}-u_{i,0})\\
\left[m^3\frac{\partial}{\partial y}\left(\frac{1}{m^2}\frac{\partial u}{\partial y}\right)\right]_{i,J-1}&=-\frac{m_{J-1}^3}{m_{J-2}^2 2\Delta^2}(u_{i,J-1}-u_{i,J-3})
\end{aligned}\right\} \tag{80}$$

and

$$\left.\begin{aligned}\left[m^3\frac{\partial}{\partial y}\left(\frac{1}{m^2}\frac{\partial v}{\partial y}\right)\right]_{i,0}&=\frac{m_0^3}{\Delta}\left[\frac{v_{i,2}}{2m_1^2\Delta}-\frac{(\partial v/\partial y)_{i,0}}{m_0^2}\right]\\ \left[m^3\frac{\partial}{\partial y}\left(\frac{1}{m^2}\frac{\partial v}{\partial y}\right)\right]_{i,J-1}&=\frac{m_{J-1}^3}{\Delta}\left[\frac{(\partial v/\partial y)_{i,J-1}}{m_{J-1}^2}+\frac{v_{i,J-2}}{2m_{J-2}^2\Delta}\right].\end{aligned}\right\} \tag{81}$$

In (81), $\partial v/\partial y$ on the boundary must be evaluated consistently with the calculation of the divergence on the boundary. For example, at $j=0$ and referring to (65) and (76) we have that

$$\left(\frac{v}{m^2}\right)_{i,-1}=-\left(\frac{v}{m^2}\right)_{i,1};$$

therefore

$$\left(\frac{\partial v}{\partial y}\right)_{i,0}=\frac{1}{2\Delta}\left(1+\frac{m_{-1}^2}{m_1^2}\right)v_{i,0}. \tag{82}$$

Similarly on the other boundary

$$\left(\frac{\partial v}{\partial y}\right)_{i,J-1}=-\frac{1}{2\Delta}\left(1+\frac{m_J^2}{m_{J-2}^2}\right)v_{i,J-2}. \tag{83}$$

Hence G_k is known everywhere and the stream function tendency may be calculated from (28) and (48).

b. COMPUTATIONAL ASPECTS OF THE ELLIPTIC PART

We may use the customary extrapolated Liebmann relaxation technique to calculate the initial ψ from (42) and ψ^* from (28). The first guess for ψ may be obtained by integrating (42) with boundary condition (43)

$${}^0\psi(y)=\frac{1}{L}\oint\psi dx=-\frac{y}{L}\left(\frac{a}{2\alpha}\oint\frac{\overline{\zeta}}{m^2}dx\right)_{y=0}+\frac{1}{L}\int_0^y\left[\int_0^y\left(\oint\frac{\overline{\zeta}}{m^2}dx\right)dy\right]dy. \tag{84}$$

The anterior superscript denotes the iterative index ν.

Equation (84) may also be employed to hasten convergence. As each row is relaxed within a given scan, ν, the mean value of ${}^\nu\psi_{i,j}$ over all i must satisfy (84). The ψ's are then adjusted accordingly before going on to the next row.

In the case of ψ^* we have the source of a better guess through extrapolation:

$$\left.\begin{aligned}&\tau=0: {}^0\psi^{*0}=0\\ &\tau=1: {}^0\psi^{*1}=\psi^{*0}\\ &\tau>1: {}^0\psi^{*\tau}=2\psi^{*\tau-1}-\psi^{*\tau-2}.\end{aligned}\right\} \tag{85}$$

We may accelerate convergence of the relaxation of (28) by again adjusting the mean value of a newly relaxed row to the integral of (26):

$$\oint\psi^*dx=-\int_0^y\left(\oint\frac{\overline{G}_x}{m}dx\right)dy. \tag{86}$$

This technique should be applied for only a few scans since the error due to adjustment quickly becomes comparable to the iterative error during the process of convergence. Such integrations have been performed on a grid of 18 x 72 points with a relaxation factor of 1.25 and a criterion $|^{\nu+1}\psi^*-{}^\nu\psi^*|/g<(15/64)m$, where $g=9.81$ m. sec^{-2}. The application of (86) was stopped when $|^{\nu+1}\psi^*-{}^\nu\psi^*|/g<(75/64)$m. The number of iterations necessary for convergence varied between 2 and 6.

c. CONSTRUCTION OF THE ϕ FIELD

Although the $\overline{\phi}$ and ϕ_k fields never enter explicitly into System II, it may be of interest to examine these quantities during the course of the calculation. This can be accomplished through integration of equations (26–27) by simple quadratures. In doing this numerically, care must be taken to avoid accumulation of systematic truncation error. That is, the numerical solution of equations (26–27) should be independent of the path taken for the numerical quadratures. Consider the scheme

$$\overline{\phi}_{i+\frac{1}{2},j+\frac{1}{2}}-\overline{\phi}_{i-\frac{1}{2},j+\frac{1}{2}}=(\psi^*_{i,j+1}-\psi^*_{i,j})+\frac{\Delta}{2}\left[\left(\frac{\overline{G}_x}{m}\right)_{i,j+1}+\left(\frac{\overline{G}_x}{m}\right)_{i,j}\right] \tag{87}$$

$$\overline{\phi}_{i+\frac{1}{2},j+\frac{1}{2}}-\overline{\phi}_{i+\frac{1}{2},j-\frac{1}{2}}=-(\psi^*_{i+1,j}-\psi^*_{i,j})+\frac{\Delta}{2}\left[\left(\frac{\overline{G}_y}{m}\right)_{i+1,j}+\left(\frac{\overline{G}_y}{m}\right)_{i,j}\right]. \tag{88}$$

Upon eliminating $\overline{\phi}$ between (87) and (88), we have

$$\psi_{i,j+1}+\psi^*_{i,j-1}+\psi^*_{i+1,j}+\psi^*_{i-1,j}-4\psi^*_{i,j}=\frac{\Delta}{2}\left[-\left(\frac{\overline{G}_x}{m}\right)_{i,j+1}+\left(\frac{\overline{G}_x}{m}\right)_{i,j-1}+\left(\frac{\overline{G}_y}{m}\right)_{i+1,j}-\left(\frac{\overline{G}_y}{m}\right)_{i-1,j}\right]$$

which is precisely the difference analogue of (28). Setting an arbitrary datum at a point, say $\overline{\Phi}_{\frac{1}{2},-\frac{1}{2}}=0$, then one can calculate $\overline{\Phi}_{\frac{1}{2},j+\frac{1}{2}}$ for $j=0, \ldots, (J-1)$ from (88). Since $i=i+I$, then with (87) we can obtain $\overline{\Phi}_{i+1\frac{1}{2},j+\frac{1}{2}}$ for $i=0, \ldots, (I-2)$; $j=0, \ldots, (J-2)$. Finally, we employ (88) again to calculate $\overline{\Phi}_{i+1\frac{1}{2},-\frac{1}{2}}$ and $\overline{\Phi}_{i+1\frac{1}{2},J-\frac{1}{2}}$ for $i=0, \ldots, (I-2)$. We now have $\overline{\Phi}_{i+\frac{1}{2},j+\frac{1}{2}}$ for $i=0, \ldots, (I-1)$; $j=-1, 0, 1, \ldots, (J-1)$. This is sufficient for an interpolation of $\overline{\phi}$ at the boundaries with a correct representation of $\partial\overline{\phi}/\partial y$ at the boundaries.

5. CONCLUDING REMARKS

We have developed a scheme for numerically integrating the baroclinic primitive equations over a domain with closed boundaries. In actual application, the methods described have yielded an analogue of the primitive

equations which is stable when integrated numerically over extended periods. At a time when it appeared unclear how numerical integration of the primitive equations could be made free of spurious gravitational instability, J. von Neumann proposed the inclusion of a compressional viscosity in the equations of motion to suppress the amplitude of gravitational disturbances of wavelength comparable to grid size. Since such a viscosity has no physical counterpart, one would expect a systematic distortion of the evolving motions. However, it appears (empirically) that the method discussed here for formulating the computational boundary conditions precludes the occurrence of spurious gravitational instability. Hence the use of an artificial compressional viscosity may be removed from consideration.

The exact integral condition for deducing computational boundary conditions must apply as well to the form of the baroclinic primitive equations which also admit external gravitational motions. Those meteorological studies for domains where flow through the boundaries is permitted present a special problem. The reason of course is that a correct statement of the appropriate physical boundary conditions is not clear. The investigation of Platzman [7] is a significant contribution in this direction.

Experience has demonstrated that a consistent use of the geostrophic approximation can yield great insight into the large-scale atmospheric processes in spite of the obvious limitations wrought by the restrictive approximations. Historically, linear techniques have played a similar role in providing a fundamental understanding of dynamical processes at the expense of relatively little mathematical effort. It appears that the step to completeness from linear and geostrophic investigations is most profitably made by going directly to the nonlinear primitive equations. The fundamental simplicity and self consistency inherent in the primitive equations, together with an assurance of stability under numerical treatment, would seem to suggest this as the logical course. The use of the balance equations as an intermediate step offers questionable diagnostic gain. This conclusion is based on the dubious increase of understanding gained in return for considerable computational complexity.

ACKNOWLEDGMENTS

The writer gratefully acknowledges the programming assistance of R. D. Graham and J. L. Holloway in performing the numerical experiments alluded to in this paper. He would also like to thank N. A. Phillips, G. W. Platzman, S. Manabe, and D. K. Lilly for their constructive comments on the manuscript.

REFERENCES

1. J. Charney, "The Use of the Primitive Equations of Motion in Numerical Prediction," *Tellus*, vol. 7, No. 1, Feb. 1955, pp. 22–26.
2. A. Eliassen, "The Quasi-Static Equations of Motion with Pressure as Independent Variable," *Geofysiske Publikasjoner*, vol. XVII, No. 3, 1949, 44 p.
3. A. Eliassen, Lectures on Physical Weather Prediction, University of California, Dept. of Meteorology, 1955, 109 pp.
4. A. Eliassen, "A Procedure for Numerical Integration of the Primitive Equations of the Two-Parameter Model of the Atmosphere," University of California at Los Angeles, Dept. of Meteorology, Large Scale Synoptic Processes Project, Scientific Report No. 4, 1956, 53 pp.
5. B. Haurwitz, *Dynamic Meteorology*, McGraw-Hill Book Co., Inc., 1941 (see p. 119).
6. N. A. Phillips, "A Map Projection System Suitable for Large-Scale Numerical Weather Prediction," *Journal of Meteorological Society of Japan*, 75th Ann. vol., 1957, pp. 262–267.
7. G. W. Platzman, "The Lattice Structure of the Finite-Difference Primitive and Vorticity Equations," University of Chicago, Dept. of Meteorology, Tech. Rep. No. 6 to U.S. Weather Bureau, 1958, 26 pp. (Recently published in *Monthly Weather Review*, vol. 86, No. 8, Aug. 1958, pp. 285–292).
8. R. D. Richtmyer, *Difference Methods for Initial-Value Problems*, Interscience Publishers, New York, 1957 (see p. 94).

APPLICATION OF NUMERICAL METHODS TO EXTENDED FORECASTING PRACTICES IN THE U.S. WEATHER BUREAU*

JEROME NAMIAS AND COLLABORATORS**

Extended Forecast Section, U.S. Weather Bureau, Washington, D.C.

[Manuscript received October 9, 1958; revised December 4, 1958]

ABSTRACT

New procedures are described for applying numerical methods to extended forecasting. These form a firm base which serves as a point of departure for the final forecast. The methods are sufficiently organized that training and actual forecasting are speeded up and the level of skill of prediction is higher than ever before.

1. INTRODUCTION

In a statement dealing with "Meteorological Research Tasks" prepared for the Natural Science Research Council of Sweden in the spring of 1956, the late Carl-Gustaf Rossby wrote, "The comments made above indicate that objective numerical methods of integration, based on current models of atmospheric behavior, probably will find their greatest practical application in the preparation of general circulation pattern forecasts of moderate range (a few days to a week), while it is more uncertain if they will be able to contribute significantly to the short-range forecasting of detailed weather phenomena." It is the purpose of the present report to indicate that at least in the first part of this statement, Rossby displayed his characteristic foresight.

Up to quite recently, methods employed in making predictions for periods up to a week in advance [1] have involved a judicious combination of physical, statistical, and synoptic techniques, but the weighting procedures have often been so subjective that Lord Kelvin's classical remark of the meager and unsatisfactory charactor of merely descriptive knowledge comes to mind. Today, after years of research in the application of numerical methods to extended forecasting, new procedures, while still not completely objective, are nevertheless sufficiently organized that (1) it takes much less time to train forecasters, (2) medium range forecasts can be prepared more easily and faster than ever before, and (3) most important, the level of skill of predictions is higher than ever before. A preliminary report of some of this research was presented earlier by the author [2]; further experiments and results are described in the present report.

The fundamental 5-day forecasting procedure still involves two steps: first, the prediction of time-averaged circulation patterns for mid-troposphere and sea level; and second, the interpretation of these patterns in terms of climatic anomalies, particularly for fields of temperature and precipitation. Once the mean patterns for the advance 5-day period have been predicted, it is also possible to estimate the general course of cyclones, anticyclones, fronts, and air masses, and thereby prepare prognostic day-to-day charts up to 6 days.

The first and most important task is to predict the 5-day mean circulation pattern which will prevail for the forecast period which covers from 2 to 7 days in advance, for this is the large-scale quasi-stationary flow pattern which appears to guide the fronts, air masses, and storms and which, to a large extent, can be interpreted in terms of regional climatic anomalies. Three numerical procedures, not independent of one another, have been developed for arriving at a prognostic 500-mb. mean contour pattern, and all three are considered carefully by the forecaster in arriving at a final prediction. While a large portion of the skill of the final forecast lies in these numerical prognoses, their improper consideration of some factors and, in fact, complete omission of others, makes it presently desirable to permit the forecaster some flexibility in the use of his experience and judgment. The three procedures are referred to as (1) the trend method, (2) the summation method, and (3) the basic current method.

2. THE TREND METHOD

Essentially this procedure utilizes recent gains made in short-range numerical prognoses by objectively viewing short-period changes in flow pattern against the background of slower-evolving time-averaged patterns. This is done by automatic construction (on the IBM 704) of a 5-day mean 500-mb. chart centered on the day of the forecast (the "trend" map). Three days of height values for this 5-day mean are observed, while the predicted information for 24 and 48 hours is extracted from short-range numerical (barotropic) prognoses.† This mean chart is quite similar in appearance to the Fjørtoft space-

*Substance of paper presented before the Scandinavian-American Meteorological Meeting in Bergen, June 19-25, 1958.

**This report represents the work of many individuals in the Extended Forecast Section of the U.S. Weather Bureau—researchers, forecasters, and technical assistants. Carlos R. Dunn, Arthur F. Krueger, and Billy M. Lewis have been especially active in the formulation and testing of these ideas.

†The barotropic forecasts referred to in this paper are derived from an older operational model used by the Joint Numerical Weather Prediction Unit at Suitland, Md. This did not include a correction for erroneous long-wave retrogression as did later models based on the work of Wolff [9] and Cressman [6].

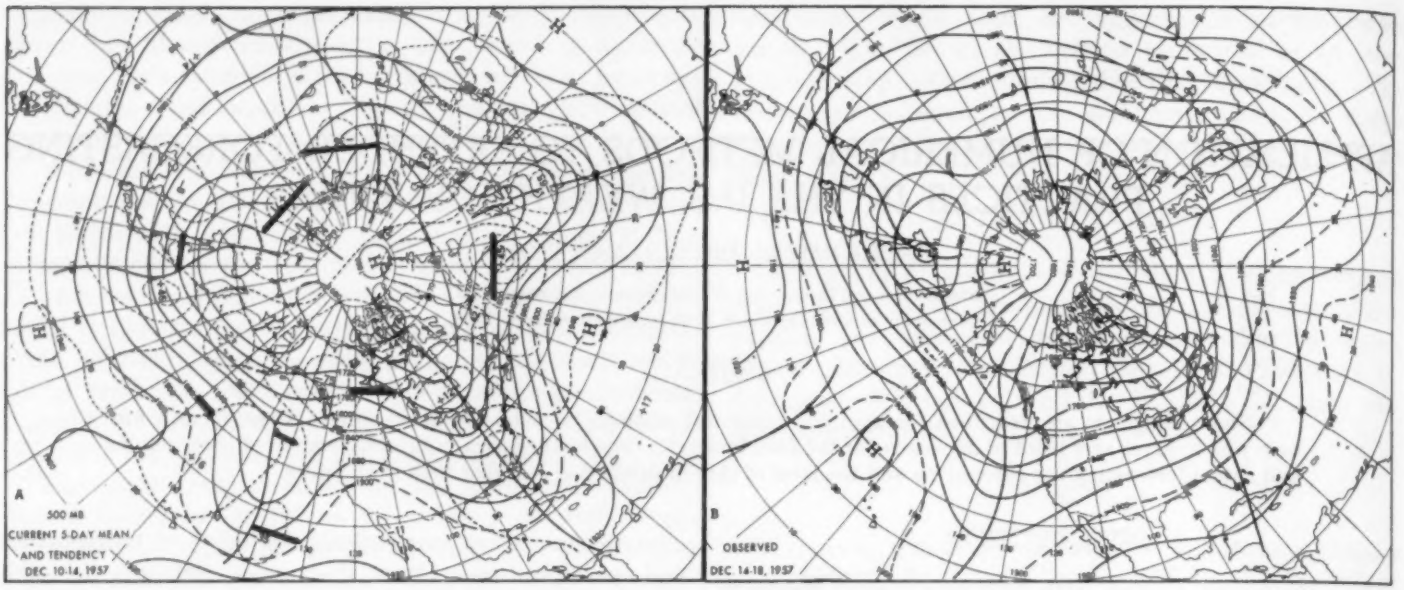

FIGURE 1.—(A) 500-mb. 5-day mean contours (solid lines drawn for every 400 feet and labeled in tens of feet) and 2-day centered height tendencies (broken lines drawn for every 200 feet and with centers expressed in tens of feet) for the period December 10–14, 1957. This chart, called a "trend map," and constructed on December 12, permits kinematical computations of 4-day ridge or trough motion, indicated by heavy arrows. (B) Observed 500-mb. contours for December 14–18, 1957.

smoothed chart. It suppresses undesired short-wave perturbations and brings into focus slow-moving long-wave phenomena. A field of centered 2-day height tendencies of the mean is also computed automatically and these are superimposed on the mean contours. The resulting fields of height and height tendency permit kinematical computations of long-wave motion and development, and thereby assist in prognosis for the desired 5-day period (which is centered 4 days in advance of the "trend map"). An example is shown in figure 1 together with the subsequent 5-day mean chart which may be inferred from the indicated kinematic evolution of the trend map. Note the fundamentally correct motions predicted for most systems except the trough over eastern United States. In this case eastward displacement of the trough must be estimated indirectly because its neighboring ridges are indicated as moving eastward.

This numerically produced trend chart, by automatically including 24- and 48-hour numerical prognoses, rather than the formerly employed statistical estimates based on auto-correlation methods, has not only made the procedure faster and more reliable, but has made it possible to eliminate many tedious and outmoded types of computation [3].

Regardless of how accurate the above-described trend map becomes, however, it will not solve the fundamental 5-day forecast problem, but will at best indicate the broad-scale, slower-evolving trends that often point the way. Therefore, experiments designed to make predictions of 5-day mean patterns centered each day up to 4 days in advance have been performed. Such charts afford not a static picture, but rather an evolving mean state, which is also a changing steering pattern for synoptic scale systems. While such a prognostic mean series might be derived from the trend method, it should be made clear that the real atmosphere is not so simple in its behavior. For example, the centers of height change often move with speeds differing from the planetary ridges and troughs, so that pure extrapolation methods based on instantaneous speed are bound to have failures.

3. THE SUMMATION METHOD

Although the accuracy of the present numerical daily prognoses employing the barotropic model declines rapidly after 48 hours, especially when verified on the basis of root-mean-square errors, numerical predictions have been carried out to 96 hours and then averaged together with the initial day's chart to form a 5-day mean (the "summation" chart). As shall be demonstrated later, the mean pattern thus obtained appears to be reasonably accurate when compared to the observed 5-day mean centered 2 days in advance. The agreement in mean ridge and trough positions, as well as cellular features, in the face of rapid decay in the 72- and especially 96-hour interval, suggests that (1) persistence (serial correlation) operates to such an extent in the real atmosphere that the first few maps imply the major features of the pattern, and (2) compensations occasionally take place wherein an error made on an early prognosis may be rectified later on (or the atmosphere appears to have a "built-in" feature for restoring itself to barotropy). Thus the most useful features (ridges, troughs, etc.) can be appreciably erroneous in intensity, yet this may not interfere with reasonably effective use of the prognosis. The summation chart has two principal functions: (1) to afford a look at the 5-day mean centered 2 days in advance so that comparison with earlier observed mean maps and with the trend map may permit further inferences regarding evolution, and (2) to obtain estimates of 5-day mean temperature anomalies as described below.

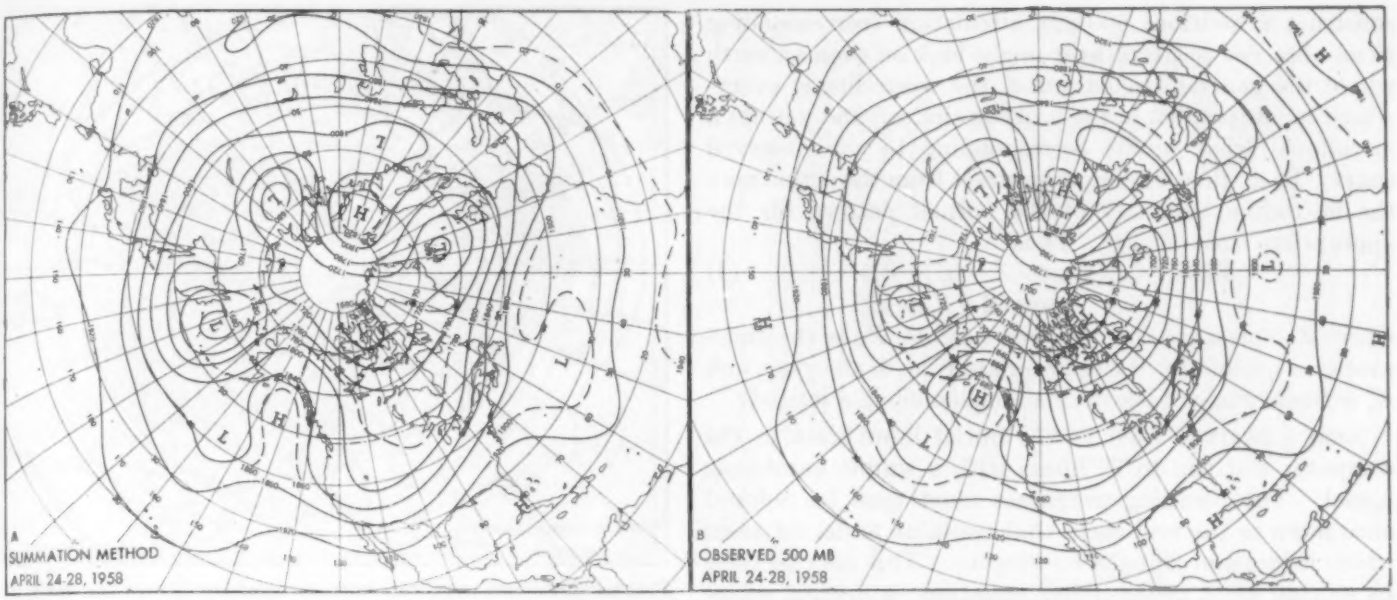

FIGURE 2.—(A) 500-mb. contours for the period April 24–28, 1958 objectively predicted by the summation method (see text). Contours drawn for every 400 feet and labeled in tens of feet. Intermediate contours dashed. (B) 500-mb. contours observed for April 24–28, 1958.

An example of a summation chart, together with the observed, is shown in figure 2. Such good correspondence is by no means rare.

4. THE BASIC CURRENT METHOD

The two methods described above essentially integrate or extend numerical short-range prognosis to bring into focus another class of motions characterized by slowly evolving systems. In both cases the final product desired, a prognostic chart of the mean circulation for the period 2 to 7 days in advance, must be inferred. If day-to-day numerical prognoses reach a point of much greater reliability than at present, it may be possible to produce medium-range forecasts by simply projecting these out to a week. In this event the concept of means would no longer be necessary, and a day-to-day description of future weather maps would be possible. However, at the present there appears to be some break-off point in the use of daily prognosis beyond which some form of statistical technique must be applied.

Since vorticity (including wavelength) concepts have been applied with some success to time-averaged mean charts for almost 20 years, a number of experiments have been performed in an attempt to employ a modified barotropic model to predict mean motions. Some of these are described below:

(1) Selected observed 5-day mean charts for the 500-mb. surface were run with the barotropic model as in routine daily forecasts by the Joint Numerical Weather Prediction Unit in Suitland, Md. These predictions were carried out to 8 days, and a print-out prediction was obtained for each day. The prognoses displayed a logical continuity throughout the period with no suggestion of computational instability; that is, the patterns remained smooth and of appropriately large scale. The patterns resembled those of the observed charts up to a few days, but they became increasingly discordant and characterized by flat fast westerlies thereafter.

(2) Next, the trend chart (the one using short-range barotropic estimates and described earlier) for one of the cases was used as initial or input data for the predictions and run for 5 days. The predictions were surprisingly similar to those obtained by using all known data (rather than half known and half estimated). This result indicated that the starting point for a 5-day mean prediction might be moved up 2 days.

(3) Although the above predictions were stable in the sense that they produced rational flow patterns, they became out of phase with the observed after a few days. It was felt that this failure was due largely to the neglect of physical processes not considered in the simple barotropic model that, after all, can only redistribute the existing vorticity. While the rigid incorporation of these missing factors is probably the central and most difficult problem facing weather forecasting, it is possible that certain statistical estimates may be used to improve the performance of the barotropic model—a philosophy that underlies current extended forecasting practice in the United States Weather Bureau.

The particular method used in the experiment was to make use of the fields of departure from normal of the initial chart (the trend chart, including 24- and 48-hr. estimates) in the manner described below.

If the earth were a smooth surface with no longitudinal temperature differences, the mean state of the general circulation would show no preferred regions for ridges or troughs in the upper westerlies and would thus consist of a vast circumpolar whirl of zonal winds. Many factors, such as mountains or other ocean-continent contrasts, that interfere with the successful operation of the barotropic model, particularly at long range, would be partially eliminated on the assumed fictitious earth. Now we can

construct a fictitious 500-mb. circulation (corresponding to an observed pattern) as it might look on such an earth where the general circulation of the westerlies is everywhere zonal (parallel to the latitude circles), and yet has a meridional wind profile corresponding to the observed chart. To do this, we simply subtract from the actual map the latitudinal anomaly of the normal pattern for the appropriate time of year. Thus:

$$\text{Fictitious Chart} = Z-(Z_n-Z_n^*) \quad (1)$$
$$\text{or} = (Z-Z_n)+Z_n^*$$

where Z represents the observed heights, Z_n is the time-averaged normal for the appropriate time of the year, and Z_n^* is the average of the normal heights along a latitude.

Such a chart is used as the initial input data in the computer and run to 96 hours with a simple barotropic model. The resulting prognoses must then be reduced once more to the real earth that contains preferred areas where ridges and troughs congregate. This may be done by solving for Z in the above equation—a process whose purpose is to incorporate once more approximations for effects of such factors as mountains and heat sources. In a sense the fictitious chart may be viewed as a catalyst used to expedite the prognosis. Viewing it in another way, this method applies the vorticity concept to the departure from normal fields, as suggested by Clapp [4], but with the important difference that a carrying current is introduced. Objections can be raised to such an oversimplified solution of such a complex problem. For example, non-barotropic effects operate at each phase in the evolution of the pattern, and cannot be removed completely or considered in one fell swoop. Of course, in the final analysis one must judge the validity of such an idea by the success it attains. Some verifications are cited below.

(4) Experiments with a coarse 483-point (600-km. mesh length) grid and utilizing the geostrophic approximation succeeded just as well as those with the more elaborate models employing more closely spaced grids and use of the balance equation. Apparently because of the large scale of systems on mean charts, great detail is not required and the geostrophic assumption is quite applicable. Moreover, this simpler model consumes much less machine time.

Expressed in other words, the core of the method described above is the premise that the general circulation consists of a broad basic current on which are superimposed free perturbations. Undulations in the basic current are established partly by geographical and seasonal factors such as mountain chains and coast lines and in a given season partly by anomalous factors whose physical nature is obscure. Subtraction of the latitudinal anomalies of the appropriate normal map from the trend map is designed to uncouple the (5-day) free perturbation from the climatologically forced flow. It is this free flow which is fed into the computer and run out barotropically to 4 days. At desired intervals of 48, 72, and 96 hours the basic current or normal is re-introduced and the machine prints out a prognostic mean chart.

In this semi-dynamic model other basic currents may be used besides the appropriate monthly normal. In fact, experiments have now proven that a better choice of a basic current is an estimate of the monthly mean circulation centered around the period of the forecast. In other words, there appears to be a controlling linkage between a fairly persistent long-period anomalous state of the general circulation and the 5-day class of motions, just as there is between 5-day phenomena and day-to-day systems. Approximations to the current long-period state of the general circulation may be obtained by statistical auto-correlation methods [5]. Thus a 30-day mean centered around the day on which a 5-day prediction is desired can be fairly well approximated by the expression:

$$\bar{h}_{30}=\frac{1}{30}(6.5h_5+8.5N+h_{-15}) \quad (2)$$

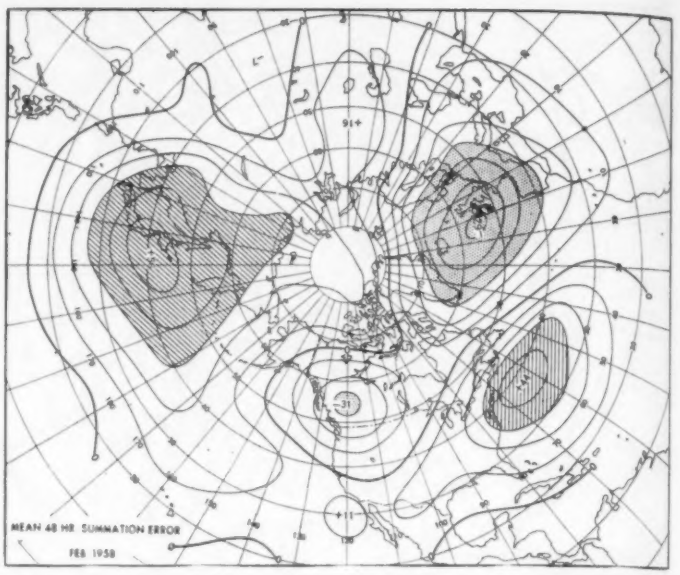

FIGURE 3.—Mean algebraic errors (isopleths drawn for each 100 feet and centers labeled in tens of feet) for summation predictions made during February 1958.

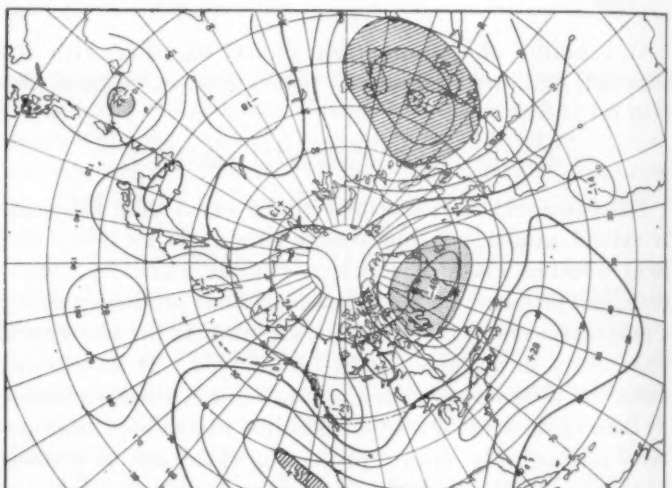

FIGURE 4.—Mean algebraic errors for basic current method predictions made during February 1958. Centers labeled in tens of feet.

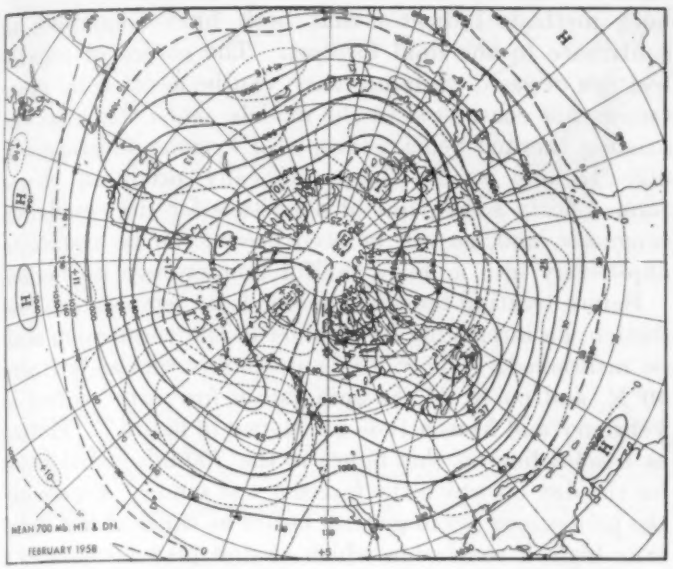

FIGURE 5.—Mean 700-mb. contours (solid lines drawn for every 200 feet) and departures from normal (broken lines drawn for every 100 feet with centers labeled in 10's of feet) for February 1958.

where $\overline{h}_{30}$ is the 30-day mean centered on forecast day, h_{-15} is the sum of the observed heights of the last 15 days, h_5 is the height given by the summation prognosis (average of next 5 days), and N is the appropriate normal.

5. VERIFICATION OF NUMERICAL PROGNOSES MADE BY SUMMATION AND BASIC CURRENT METHODS

Algebraic mean error fields for all forecasts made by the summation and basic current methods for a 5-day period centered 2 days ahead during February 1958 are shown in figures 3 and 4. The large positive errors in the summation prognoses off the east coasts of the continents appear to be due, at least in part, to the absence of heating terms in the simple barotropic model used. (The outflow of air off the Asiatic and North American coasts during February 1958 was even colder than normal for February.) The reduction in mean error over these areas indicated by the normal basic current predictions (fig. 4) suggests that to some extent these complex effects are being taken into consideration, although in some areas (e.g., over Europe) errors not found in the summation chart are introduced.

If one compares the mean error fields obtained by using the normal basic current method (fig. 4) with the departures from normal for the month during which the forecasts were made (February 1958, shown in figure 5), it is at once clear that a good *negative* correlation exists. In other words, the predictions are generally too high in areas where the month was below normal and too low in areas of positive anomaly. This strongly indicates that improvements would result from the use of a basic current bearing greater resemblance to the *anomalous* condition of the month. Indeed, material improvement results from substituting the estimated centered 30-day mean for Z_n in formula (1) when solving for Z at the end of the

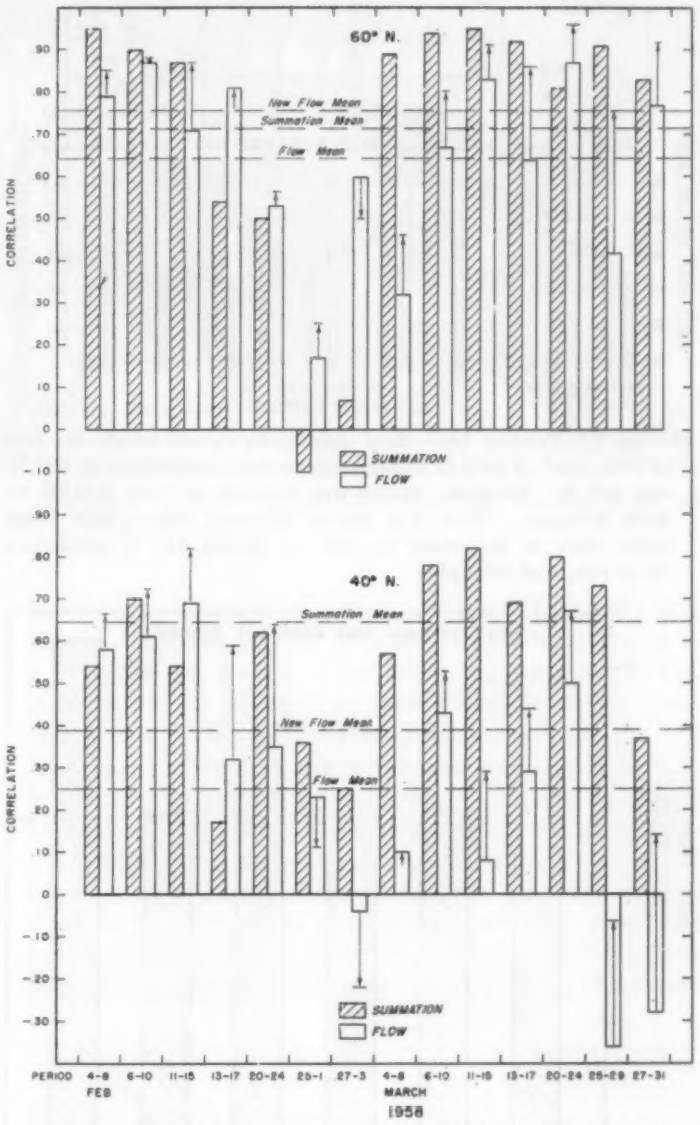

FIGURE 6.—Verifications for 5-day mean 500-mb. forecasts made by summation and basic current (labeled "flow") methods during February and March 1958. Bars indicate correlation between predicted and observed height anomalies at the indicated latitude. Horizontal lines show average of all forecasts at that latitude. Arrows indicate change in score from flow method to new flow method. See text for detailed explanation.

forecast interval. This abbreviated basic current method produces improvements, as seen from verifications shown in figure 6. Here two months of available verifications for summation and basic current charts are shown in terms of the correlation of the profile of predicted vs. observed departures from normal at latitudes 60° N. and 40° N. The changes in individual forecast scores from inserting the 30-day approximation instead of the normal are represented by arrows superimposed on the open bars. Average performances are shown by horizontal dashed lines.

While the abbreviated basic current method was about the same as the summation chart at 60° N. it was inferior at 40° N. More recent verifications show similar results, although newly introduced short-range models [6] appear to have improved the summation chart.

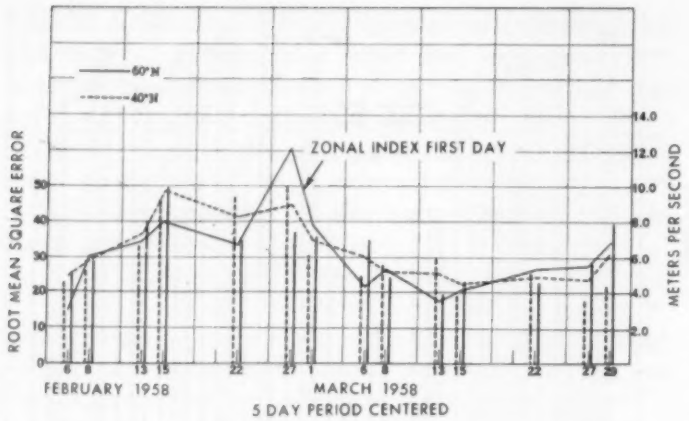

FIGURE 7.—Vertical bars show root-mean-square errors (in tens of feet, scale at left) of summation method predictions at 60° N. and 40° N. Irregular dashed line connects average RMSE for both latitudes. Thin line shows Western Hemisphere zonal index from 0° westward to 180° on initial day of prediction (in m.p.s., scale at right).

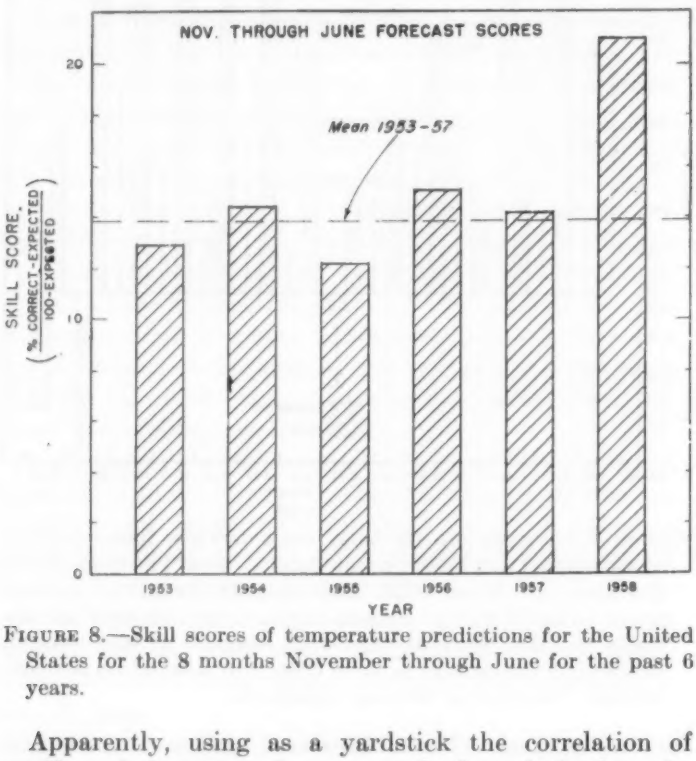

FIGURE 8.—Skill scores of temperature predictions for the United States for the 8 months November through June for the past 6 years.

Apparently, using as a yardstick the correlation of profiles of departure from normal along latitudes, the summation method of prognosis for a 5-day mean centered 2 days in advance is somewhat superior to the abbreviated basic current method. For a mean centered 4 days in advance the scores, while positive, are so low as to leave much room for improvement.

In view of these results work is currently proceeding to improve the prognoses by (1) applying the basic current method in the complete manner (i.e., by uncoupling the free perturbation from the 30-day mean basic current rather than from the normal), and (2) by introducing a more sophisticated model which also incorporates the philosophy of the basic current method.

In spite of the verification statistics cited, a subjective appraisal of routinely prepared numerical prognoses by both methods indicates that both have something to contribute to the final forecast. The choice of reliable features of each, while not easy, can be assisted by other factors not considered in the models—such things as the existing thermal fields, concepts of cyclone development, etc. In any event, the numerically produced charts form a fairly solid point of departure for the circulation prognosis, and, as will be seen below, can be translated objectively into a fairly skillful temperature prediction.

Before treating objective methods of temperature prediction, an interesting by-product of the verification shall be mentioned. The root-mean-square errors at latitudes 40°N. and 60°N. of the summation forecasts verified in February and March 1958 are shown in figure 7. Plotted as a solid line on this figure is the 700-mb. zonal index for the day on which the forecast was made. Apparently the predictions are in general better at times of low index than high, a conclusion which at first glance comes as a surprise. However, it must be borne in mind that low index states are frequently characterized by cellular features with isotherms and contours in mid-troposphere in phase—states more barotropic than those of high index in which meridional temperature gradients are steep and sudden baroclinic developments are frequent.

6. OBJECTIVE TEMPERATURE PREDICTIONS

Once a mean circulation pattern has been determined it is possible to estimate from it the accompanying departures from normal of surface temperature. A detailed discussion of this problem will be found in references [5] and [7]. The essence of the presently used technique depends upon the position and intensity of key centers of height anomaly as determined by subtracting the appropriate normal contour pattern from the predicted. The key centers naturally vary from station to station and from one season to another, but in general a large part of the variability of surface temperature of 5-day means is accounted for by the departure from normal of mean mid-tropospheric height near the station and also, equally or more important, at a point a few thousand miles or more to the northwest of the station—removed by about one-half the length of a planetary wave. The location of the centers is determined by computing correlation fields between each station's temperature departure and the contemporary height anomalies—a procedure greatly facilitated by the use of high-speed computing machines. The latest studies in this direction have just been reported by Klein and Lewis [8].

While the mid-tropospheric height pattern accounts for a reasonably high (about 50 percent) proportion of sea level temperature variability, it obviously cannot uniquely specify the field, for it is probable that both the initial air mass distribution and the character of the earth's surface (e.g., presence or absence of snow cover) must be taken into consideration. The *net* influence of these complex factors is to some extent reflected in errors made by the initial objective estimates in a given case. Hence, if one is able to obtain the error field of objective estimates

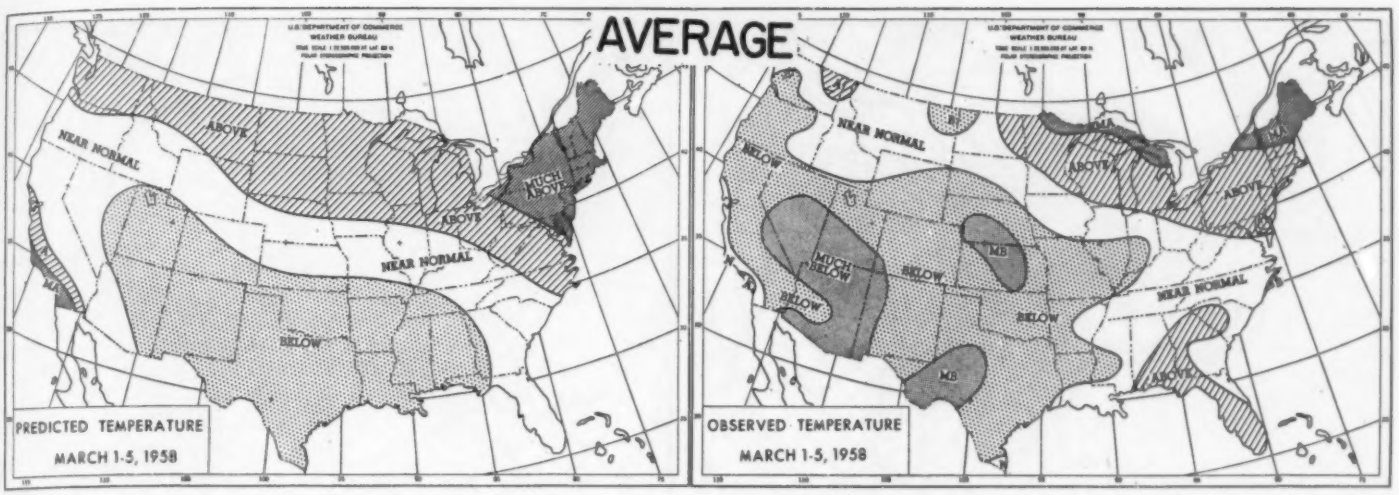

FIGURE 9.—Example of the success of an average temperature prediction made during the period November 1957 through June 1958, following the introduction of numerical techniques.

for a period close enough to the forecast period so that the changes in mean flow pattern are slight, he may reasonably suppose that the *errors* remain the same. Therefore, the initial error may be used as a correction term to the subsequent objective estimate based on the contour pattern alone. Now it will be remembered that a 5-day mean chart centered on forecast day is available. Likewise, it is possible to prepare a centered 5-day surface temperature estimate by making use of official short-range forecasts of maximum and minimum temperatures for the following 2 days in addition to 3 days of known values. This field of temperature anomaly is then compared with the objective estimate afforded by the trend map contour pattern and the "error" determined. This error is then applied as a corrective term to objective estimates made on the numerical prognosis. So far, this technique has been applied only to the summation chart. The results have been gratifying in that this method produces an anomaly forecast which, even when taken as a forecast for the 5-day period 2 to 7 days in advance, gives temperature scores equal to those obtained using all available tools in a subjective fashion during the pre-numerical period 1953–1957! In other words, an objective base has been established for temperature just as for contour pattern and this forms a good point of departure.

Because of the obvious oversimplification of the underlying objective method, it is possible to improve on this objective base, so that the net improvement in temperature scores over the 1953–57 period has been dramatic. The extent of this improvement is indicated in figure 8 where the averages of temperature scores for the 8-month period November through June for the last 6 years are presented. (November 1957 was the month of institution of the new forecast tools described in this paper—and also the month of discard of older outmoded techniques.) The scores consider only the percentage of the United States predicted in the exact temperature class out of five categories—above, near, and below normal and much above and much below normal. The first three named classes have a probability of occurrence of ⅓ and the latter two ⅙. The roughly 50 percent increase in scores in the post-numerical period (1958) over the preceding 5 years is striking. A statistical analysis of the monthly averages of scores entering into figure 8 indicates that the 1958 scores *are* higher than the earlier scores at a level of significance of 3 in 10,000! Some idea of the correspondence of such forecasts with observed conditions is afforded by an example (fig. 9) selected only because it fell on the average 1958 score. Of course, there are large areas of imperfection, but taken as a whole, predictions of this sort are economically valuable. Further demonstrating the skill of these forecasts is table 1 which shows the percent

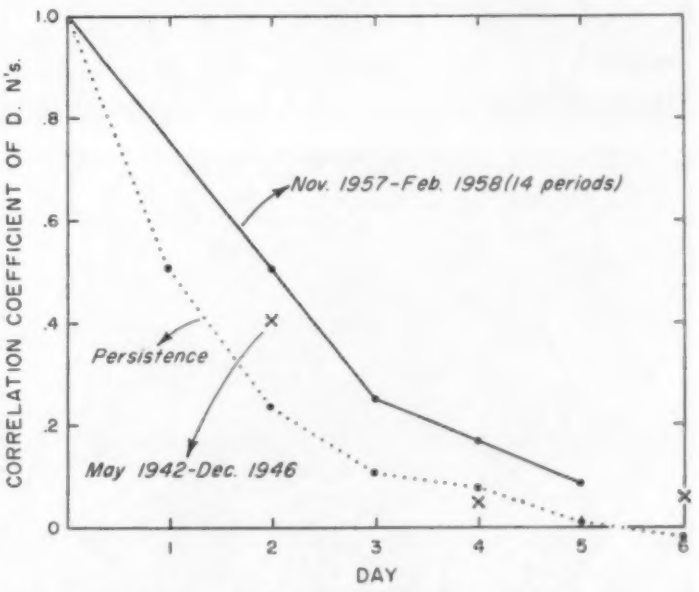

FIGURE 10.—Verification of prognostic daily sea level pressure maps for North America for 14 forecasts made from November 1957 to February 1958 (solid) and persistence scores from an earlier 8-month period (dotted). Crosses give scores for an earlier 4-year period. Ordinate is averaged correlation between predicted and observed pressure anomalies, and abscissa is number of days after forecast day.

494192—59——2

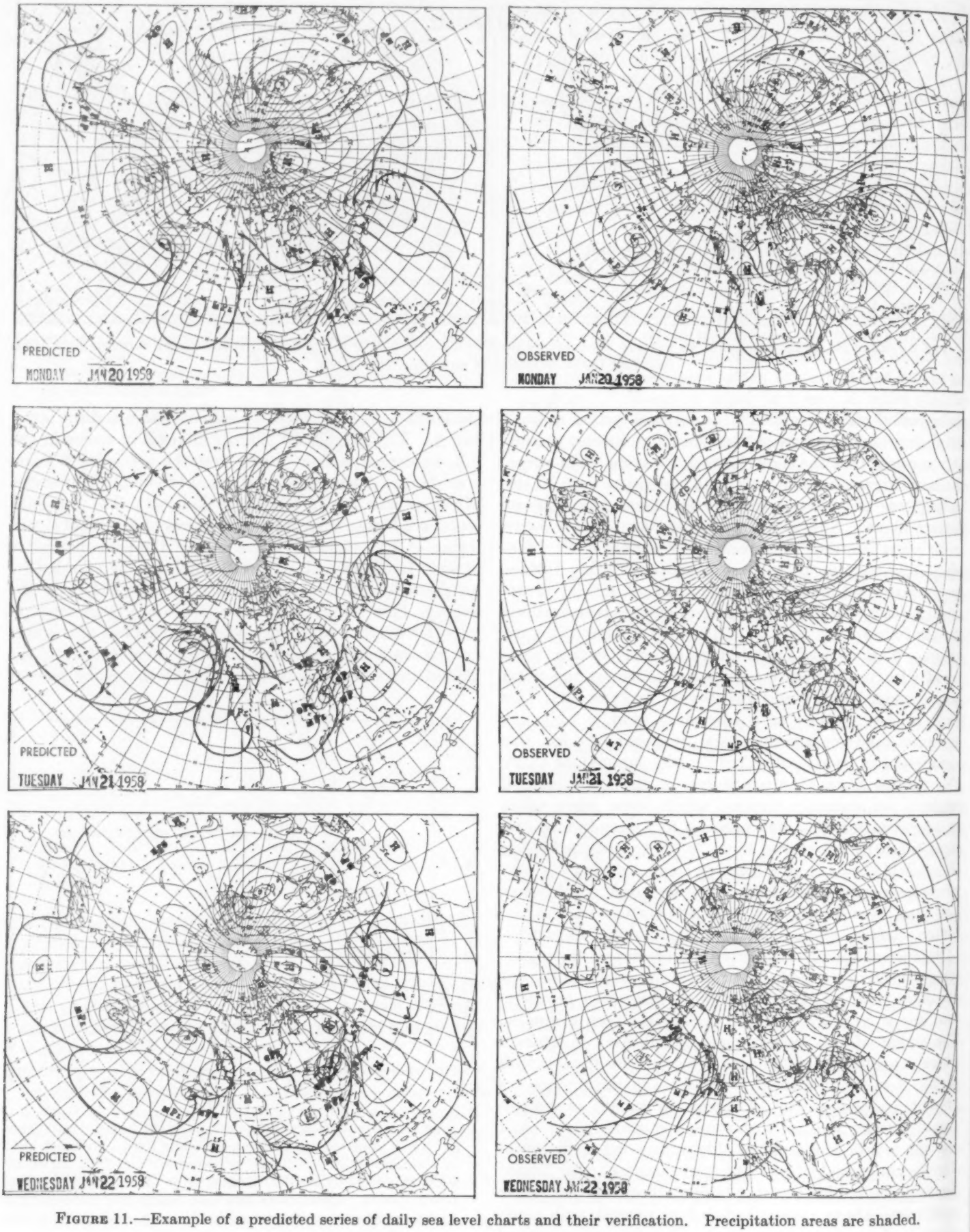

FIGURE 11.—Example of a predicted series of daily sea level charts and their verification. Precipitation areas are shaded.

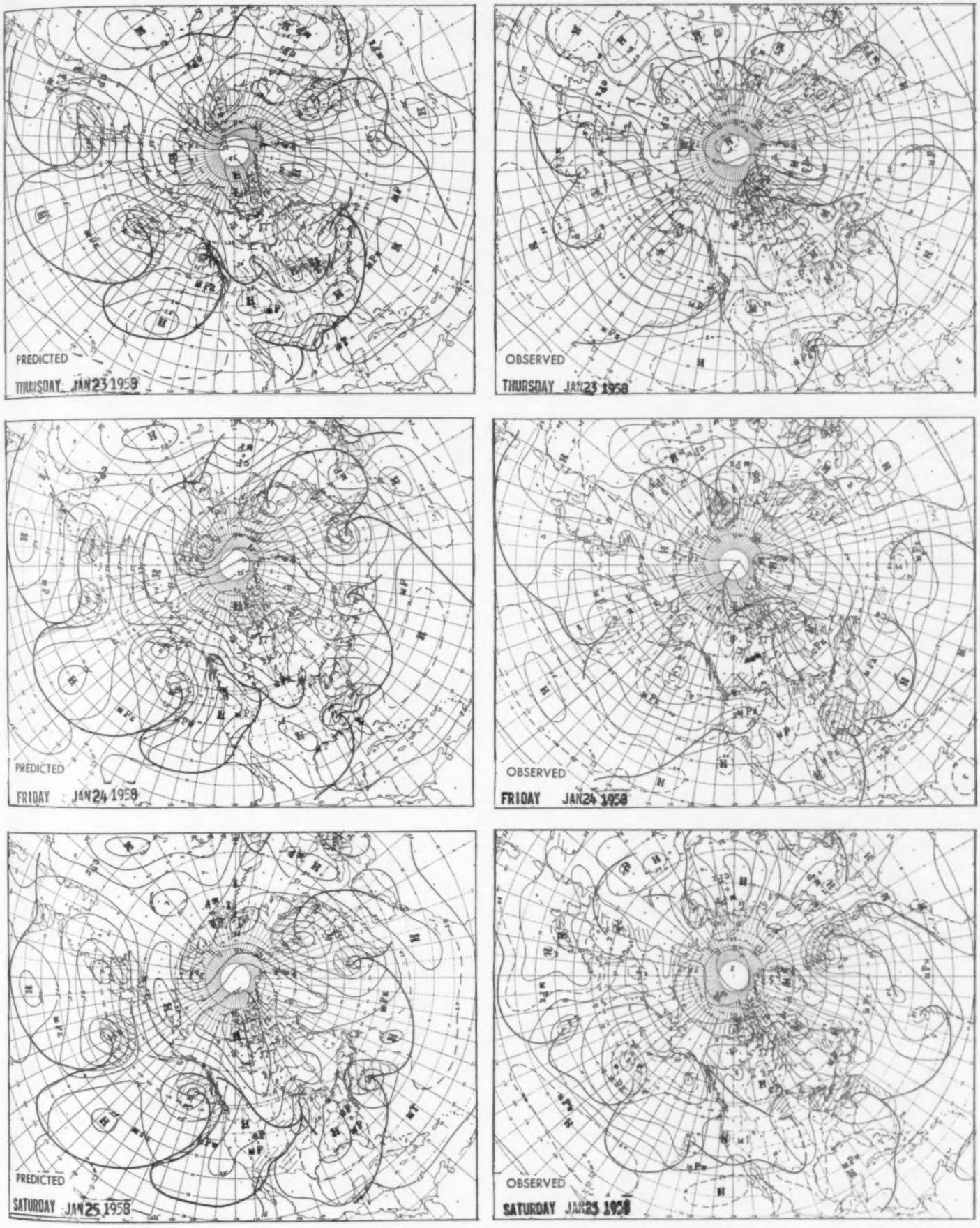

FIGURE 11.—Continued.

TABLE 1.—*Probability of obtaining temperature categories (percent).*

Observed	Forecast				
	MB	B	N	A	MA
MB	44.6	16.3	5.9	2.6	0.6
B	30.6	40.1	26.4	13.0	6.4
N	11.1	22.7	28.5	23.1	13.0
A	4.5	17.3	30.4	40.7	38.4
MA	0.3	3.6	8.8	20.6	41.6

of the time for the country as a whole each forecast class occurred or was observed in another category.

For example, when much below normal was predicted the observed category was much below normal 44.6 percent of the time and below normal 39.6 percent of the time. Note the almost negligible error of four classes; i.e., much below forecast and much above normal observed or vice versa.

It has been suggested that the high 1958 scores indicate that the temperature patterns were easier to predict because of more persistence than normal during the 8-month period. Actually, statistics show that (1) the period as a whole was certainly no more persistent from one 5-day period to another (and perhaps was less persistent) than during the past 5 years, and (2) earlier 5-day forecast scores show no correlation with persistence scores. It seems difficult to attribute the increase in skill to anything other than increased objectivity in which numerical contour predictions play a large role.

While precipitation forecasts were slightly improved over the averages of the past 5 years, no such significance as with temperature is indicated. Although this is a puzzling and disconcerting circumstance, the following facts undoubtedly play a part:

1. No objective methods have been developed for satisfactorily interpreting mean contour patterns in terms of precipitation.

2. Precipitation, a discontinuous element unlike temperature, is probably less related to mean contour patterns than temperature.

3. 5-day precipitation forecasts involve more degrees of freedom (subjectivity) on the part of the forecaster, and are often overly influenced by short period "indications" which may turn out to be erroneous. At any rate, the lack of comparable success in improving precipitation forecasts points up this problem as one of high priority.

7. THE CONSTITUENT DAYS OF THE FORECAST PERIOD

One of the most difficult tasks in the 5-day forecast routine is the preparation of a prognostic series of six sea level maps—the pressure distribution, the fronts, air masses, and precipitation. The methods for drawing these charts are far from objective, although there are broad guide lines:

1. The series of maps must possess a logical evolution.

2. The forecaster is tied down to the last observed map and to short period prognoses, and obtains some assistance from the daily numerical prognoses up to 72 hours in advance.

3. The steering and development of synoptic-scale systems must be consistent with the evolving mean patterns predicted (steering, etc.).

4. The daily series must be consistent with the broad-scale temperature field predicted.

While these constraints still leave considerable flexibility, the new methods have resulted in some improvement in the ability to prognosticate maps out to 6 days in advance. Some evidence for this is shown in figure 10 where the departures from normal of predicted and observed pressure patterns over North America are correlated for days 1 to 6 after forecast day. The scores for 14 weeks of forecasts (taking one forecast series a week) are shown along with persistence scores (computed from an earlier 8-month period) and also with earlier attempts over a 4-year period shown by crosses. Perhaps a better idea of the possibilities of such predictions is obtained from one of the better series, reproduced together with the observed charts in figure 11. Note the proper development and course of both major cyclones affecting the United States—the Texas wave at the first of the period and the wave from southern California moving eastward and then northeastward.

REFERENCES

1. J. Namias, *Extended Forecasting by Mean Circulation Methods*, U.S. Weather Bureau, Washington, D.C., Feb. 1947, 89 pp.
2. J. Namias, "Progress in Objectivization and Automation of Extended Forecasting," *Transactions of the New York Academy of Sciences*, Ser. II, vol. 19, No. 6, Apr. 1957, pp. 581–592.
3. C. R. Dunn, "Automatic Incorporation of Numerical Short-Range Prognoses in 5-day Circulation Forecasts," *Monthly Weather Review*, vol. 86, No. 2, Feb. 1958, pp. 45–52.
4. P. F. Clapp, "Some Considerations Involved in Preparing Long-Range Forecasts by Numerical Methods," *Journal of Meteorology*, vol. 13, No. 4, Aug. 1956, pp. 341–350.
5. J. Namias, "Thirty-Day Forecasting: A Review of a Ten Year Experiment," *Meteorological Monographs*, vol. 2, No. 6, American Meteorological Society, July 1953, 83 pp.
6. G. P. Cressman, "Barotropic Divergence and Very Long Atmospheric Waves," *Monthly Weather Review*, vol. 86, No. 8, Aug. 1958, pp. 293–297.
7. H. F. Hawkins, Jr. and D. E. Martin, "Forecasting the Weather: The Relationship of Temperature and Precipitation over the United States to the Circulation Aloft," *Weatherwise*, vol. 3, No. 1, pp. 16–19, No. 2, pp. 40–43, No. 3, pp. 65–67, No. 4, pp. 89–92, No. 5, pp. 113–116, No. 6, pp. 138–141, 1957.
8. W. H. Klein and B. M. Lewis, "Numerical Prediction of Five-Day Mean Temperature during Winter," paper presented at Program of the National Conference on Practical Problems of Modern Meteorology, American Meteorological Society, Denver, Colo., Sept. 22–24, 1958.
9. P. M. Wolff, "The Error in Numerical Forecasts Due to Retrogression of Ultra-Long Waves," *Monthly Weather Review*, vol. 86, No. 7, July 1958, pp. 245–250.

THE HURRICANE SEASON OF 1958

Staff, Weather Bureau Office, Miami, Fla.

1. GENERAL SUMMARY

Ten tropical cyclones, seven of full hurricane intensity, developed in Atlantic waters during the hurricane season of 1958. This number compares with an annual average of 10 storms for the past 20 years, 9 for the past 40 years, and 8 for the last 75 years. Except for a short-lived minor tropical storm in the western Gulf of Mexico in mid-June, conditions over the tropical Atlantic remained stable until the second week in August. Thereafter conditions were very active until the last hurricane of the season, Janice, formed during the first week in October.

In contrast to the concentration of most of the activity in the Gulf of Mexico during 1957, major tropical storm activity shifted to the western Atlantic in 1958 (fig. 1). Only two storms, both lacking hurricane intensity, occurred in the Gulf of Mexico and storm activity affected only the extreme northern Caribbean. While no hurricane center reached the coastline of the United States, one—Helene—caused hurricane winds of major intensity on the North Carolina coast. Ella crossed the Texas coast near Corpus Christi with less than hurricane winds and Alma, Ella, Daisy, and Janice caused fringe squalls at one point or another along the United States coastline. Only two deaths in the United States were directly attributable to tropical cyclones and total damage was estimated at between 11 and 12 million dollars, mostly in the Carolinas in connection with Helene. In the Antilles, tropical cyclones killed 6 or 7 persons in Cuba, 35 or more in Haiti, 3 in Puerto Rico, and 2 in the Bahamas. Total damage outside the United States has been difficult to determine but is estimated at several million dollars, mostly in Hispaniola, Cuba, Jamaica, and Puerto Rico.

Following the formation of tropical storm Alma on June 14, a broad trough developed along the Atlantic coast and persisted throughout the remainder of the month. The accompanying westerlies at comparatively low latitudes are thought to be inimical to tropical storm formation. In July, intense blocking over the Atlantic continued to depress the westerlies [5], and the circulation was highly unfavorable for tropical storms in this area [2] [9].

Tropical storm activity was high during the last two decades of August and the mean circulation for the month as described by Woffinden [16] showed a reasonable similarity to the composite chart developed by Ballenzweig [3] favorable for tropical storm formation in the vicinity of the Lesser Antilles. The somewhat greater than normal amplitude of the trough along the Atlantic coast permitted Becky, Cleo, and Daisy to recurve over the western Atlantic. However, Ella, which formed at a low latitude just east of the Windward Islands at the close of the month, remained in the easterlies when the east coast trough was replaced by a ridge during the first few days of September

494192—59——3

2. INDIVIDUAL TROPICAL CYCLONES

Alma, June 14–15.—Tropical storm Alma developed in an easterly wave that was first detected in the central Caribbean on June 9 and 10. Abnormally heavy shower activity was occurring on these dates over the western and central Caribbean Sea and northward across Cuba into the Bahamas. There was some evidence of a closed circulation at 1800 GMT on the 10th near latitude 15° N., longitude 78° W. On succeeding maps, a weak circulation was observed and heavy rains continued over the northwestern Caribbean and eventually spread into Central America.

The weak circulation moved westward into the Yucatan Peninsula-Guatemala area on the 12th and into the Gulf of Campeche on the 13th. The disturbance continued northwestward along and off the Mexican coast and developed into tropical storm Alma about midday on the 14th some 150 miles east of Tampico.

At 2100 GMT on the 14th, the Motor Vessel *Mada*, at latitude 22.8° N., longitude 95.6° W., reported a south-southeast wind of 45 m.p.h., pressure of 997 mb., and mountainous seas. At 0500 GMT on the 15th, this ship, located about 100 miles northwest of Carmen, Mexico, was encountering south-southwest winds of 35 to 40 m.p.h., pressure of 1006 mb., and very rough seas.

A Navy reconnaissance aircraft was dispatched to the storm on the 14th. However, the center had apparently moved inland and broken up before the aircraft reached the area. The plane reported maximum winds of 22 knots and minimum pressure of 1008 mb., and observed no radar echoes.

Highest winds reported were 45 to 50 m.p.h. from the MV *Mada* on the 14th, 50 knots from a Coast Guard aircraft 50 miles south of Port Isabel, Tex., at 0800 CST and 40 to 45 m.p.h. at south Padre Island, Tex., at 1000 CST on the 15th. Heavy rains fell over the hill country to the west of San Antonio, generally averaging 7 to 10 inches with some amounts reported as high as 20 inches a little to the west of Medina, Tex.

Very little damage was caused by wind and tides associated with this storm and major damage to crops and property was associated with floods caused by the attendant rains. One death by drowning occurred in the Galveston area during passage of the storm.

Becky, August 11–15.—Becky, the second tropical storm of the season, was first positively identified on August 11. A series of reports from the ship *Industrious* indicated the storm's existence near latitude 18° N., longitude 45° W., halfway between Puerto Rico and the Cape Verde

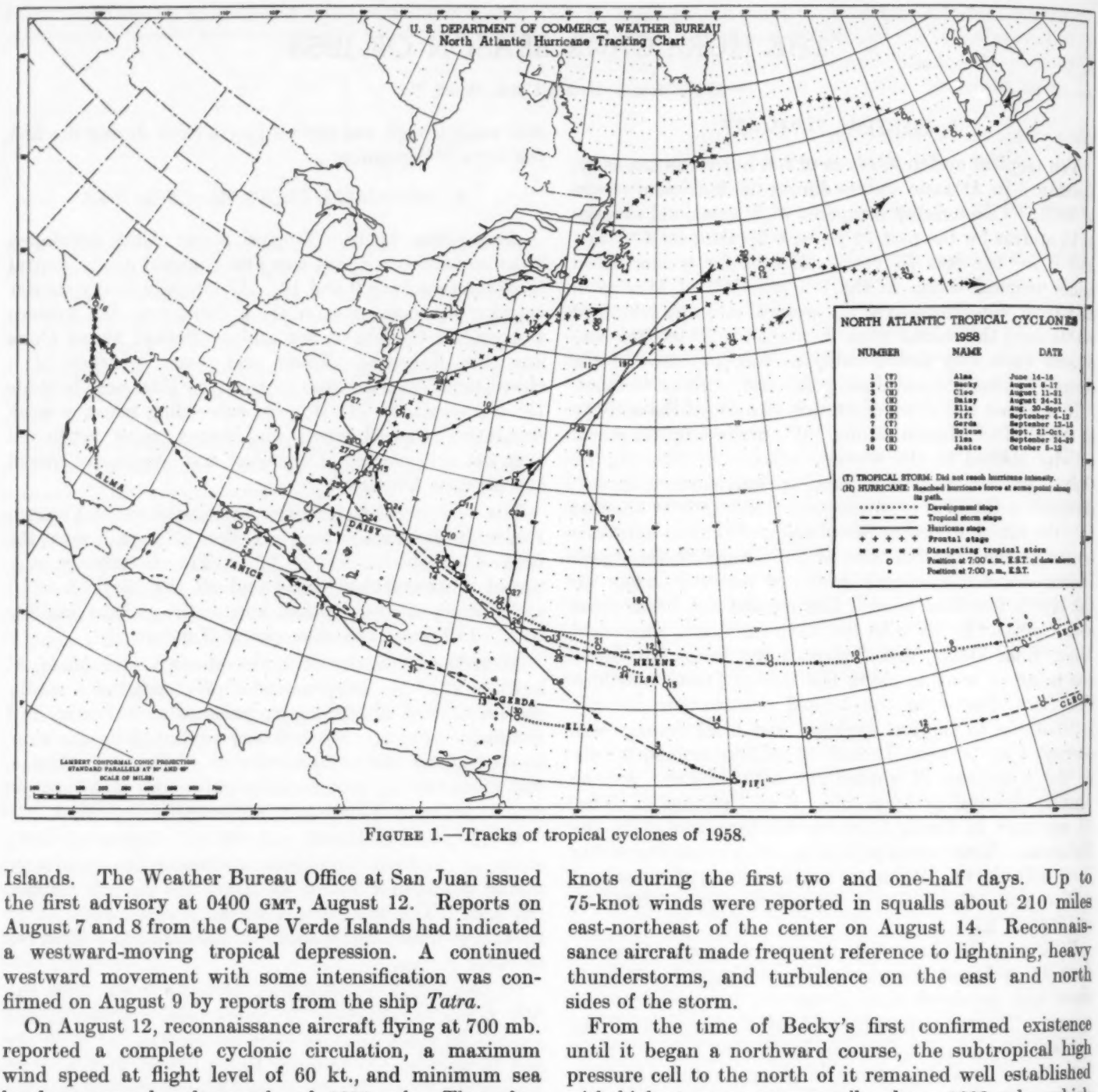

FIGURE 1.—Tracks of tropical cyclones of 1958.

Islands. The Weather Bureau Office at San Juan issued the first advisory at 0400 GMT, August 12. Reports on August 7 and 8 from the Cape Verde Islands had indicated a westward-moving tropical depression. A continued westward movement with some intensification was confirmed on August 9 by reports from the ship *Tatra*.

On August 12, reconnaissance aircraft flying at 700 mb. reported a complete cyclonic circulation, a maximum wind speed at flight level of 60 kt., and minimum sea level pressure by dropsonde of 1006 mb. Thereafter Becky continued on a westward to west-northwestward course passing about 290 miles northeast of Puerto Rico at the nearest point. Then the storm began to recurve broadly to the northwest and north and on the 16th toward the northeast around the western periphery of the subtropical high pressure area.

The minimum pressure of 1006 mb. reported by the first reconnaissance into Becky was as low as any succeeding central pressure report while the storm was under close surveillance by aircraft. The area of gale winds gradually increased in size but remained mostly north and east of the center. Maximum reported winds increased very slowly from about 35 knots up to an estimated 55 or 60 knots during the first two and one-half days. Up to 75-knot winds were reported in squalls about 210 miles east-northeast of the center on August 14. Reconnaissance aircraft made frequent reference to lightning, heavy thunderstorms, and turbulence on the east and north sides of the storm.

From the time of Becky's first confirmed existence until it began a northward course, the subtropical high pressure cell to the north of it remained well established with highest pressures generally above 1023 mb., which is about normal for the month of August. The average speed of the storm during the time it was under close surveillance by aircraft was about 20 knots. The reason for lack of intensification is not known, but an old empirical forecasting rule states that movement of 20 m.p.h. or more is unfavorable for intensification.

Reconnaissance aircraft and ship reports in the region early on August 15 indicated that Becky had degenerated into an area of squalls with little if any cyclonic pattern. However, late on the 16th, after Becky moved into an old frontal zone and became extratropical, rapid intensification took place, with one ship for a short time reporting hurricane-force winds.

Cleo, August 11–21.—The existence of hurricane Cleo was first suspected on August 11 based on reports from the Cape Verde Islands. Weather conditions and 24-hour surface pressure changes indicated that a fairly well developed easterly wave was passing through the area. Judging from surface and low-level wind reports, any possible circulation associated with the wave must have passed well to the south of the Cape Verdes. On August 12 and 13, reports from several ships on the outer periphery of the suspected storm indicated that a large cyclonic circulation was developing; however, none was close enough to even estimate the location or intensity of Cleo.

On August 14, an Air Force reconnaissance aircraft located hurricane Cleo at 1820 GMT near latitude 14.7° N., longitude 47.1° W. By this time, Cleo had developed into a very intense storm with lowest pressure of 962 mb. and winds estimated at 146 m.p.h. On the basis of fringe data, it is believed the storm was moving at about 21 m.p.h. from August 11 to 13; however, on August 14, the time of first aircraft penetration, the storm undoubtedly was decelerating as it began turning northward under the influence of a weak upper trough near longitude 50° W.

On the 16th, the storm turned toward the north-northwest and gradually increased its forward speed. Recurvature south of latitude 20° N. during August is very unusual and in this case was never completed (fig. 1). The trough that influenced Cleo was naturally weak at this latitude and it soon collapsed from the outflow from the hurricane. Again, under the control of a large warm anticyclone over the eastern Atlantic, Cleo resumed a more northwestward course until the 18th.

An active short wave which passed through the Northeastern States on the 16th and 17th began to affect Cleo by the 18th as the storm slowed to about 14 m.p.h. and gradually turned to a northward course. On the 19th Cleo accelerated to around 29 m.p.h. on a northeastward and later a more eastward course until becoming extratropical on the 20th.

Although the highest winds were reported by reconnaissance aircraft on first penetration, the hurricane did not reach maximum intensity (based on pressure and radar pattern) until the 15th when a dropsonde in the eye at 2030 GMT indicated a sea level pressure of 947 mb. (See fig. 2 for minimum pressure as reported by the reconnaissance aircraft.) It is probable that the aircraft did not find the area of maximum winds on this day so it still may be assumed that this was the date of maximum intensity.

Fortunately hurricane Cleo remained at sea throughout its history and no reports were received of any severe damage to shipping or loss of life despite the storm's traversal of the principal transatlantic shipping lanes. An interesting account of a vessel passing through the eye of Cleo can be found in the November *Mariners Weather Log* [15].

Daisy, August 24–31.—Hurricane Daisy formed in a strong easterly wave which passed through the Lesser

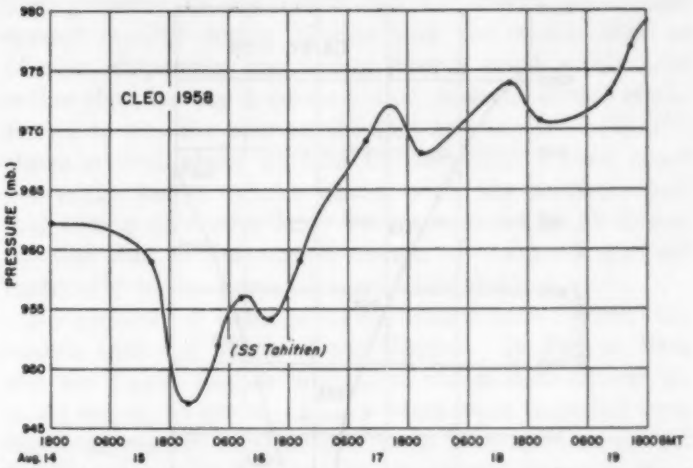

FIGURE 2.—Minimum sea level pressures in hurricane Cleo, reported by reconnaissance aircraft, Aug. 14–19, 1958.

Antilles during August 20–21. There was little indication of intensification, however, until the 23d, when the wave passed through the Windward Passage and a definite increase in its amplitude was evident. A vortex developed on the 24th and reconnaissance aircraft located an eye just north of the central Bahamas with maximum winds of about 55 m.p.h. and a central pressure of 1002 mb. The first advisory was issued at 0100 GMT August 25.

Hurricane Daisy moved very slowly north-northwestward during the 25th and the morning of the 26th. The hurricane recurved initially near latitude 28° N. on the 26th, and its forward speed accelerated. The center passed about 75 miles east of Hatteras on the 28th moving about 20 m.p.h. It then passed about 70 miles southeast of Nantucket, moving east-northeastward about 25 m.p.h. on a second recurve. Neither the North Carolina nor the New England coasts, however, felt much effect of this severe hurricane. The strongest wind at Hatteras was NNW 27 m.p.h., with gusts to 36; Block Island reported 40 m.p.h., with gusts to 45. A Texas Tower, 120 miles east of Cape Cod, experienced a sustained wind of 69 m.p.h. with gusts to 87. There was no loss of life or appreciable property damage in the United States from Daisy.

At the time Daisy formed, the westerlies over the United States were far south of their normal position for the second half of August. At 500 mb. on the 24th, westerly winds extended southward into the Gulf of Mexico. A similar pattern had prevailed during most of the month, a circulation feature which steered Daisy away from the coastal areas of the United States. While the hurricane was forming, however, the subtropical ridge over the western Atlantic at 500 mb. was north of Bermuda. During the first two days of Daisy's history, a weak extension of this ridge separated the hurricane from the westerly flow just to the north. While the storm was small and relatively weak, it was unable to break through this ridge, which partly explains the very slow movement prior to first recurvature. Deepening of the storm took place simultaneously with the passage of a strong short-wave trough through the central portions of

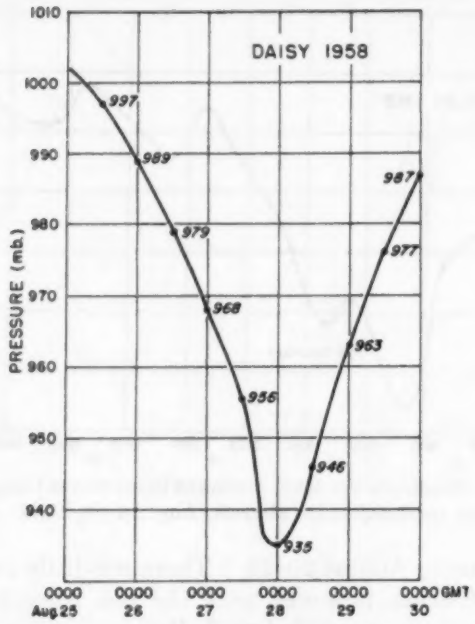

FIGURE 3.—Minimum sea level pressures in hurricane Daisy, Aug. 25–30, 1958.

the United States. The intensification of the storm increased the internal forces which tend to drive a hurricane northward at the same time that the approach of the short wave weakened the already weak ridge north of Daisy. This combination permitted the subsequent rapid northward progress of the storm.

The central pressure dropped steadily from 1002 mb. at the time the first advisory was issued to a minimum of 935 mb. (fig. 3). Thereafter the pressure rose and by the 30th the central pressure was 987 mb. The strongest winds, reported by aircraft, were about 115 m.p.h. It appears likely, however, that the aircraft did not encounter the actual maximum winds within the storm, inasmuch as Fletcher's [6] formula* would indicate a maximum wind in excess of 150 m.p.h. at the time of minimum pressure.

The intensification of the storm is not easy to explain. The initial deepening on the 24th took place while the low-level disturbance was situated under a small 200-mb. anticyclone, a situation postulated by Riehl [10] as favorable for deepening. At the same time there was a large cyclonic vortex (cold) south of Bermuda. On the 25th the small warm anticyclone over the storm disappeared, although the low-level vortex was still under a weak anticyclonic flow. The presence of the cold vortex to the east in all probability inhibited the growth of the high-level anticyclone typically associated with developing hurricanes and the absence of a well developed High at 200 mb. may have retarded Daisy's intensification.

On the 26th, however, the cold 200-mb. Low weakened and moved northward to the west of Bermuda. At the same time the 200-mb. anticyclone in the area of the storm began to increase in size and intensity, and a well-developed trough approached the storm area from the west. Although the size of the 200-mb. High was much smaller, the overall situation closely resembled that described by Miller [7] as being most favorable for maximum intensification. During the 24-hour period beginning at 2100 GMT on the 26th the central pressure in Daisy fell about 40 mb. That intensification was also accompanied by growth of the 200-mb. anticyclone is evidenced by the fact that during a comparable 24-hour period beginning at 0000 GMT on the 27th, the size of the high-level anticyclone more than quadrupled.

Daisy was within range of land-based radar during much of the time it retained its tropical nature. Various radar installations all the way from Miami, Fla., to New England had Daisy's eye under surveillance at one time or another. The Weather Bureau station at Hatteras was particularly effective in tracking the storm during the period when the forecast problem was most acute.

The forecasts on this hurricane at the critical times when it posed a threat to coastal areas were excellent. The turn to a more northerly course while the first recurving was in progress was forecast. The recurving south of the New England coast was also forecast because it was indicated by all except one of the techniques for forecasting movement now in general use. However, hurricane warnings were eventually issued for the area from Provincetown, Mass., to Block Island, R.I., when it appeared that the center would come close to Nantucket Island. This hurricane warning was fully warranted in view of the normal error in forecasting the path of any storm continually changing direction and speed of movement with time.

Ella, August 30–September 6.—First indication of Ella was a fairly active easterly wave in the vicinity of longitude 50° W. on August 29. Reconnaissance aircraft on a routine flight east of the Windward and Leeward Islands reported a wind shift and above average shower activity, but no indication of a cyclonic circulation. The wave moved through the islands during the 30th causing heavy rains and winds of 35 to 40 m.p.h. and lowest pressure around 1010 mb. Reconnaissance aircraft located a center by radar at latitude 16.3° N., longitude 64.7° W., during the evening of the 30th (local time) and the first advisory was issued on tropical storm Ella. Highest winds were estimated at 55 to 60 m.p.h. near the center and the minimum pressure had dropped to about 1009 mb. Advice to small craft and residents of the islands from Puerto Rico eastward and southward had been given previously by bulletins from the San Juan Weather Bureau Office.

The storm intensified rapidly as it moved westward at about 18 m.p.h. in the eastern Caribbean and by 1600 GMT of the 31st winds were estimated by aircraft at 85 m.p.h., increasing to 110 m.p.h. by 0400 GMT of September 1. The course had changed to the west-northwest during the day, as the center skirted along and just south of the Dominican Republic and Haitian coasts, causing torrential rains and considerable damage on the southern slopes of the mountains. It was thought that the hurricane passed over the southwestern peninsula of Haiti, however, since the original intensity was maintained until it encountered

*There is some evidence that Fletcher's formula is more nearly indicative of gusts than of sustained wind (c.f., Myers [8]).

the Sierra Maestra in eastern Cuba, the center of the hurricane may have skirted along the immediate south coast of Haiti. In fact, reports from the Haitian Meteorological Service indicate the hurricane followed a path parallel to the peninsula.

Reconnaissance aircraft on September 1 reported winds of 115 m.p.h. and lowest pressure of 989 mb. while the center was over the Caribbean Sea between Jamaica, Haiti, and eastern Cuba. The center passed inland over the Sierra Maestra in Oriente Province in eastern Cuba a short distance west of Santiago and the storm weakened below hurricane strength. It never regained hurricane force in its long path along the southern coast of Cuba, across the Gulf of Mexico, to the lower Texas coast.

As the storm moved west-northwestward along the southern coast of Cuba, a building high pressure system was moving into the Atlantic States, and consequently gale warnings were hoisted on the lower east coast of Florida and in the Florida Keys, because of the anticipated increase of pressure gradient caused by interaction between the two systems. Highest winds had dropped to 40 to 50 m.p.h. in squalls but the area of squalls and rather heavy rains extended across Cuba into the southern Bahamas and the Florida Straits and Keys. The center crossed extreme western Cuba on the 3rd, moving toward the west-northwest at 12 m.p.h. A west-northwestward course was continued at 12 to 15 m.p.h. across the Gulf of Mexico, with highest winds generally about 50 m.p.h.; however, Grand Isle, La., reported gusts to 75 m.p.h. during a squall on the morning of the 5th, and the SS *Jean Lykes* reported a wind of 55 knots near latitude 24.5°N., longitude 85.5°W. late on the 3d. Highest winds on the Texas and Louisiana coasts were generally around 40 m.p.h. with tides 2 to 4 feet above normal.

As the easterly wave in which Ella was spawned moved into the eastern Caribbean, deep easterlies existed to elevations beyond 500 mb. and at 200 mb. a vigorous anticyclone appeared, with a weak cyclone at this height 600–800 miles to the northwest. Rapid intensification occurred during the night of the 30th and on the 31st. The high-level anticyclone was in a position to give rapid outflow to the hurricane, a necessity for deepening according to Riehl [10], but became steadily less so after the storm entered the Gulf. Riehl [11], in studying a number of the tropical cyclones during the past several years, has found the problem of hurricane formation and intensification much more complex than earlier thought. There are apparently additional constraints not yet known or defined.

Several factors may have contributed to the nondeepening of Ella after it was weakened by passage through the Sierra Maestra of Cuba: (1) The storm lost, to some extent, its high-level anticyclone which seems to be a necessity for deepening and maintaining strength. The vortex was deep vertically even after passage into the Gulf. (2) The storm moved quite a bit faster during the previous and succeeding 48-hour periods than while passing south of Cuba. The bad weather pattern, caused by the combination of growing surface high pressure to the north and the storm circulation, spread rapidly across Florida and the entire Gulf of Mexico, dispersing the energy over a considerable area rather than having it concentrated near the center of the storm, as was the case on the 31st and the 1st. (3) The storm moved along parallel to the south Cuban coast the entire length of the island, with the northern half and strong side over land for approximately 48 hours. Friction due to the rugged terrain of Cuba contributed materially to the prevention of intensification there.

No reports of damage have been received from the islands east and south of the Virgins. In Puerto Rico and the Virgin Islands, maximum winds were around 40 to 50 m.p.h. in gusts. Heavy rains were recorded over the southwestern sections of Puerto Rico and some local flooding occurred, but damage in general was minor.

Heavy rains and floods caused damage estimated at $100,000 in the Dominican Republic, most of which occurred in the southwestern portion. No fatalities were reported there.

Torrential rains along the entire southern portion of Haiti caused considerable flooding. Thirty persons were reported drowned near Aux Cayes, probably due to a flash flood in a small rivulet. There were no casualties or losses of property in Jérémie or in general in any of the towns and villages located in the northern half of the southwestern Haiti peninsula; however, three persons were reported missing. After the passage of the hurricane, thousands of people along the southern coast were without shelter because of damaged or unroofed homes. Although no monetary estimate of the damage has been received, it would appear to be considerable.

In Cuba, six to eight persons were drowned due to floods resulting from torrential rains. Total damage to property on the island was estimated at $100,000.

Damage was minor in extreme southern Florida and the Florida Keys, where strong to gale force winds and rather heavy rains occurred. A vessel, the *Erikboye*, was disabled southeast of Miami due to the storm and towed in by the Coast Guard.

Very little damage was reported in Texas as a result of Ella. Rainfall was spotty but quite heavy in some localities. Galveston Airport measured 13.60 inches in three and a half days, with 8.44 inches occurring on September 7. A shrimp trawler was lost on the Galveston Jetty on the night of September 3. One man was washed overboard from a snapper boat near Galveston on the same night.

Fifi, September 4–12.—Possibly the increase in winds at 700 mb. shown by the regular Gull Papa reconnaissance flight on September 3 was the first bit of evidence of the existence of the easterly wave which later developed into Fifi. On the 4th, the suspicious area was confirmed by the SS *Robin Hood*, located near latitude 12° N., longitude 48° W., which reported squalls and pressure of 1008.8 mb., falling. Later that day the *Robin Hood*'s wind veered from east to south but the development was so weak and slow that no cyclonic circulation could be found by the aircraft. The flight did observe cumulonimbus

tops being blown toward the northeast and this was in agreement with a high-level vortex over the extreme eastern part of the Caribbean Sea.

Early on the 5th, reconnaissance indicated possibly two centers of action, but by afternoon a single center was firmly established. The first advisory, at 2200 GMT September 5, located tropical storm Fifi at latitude 15.1° N., longitude 55.0° W. with highest winds of 50 to 55 m.p.h. A solid wall cloud was observed and the sea level pressure was 1000 mb. This was the lowest central pressure observed during the history of the storm although it was equaled at a later date.

Fifi had been moving rapidly northwestward about 23 m.p.h., but by early afternoon of the 6th the forward speed had decreased to 16 m.p.h. and the storm had increased to hurricane intensity. It was located near latitude 17.0° N., longitude 57.5° W. at 1330 GMT on the 6th, attended by surface winds up to 92 m.p.h. north of the center. This was the maximum intensity of hurricane Fifi. The storm slowed to around 12 m.p.h. and highest winds decreased to 75 m.p.h. on the 7th.

During the 8th, Fifi continued on a northwestward course at 7 m.p.h. and maximum winds dropped to 60 m.p.h. Prior to this time, a jet maximum at high levels had worked around peninsular Florida, and by evening of the 8th it was located from the central Bahamas to Bermuda. It was this wind field which influenced the storm to make a turn to the north during the 9th and 10th. There were times when the jet appeared to be in a favorable position for an increased divergent field over the storm. The analysis delineating the jet maximum at this high level may have been in error due to lack of data.

Fifi turned northeastward and accelerated during the 11th. The storm passed within 150 miles of the Leeward Islands and approximately the same distance southeast of Bermuda. No loss of life or property damage was reported.

Gerda, September 13–15.—The seventh tropical cyclone of the season, Gerda, developed in an easterly wave which was first identified about 400 statute miles east of the Lesser Antilles on September 11. Reconnaissance aircraft found no evidence of cyclonic flow or unusual weather in the wave on September 12 but on the following day, September 13, surface reports from the Windward Islands indicated that the wave had intensified. The same reports indicated some evidence of cyclonic circulation in the Caribbean Sea, a short distance west of Martinique, but apparently it was not well defined because aircraft reconnaissance did not confirm its existence until about noon (EST) of September 14. At that time the cyclonic circulation was centered 75 miles southwest of Ciudad Trujillo, Dominican Republic, with highest winds 60 kt. in the southeastern quadrant and a minimum central pressure of 1004 mb.

The center of Gerda, moving west-northwestward about 18 m.p.h., passed over the southern peninsula of the Dominican Republic and evidently the mountainous terrain of that island disrupted the cyclonic flow around its center. On September 15, reconnaissance planes could not locate evidence of a circulation and reports thereafter indicated that tropical storm Gerda had again degenerated into an easterly wave.

Gale warnings were issued for the southern coasts of Puerto Rico and Dominican Republic in connection with Gerda. Three deaths in Puerto Rico, two of which were drownings, were attributed to the storm.

On September 19 and 20, the Weather Bureau Office in New Orleans issued bulletins in connection with a low pressure center which moved north-northwestward out of the Gulf of Campeche having apparently formed in the same easterly wave in which Gerda had developed earlier. A weak polar trough moving into the western Gulf of Mexico at the time of the easterly wave's arrival there appears to have initiated reintensification and development of a vortex. The small low center moved inland near Brownsville, Tex., on September 20, then continued along the Texas coast to the Louisiana border, losing its identity on September 21. Its minimum pressure, as indicated by a barograph record mailed in by the SS *Kendall Fish* was 1003.5 mb., and the highest wind reported was a gust of 52 m.p.h. at Nederland, Tex.

Helene, September 22–29.—Hurricane Helene, one of the most intense storms of the 1958 season as well as the most destructive, developed from an easterly wave which can be traced back to the Cape Verde Islands on September 16. Slow intensification of the wave began near longitude 50° W. on September 20 with pressure falls and above normal shower activity reported by shipping in the area. On the 21st, aircraft located evidence of a weak circulation near 19° N., 54° W. with maximum winds of 35 to 40 m.p.h. in scattered squalls.

The incipient storm moved on a west-northwestward course at approximately 20 m.p.h. on the 22d with little change in intensity. However, an extensive anticyclone in the upper troposphere was developing off the South Atlantic coast during this period so that the disturbance was moving into a much more favorable environment for the deepening process to begin. On the morning (EST) of the 23d, reconnaissance aircraft located a center near 23° N., 68° W., indicating a slowing of forward speed to 12 m.p.h. and an increase of winds to 50 m.p.h. in squalls. Helene continued on a west-northwestward course at 12 to 15 m.p.h. through the 24th with slow intensification.

On September 23, a large and very warm upper tropospheric anticyclone, which had been located over Texas for several days, began to move rapidly eastward (approximately 45 m.p.h.) reaching the middle Atlantic coast on the 25th. This displacement resulted from a temporary change in the long-wave pattern over the Northern Hemisphere. In the lower troposphere, a mean trough was located off the Atlantic coast during September according to Ballenzweig [4], but this trough was either very weak or entirely absent on the Extended Forecast Section's mean charts during the period September 13–27. Without this large-scale adjustment in the general circulation, Helene would have moved around the western edge of the Azores-Bermuda anticyclone a safe distance off the east coast of the United States in the same manner as

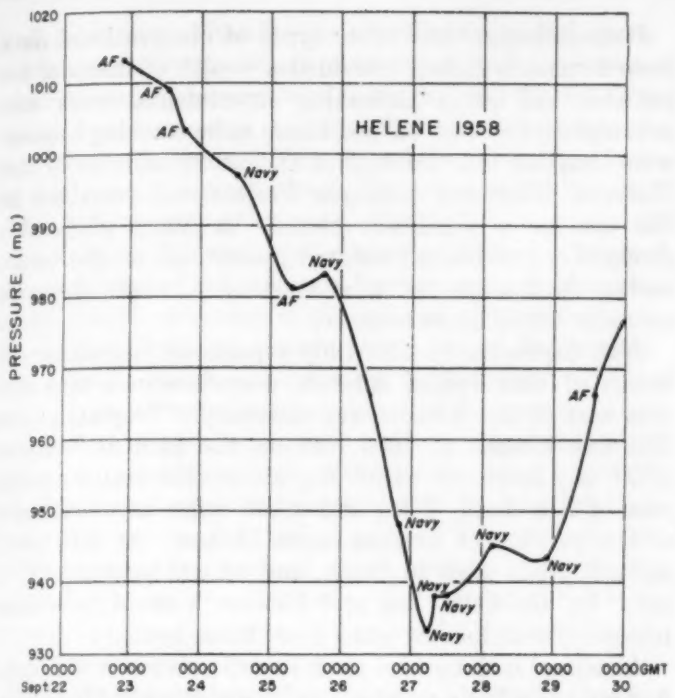

FIGURE 4.—Pressure profile for hurricane Helene, from Air Force and Navy dropsondes, Sept. 22–30, 1958.

Becky, Daisy, and later, Janice. In response to the arrival of the anticyclone in the upper troposphere, hurricane Helene slowed to about 8 m.p.h., veered to the left on a northwestward course with rapid deepening, in the manner described by Riehl [12] and Miller [7] for a hurricane moving under an intense anticyclone. The minimum pressure curve of the hurricane is shown in figure 4.

On the 26th, reconnaissance aircraft found that the hurricane's central pressure had dropped to 948 mb. with winds near the center in excess of 100 m.p.h. compared to 988 mb. and 75 to 90 m.p.h. winds the day before. Helene moved on a northwestward course at 8 to 10 m.p.h. during the 26th as it continued to deepen, finally attaining a minimum pressure of 933 mb. around midnight (local time) at a position some 80 miles east of Charleston, S.C.

On September 26, at 1100 EST, hurricane emergency warnings were issued for the coastal areas from Savannah, Ga., to Cape Fear, N.C. At this time the center of Helene was located about 260 miles east of Brunswick, Ga., moving northwestward toward the coast at 14 m.p.h., and the hurricane center was forecast to reach the coast in the vicinity of Charleston. During the evening it became apparent that Helene was gradually acquiring a more northward component of motion and hurricane warnings were extended northward along the North Carolina coast to Cape Hatteras. The western edge of the hurricane eye came within approximately 10 miles of the coast at Cape Fear and a portion of the intense convective wall cloud passed over land in this area. After recurvature, Helene moved northeastward at an accelerated rate and crossed Newfoundland on the 29th. The storm continued across the Atlantic as a large and vicious extratropical Low that dominated the weather over a large area for several more days.

As indicated by Ballenzweig [4] the broadscale circulation continued to change rapidly and heights fell strongly on the 26th at 70° and 80° W. at all levels as a trough approached the east coast inducing the recurvature. At midnight on the 25–26 (EST) winds at 200 mb. had already shifted from east to southeast and in retrospect it is believed clues were available which might have permitted a more accurate 500-mb. prognostic and consequently a stronger inference of recurvature.

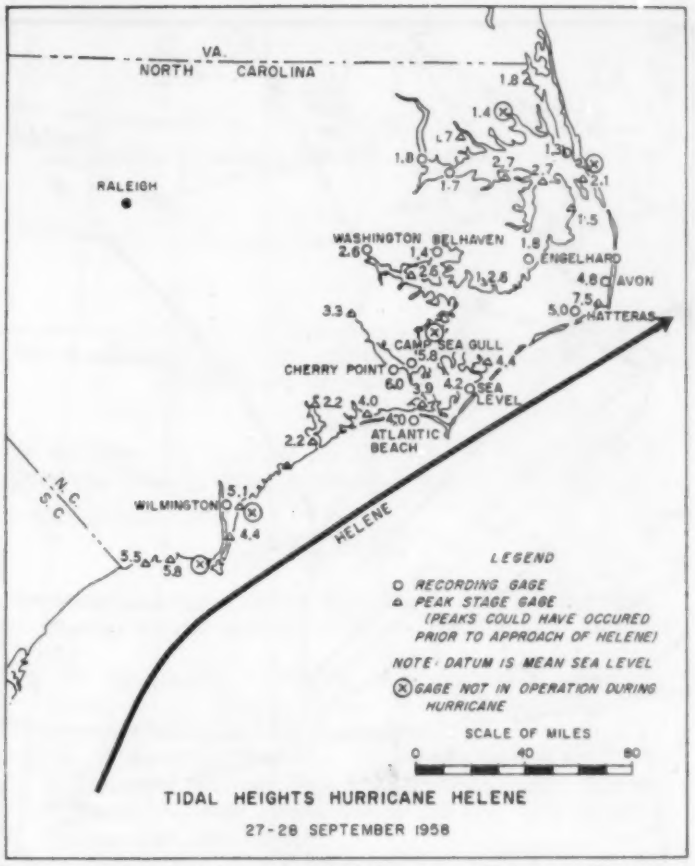

FIGURE 5.—Storm tide produced by hurricane Helene. (Data furnished by U.S. Army Engineer District, Wilmington, N.C.)

Hurricane-force winds, accompanied by high tides and torrential rains, pounded the coastal areas from Cape Fear to Cape Lookout. The Weather Bureau at Wilmington, N.C. recorded a maximum wind (one mile) of 88 m.p.h. and a peak gust of 135 m.p.h. Both of these speeds greatly exceeded all previous records there. Total rainfall at Wilmington during the hurricane was 8.29 inches. At Cape Fear, winds were estimated at 125 m.p.h. with gusts to 150 to 160 m.p.h. According to Sumner [14], the wind speeds and wind damage associated with Helene indicate a more intense hurricane than Hazel of 1954, but the fact that the center of Helene passed about 20 miles off the coast prevented the extremely high tides and wave damage associated with the 1954 hurricane.

A careful swell count made at Wrightsville Beach on the morning of September 27 by a staff member of the Weather Bureau Office at Wilmington, showed only 2½ to 3 per minute. This figure is probably the lowest count ever recorded for the area and indicates a storm of exceptional intensity. Figure 5, prepared from data furnished by the U.S. Army Engineer District, Wilmington, shows the elevation and extent of the storm tide produced by

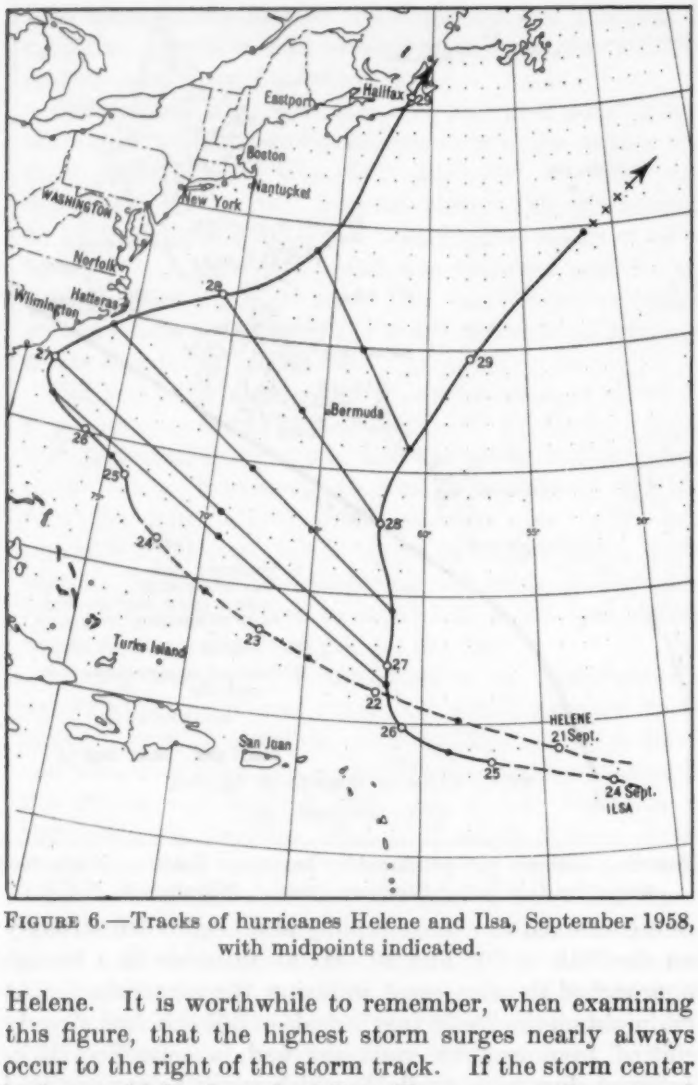

FIGURE 6.—Tracks of hurricanes Helene and Ilsa, September 1958, with midpoints indicated.

Helene. It is worthwhile to remember, when examining this figure, that the highest storm surges nearly always occur to the right of the storm track. If the storm center had moved inland south of Cape Fear on a northwestward or northward trajectory, the accompanying tides might have exceeded the 16 feet of Hazel. The Carolina coast missed a potential disaster of the first magnitude by a very close margin.

Although property damage was estimated at $11,000,000 in North Carolina and $200,000 on the upper South Carolina coast, no lives were lost directly as a result of the hurricane and only one indirectly. The lack of fatalities was due to extensive and detailed warnings, excellent detection and tracking by land-based and airborne radar, and effective community action with respect to evacuation and other protective measures. Evacuation of beaches was complete in most cases.

Reconnaissance and other types of observational data from hurricane Helene provided a wealth of material for research and some interesting experimental work was accomplished. Two balloon-borne radio tracking beacons were dropped into the eye of Helene by aircraft of the National Hurricane Research Project and remained in the eye for a significant period. A Navy plane also dropped a metallicized inflated plastic ball on the ocean surface in the eye for radar tracking. It was observed on radar for 12 hours or more.

Ilsa, September 24–29.—Ship reports on September 23 indicated that special aircraft reconnaissance into the area east of the Antilles was necessary. Tropical storm Ilsa was located at 1606 GMT on the 24th at latitude 17.7° N., longitude 54.0° W., about 800 statute miles east of San Juan, P.R., and 1,300 miles east-southeast of the position of tropical storm Helene. At this time, highest winds were 40 m.p.h. and central pressure 997.6 mb. By the 25th, Ilsa and Helene, both of hurricane intensity, were located some 1,100 miles apart.

A method to determine the interaction between vortices, first noted by Fujiwara and later investigated by Haurwitz, is described by Riehl [13]. The results of this check are given in table 1. The tracks of Ilsa and Helene and a plot of the midpoint between the two hurricanes are shown in figure 6. That there was some relative counterclockwise rotation is shown in figure 7, where a plot has been made of the relative motion during the last 36 hours of table 1.

Ilsa deepened rapidly on the 26th, reaching 932 mb. (dropsonde), a fall of 48 mb. in about 24 hr. The eye was well defined, and spiral bands were described as a typical textbook picture. Winds were estimated to exceed 125 m.p.h. The storm began to fill on the 27th and regular advisories were discontinued on the 30th. No loss of life or property damage was reported.

Janice, October 5–11.—A fairly active easterly wave passed through the Lesser Antilles on September 30 and into the Virgin Islands on October 1. By midday of the 2d, the wave had reached central Hispaniola, and 24 hours later extended from extreme eastern Cuba southward near Jamaica. By the 4th the wave had moved to the central Cuba-Grand Cayman Island area.

This wave had been attended by heavy shower and thunderstorm activity from the central Caribbean northward across Puerto Rico, Hispaniola, Cuba, and into the Bahamas as it progressed westward. A broad flat quasi-circulation was evident southwest of Jamaica on the 3d, however, reconnaissance aircraft on this date found no

TABLE 1.—*Data for checking interaction between vortices, Helene and Ilsa.*

Date (Sept.)	Time (GMT)	Ilsa		Helene		Midpoint		Ilsa–Midpoint [2]		Helene–Midpoint [2]	
		Course [1]	Speed [1] (kt.)	Course [1]	Speed [1] (kt.)	Course [1]	Speed [1] (kt.)	Course	Speed (kt.)	Course	Speed (kt.)
27	0000	335°	8.0	305°	10.0	320°	9.6	090°	3.0	235°	2.0
27	1200	360	5.0	350	7.5	355	5.6	140	0.8	340	2.5
28	0000	360	10.4	045	12.4	030	10.4	285	5.5	095	3.5
28	1200	360	17.5	070	23.0	035	15.0	300	9.5	110	12.5
29	0000	015	16.5	070	21.8	040	17.1	290	7.5	120	11.0

[1] Mean during 12 hours prior to time indicated.
[2] Subtraction of the displacement of the midpoint from the tracks. (During period of study hurricanes were near same intensity so midpoint was considered center of gravity.)

closed circulation. Squalls in the northern semicircle were attended by maximum winds of 40 m.p.h. and the lowest sea level pressure observed was 1010 mb. By the 4th this circulation was located a short distance southwest of Grand Cayman Island. The aircraft found a large but very weak circulation with minimum pressure of 1008 mb. and maximum winds of 25 m.p.h.

The weak circulation drifted slowly north-northwestward during the night, gradually becoming better organized, and by afternoon of the 5th had developed into a tropical storm with the center just south of the central Cuban coast. Winds had increased to 40 to 45 m.p.h. in squalls within 60 miles north and east of the center. The storm turned northeastward and crossed Cuba during the night and by midday of the 6th was centered between New Providence and Andros Island in the central Bahamas. The storm, gradually increased in force and size and accelerating in forward speed during this period, reached hurricane intensity during the evening of the 6th. Minimum sea level pressure at this time by dropsonde was around 996 mb.

A cold front extending from the Ohio Valley northeastward across New England on the morning of the 6th was being followed by a cold, growing, 1026-mb. high pressure area centered in northeastern Minnesota at that time. Twenty-four hours later the cold front had moved to southern Georgia and the high pressure center to the New York-Pennsylvania area. The hurricane decelerated in forward speed from 15–20 m.p.h. to 7 m.p.h. by afternoon of the 7th.

The hurricane drifted slowly north-northeastward to northeastward then began accelerating northeastward to east-northeastward on the 9th, and continued until the 11th when it began losing tropical characteristics and later merged with a deep low pressure system that moved from the Canadian Maritime Provinces into the North Atlantic.

Gale warnings for northeasterly winds were hoisted at 2300 EST on October 6 from Cape Hatteras, N.C., southward to Vero Beach, Fla., and lowered on the 8th and 9th as the hurricane began its definite track away from the United States mainland. Minimum sea level pressure by dropsonde was 968 mb. on the 10th. Highest winds were estimated at 90 m.p.h. over a small area near the center of the hurricane on the 7th and again on the 10th, with slightly lower wind speeds on intervening days. Minimum pressure in the Bahamas was 988 mb. at Harbour Island, Eleuthera. Highest wind was 63 m.p.h. at San Salvador, although Nassau reported 61 m.p.h.

One man lost his life in Nassau harbor while attempting to move a skiff. Eighteen Haitians were reported lost when their craft capsized in the Central Bahamas, but this later proved false. Total monetary damage in the Bahamas was probably between $200,000 and $300,000. One yacht was seriously damaged and a dredger lost. In Jamaica, rains in excess of 20 inches caused floods which destroyed homes and caused severe crop damage. Most of the loss was from damage to wharves, coastal roads, and crops.

In mid-October a reversal of the hemispheric trough-ridge systems [1] resulted in a split jet and polar air flooded the Florida area. Tropical cyclone development abruptly terminated.

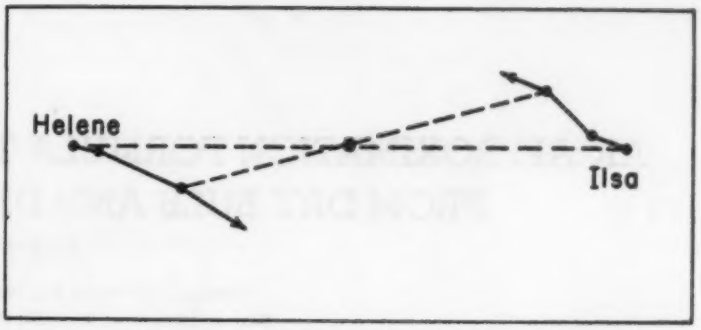

FIGURE 7.—Diagram of relative motion of Helene and Ilsa during last 36 hours shown in table 1.

REFERENCES

1. J. F. Andrews, "The Weather and Circulation of October 1958," *Monthly Weather Review*, vol. 86, No. 10, Oct. 1958, pp. 408–415.
2. E. M. Ballenzweig, "Relation of Long-Period Circulation Anomalies to Tropical Storm Formation and Motion," *Journal of Meteorology* (to be published).
3. E. M. Ballenzweig, "Formation of Tropical Storms Related to Anomalies of the Long-Period Mean Circulation," *National Hurricane Research Project Report* No. 21, U.S. Weather Bureau, Sept. 1958, 16 pp.
4. E. M. Ballenzweig, "The Weather and Circulation of September 1958," *Monthly Weather Review*, vol. 86, No. 9, Sept. 1958, pp. 359–367.
5. C. R. Dunn, "The Weather and Circulation of July 1958—Heavy Precipitation Associated with a Trough in Central United States," *Monthly Weather Review*, vol. 86, No. 7, July 1958, pp. 268–276.
6. R. D. Fletcher, "Computation of Maximum Surface Winds in Hurricanes," *Bulletin of the American Meteorological Society*, vol. 36, No. 6, June 1955, pp. 247–250.
7. B. I. Miller, "On the Maximum Intensity of Hurricanes," *Journal of Meteorology*, vol. 15, No. 2, Apr. 1958, pp. 184–195.
8. V. A. Myers, "Maximum Hurricane Winds," *Bulletin of the American Meteorological Society*, vol. 38, No. 4, April 1957, pp. 227–228.
9. J. Namias, "Long-Range Factors Affecting the Genesis and Paths of Tropical Cyclones," *Proceedings, UNESCO Symposium on Typhoons, 9–12 November 1954, Tokyo*, pp. 213–219.
10. H. Riehl, "Formation of Hurricanes," *Final Report of the Caribbean Hurricane Seminar held at Ciudad Trujillo, D.N., Dominican Republic, February 16–25, 1956*, Ciudad Trujillo, 1956, pp. 69–79.
11. H. Riehl, "Comments on the Formation of Hurricanes," *Proceedings of Technical Conference on Hurricanes*, Miami Beach, Fla., Nov. 1958, pp. G1–1—G1–7.
12. H. Riehl, "Intensification of Tropical Cyclones, Atlantic and Pacific Areas," 4th Research Report Task 12, Project AROWA, 1956.
13. H. Riehl, *Tropical Meteorology*, McGraw-Hill Book Co., Inc., New York, 1954, 392 pp. (See pp. 345–347).
14. H. C. Sumner, "North Atlantic Tropical Storms, 1958," *Mariners Weather Log*, vol. 3, No. 1, Jan. 1959, pp. 5–11.
15. U. S. Weather Bureau, *Mariners Weather Log*, vol. 2, No. 6, Nov. 1958, pp. 185–186.
16. Charles M. Woffinden, "The Weather and Circulation of August 1958—A Month with an Unusual Temperature Reversal," *Monthly Weather Review*, vol. 86, No. 8, Aug. 1958, pp 312–318.

AN APPROXIMATION FORMULA TO COMPUTE RELATIVE HUMIDITY FROM DRY BULB AND DEW POINT TEMPERATURES

JULIUS F. BOSEN

Office of Climatology, U.S. Weather Bureau, Washington, D.C.

[Manuscript received November 17, 1958; revised December 3, 1958]

The WBAN punched card library at the National Weather Records Center, Asheville, N.C., contains millions of observations of simultaneous dry bulb and dew point temperatures for which relative humidities have never been computed. Relative humidity, however, is frequently required for climatological analysis, and must be computed from the available dry bulb and dew point temperatures.

The conventional approach for machine computation of relative humidity involves table lookup of the relative humidity, or of saturation vapor pressures over water for the dew point and dry bulb temperatures, respectively, in order then to compute the ratio

$$U=\frac{e}{e_s}$$

where U is the relative humidity, e the actual vapor pressure (saturation vapor pressure over water for the dew point temperature) and e_s the saturation vapor pressure over water for the dry bulb temperature.

The table lookup process requires either (a) sorting of the punched cards into dry bulb and dew point temperature sequence, matching with a punched card table of pre-computed relative humidities, and gang-punching the appropriate relative humidity values; or (b) the use of a relatively expensive electronic computer with sufficient memory to contain the saturation vapor pressure table for internal reference and computation of relative humidity. Either alternative represents a costly process. A third alternative might be the computation of vapor pressures by the approved Goff-Gratch formula [1]. This would use even more time on an electronic computer capable of performing the required complex of power series expansions, and has never been considered practical as an alternative to table lookup.

The cost of punched-card computation of relative humidity is cut to one-third or less by use of an approximation equation which has been developed and is now being used for this purpose:

$$U\cong\left(\frac{173-.1t+t_{dp}}{173+.9t}\right)^8$$

where t is the dry bulb temperature in °F. and t_{dp} is the dew point temperature in °F. This equation can be solved in a single operation on simple, relatively inexpensive punched card calculating machines, with no preprocessing of the cards.

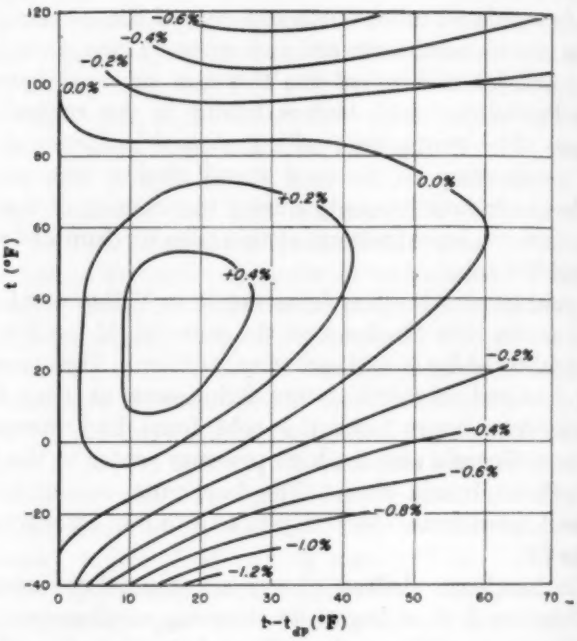

FIGURE 1.—Error in the approximation $U\cong[(173-.1t+t_{dp})/(173+.9t)]^8$

In the meteorological range of temperatures and humidities, the equation approximates relative humidity to within 1.2 percent; over the common range, the error is 0.6 percent or less. This is well within the limits of accuracy of the data.

The error of approximation over the meteorological range of atmospheric conditions is shown in figure 1.

ACKNOWLEDGMENT

The author is grateful to Mr. Louis P. Harrison for a suggestion that resulted in revision and improvement in the subject formula which cuts the error range in half without increasing the number of computational steps.

REFERENCE

1. R. J. List (Ed.), "Smithsonian Meteorological Tables," 6th Rev. Ed., *Smithsonian Miscellaneous Collections*, vol. 114, The Smithsonian Institution, Washington, D.C., 1951, 527 pp. (p. 350).

THE WEATHER AND CIRCULATION OF DECEMBER 1958[1]

RAYMOND A. GREEN

Extended Forecast Section, U.S. Weather Bureau, Washington, D.C.

1. GENERAL CIRCULATION

Waves of large amplitude characterized the mean circulation at middle latitudes of the Western Hemisphere during December 1958 (fig. 1). At the same time fast westerlies in waves of small amplitude dominated the Eastern Hemisphere at similar latitudes. Just the opposite was true in November when large amplitudes prevailed over the Eastern Hemisphere with the remainder of the pattern rather zonal [1]. In December deep mean troughs extending from the Aleutians to Hawaii and from the Maritime Provinces to the Gulf of Mexico were separated by a strong ridge over western North America. For the most part these systems lay well within climatologically favored areas as outlined in the study by Klein and Winston [2]. At middle latitudes these mean waves were amplified counterparts of systems already existing in November (fig. 5 of [1]).

A comparison of the field of changes in mean 700-mb. height anomaly from November to December (fig. 2A) with the December pattern (fig. 1) helps to delineate the areas of greatest amplification; namely, the east-central Pacific, western and southeastern United States, and the west-central and northeastern Atlantic. Large changes from Great Britain to northwestern Siberia accounted for the flattening of an extensive November ridge over Europe. The two months differed markedly at high latitudes where a huge anticyclone (470 ft. above normal) dominated the December pattern (fig. 1). This system was centered about 400 miles poleward from the northern tip of Alaska and was the most intense in 12 Decembers of record for that section of the Arctic. The surrounding channel of negative height departures from normal (frequently found around blocking Highs) was far from uniformly intense, and its displacement from the high center varied greatly. A strong ridge connection was maintained toward a second blocking High near Greenland, and a weaker southward extension of positive anomalies damped the Asiatic coastal trough. A third connection through western Canada and United States attended amplification of the normal pattern to an extensive mean ridge (also at sea level, Chart XI) which markedly affected United States weather.

Mean wind speeds at the 700-mb. level (fig. 3A) were strongest at middle latitudes of the Pacific and the Atlantic. The belt of maximum mean westerlies curved northeastward from the central Pacific with diminishing speeds to northwestern United States, then southeastward with increasing speeds to a maximum centered in the western Atlantic. Numerous Alberta waves traversed paths paralleling, but northward from, the axis of the main branch of maximum westerlies over North America (see Chart X). Several daily anticyclones (Chart IX) followed a track nearly coincident with the path of a secondary wind maximum from western Canada to the Dakotas, then southeastward along the main wind branch to the Atlantic.

Greatest positive departures from normal of mean wind speed (fig. 3B) were located in middle latitudes of the Pacific and the Atlantic. A smaller center appeared over the Northern Plains at the confluence between the main branch of maximum westerlies and a secondary branch from Canada. Large negative areas associated with high-latitude blocking were centered near Iceland, the Aleutians, and just east of Hudson Bay.

After a dip in early December, the 5-day mean index of the strength of the temperate westerlies recovered rapidly during the first week and remained above normal to exceed the monthly average of November. This made the eighth consecutive month with above normal values of the zonal index. However, the classical association of high index with predominantly warm, zonally oriented temperature anomalies over the United States did not apply this month (Chart I–B).

2. CIRCULATION CHANGE RELATED TO UNITED STATES TEMPERATURE ANOMALY

Temperature anomalies in December 1958 changed much more from November than the 1932 to 1954 average determined by Namias [3]. For that period he found the November to December change averaged more than one class out of five at only 33 percent of the stations. In 1958 the changes exceeded one class at 68 percent of the representative stations. Figure 2B illustrates the distribution, direction, and magnitude of the changes, with mainly warming to the west and cooling to the east of the Continental Divide.

Several interrelated circulation characteristics favored these changes of the temperature anomaly pattern. Increased 700-mb. heights (fig. 2A) over Alaska and the Yukon, coupled with strengthened northerly flow across

[1] See Charts I–XVII following p. 492 for analyzed climatological data for the month.

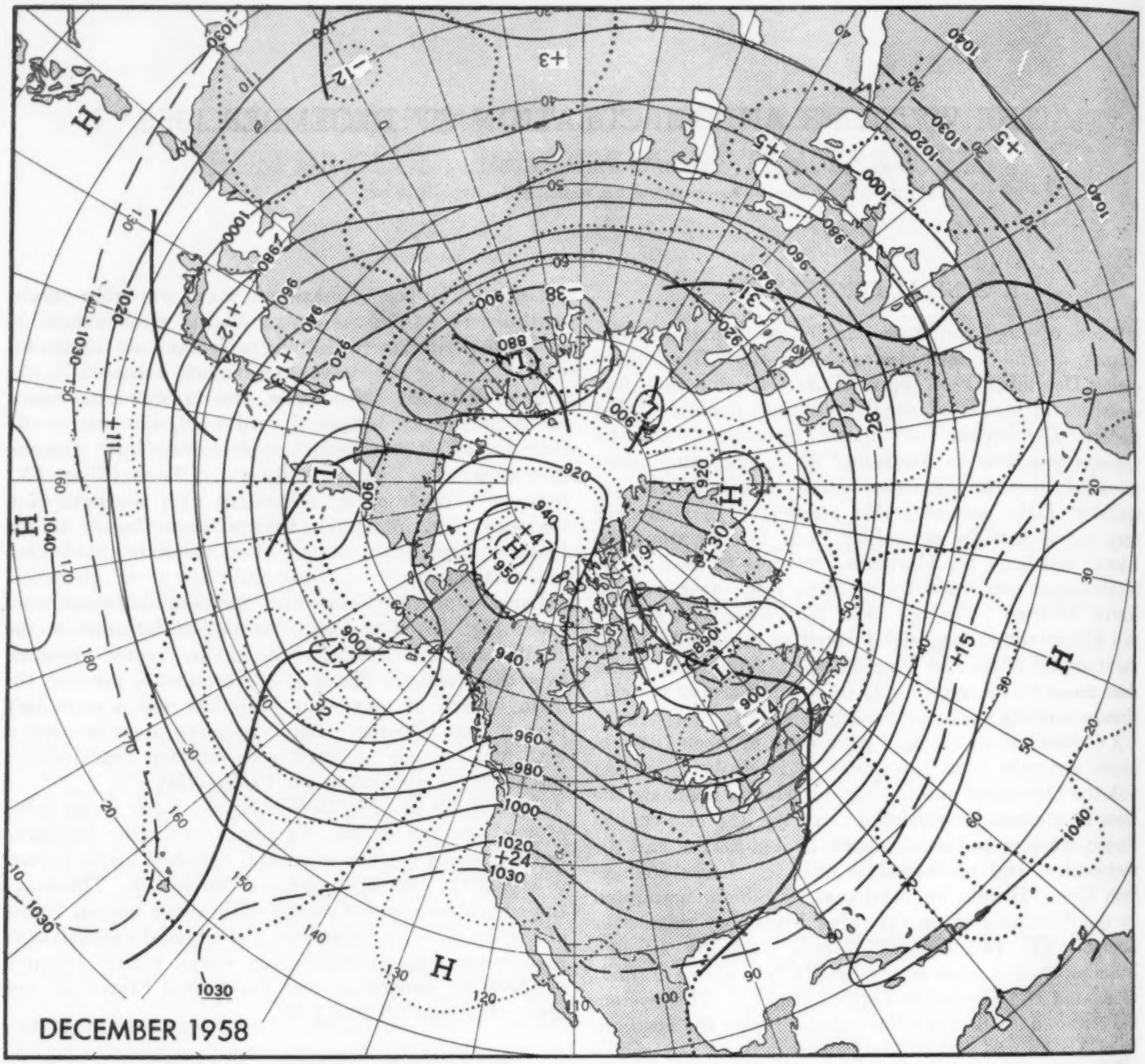

FIGURE 1.—Mean 700-mb. contours (solid) and height departures from normal (dotted), both in tens of feet, for December 1958. Troughs are indicated by heavy lines. Middle-latitude waves with strong amplitudes were surmounted by high-latitude anticyclones in the Western Hemisphere.

a cold source, enhanced cooling over central and eastern United States. Lowered 700-mb. height anomalies accentuated the effect of these factors over the eastern States where the greatest cooling occurred. Most of the warming must be attributed to the local effect of increased 700-mb. height anomalies attending anticyclogenesis west of the Divide.

Temperature records for extremes of both cold and warmth for December were broken in the areas just described. New records for cold were set by the mean monthly temperature at Grand Rapids and Muskegon, Mich., Toledo and Akron, Ohio, and Allentown, Pa. Numerous stations east of a line from Louisville, Ky. to Sault Ste. Marie, Mich., recorded the coldest December since 1917, when December sea level activity [4] was very similar to that of 1958. Record warmth occurred at San Diego, Los Angeles, Burbank, San Francisco, Red Bluff, and Blue Canyon in California.

3. INTRA-MONTHLY VARIABILITY

A. CHANGES BETWEEN THE HALF-MONTHS

A crude evaluation of variability within the month was obtained from tracks (not shown) of 5-day mean 700-mb.

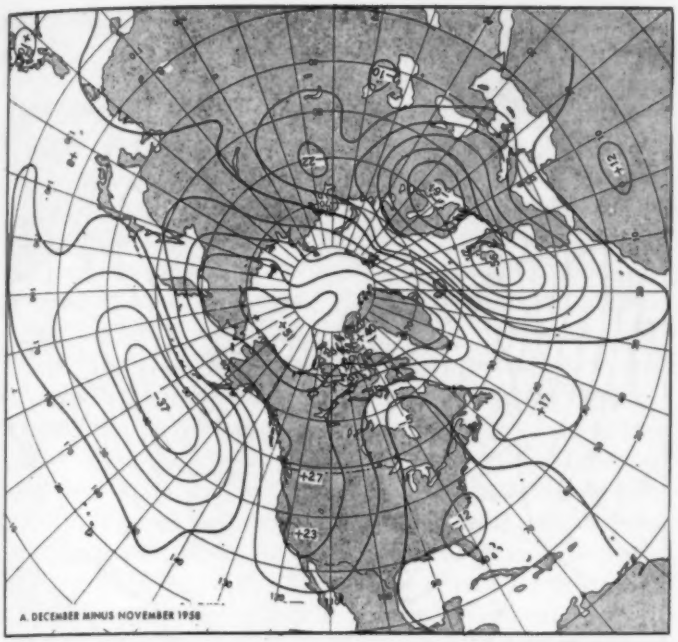

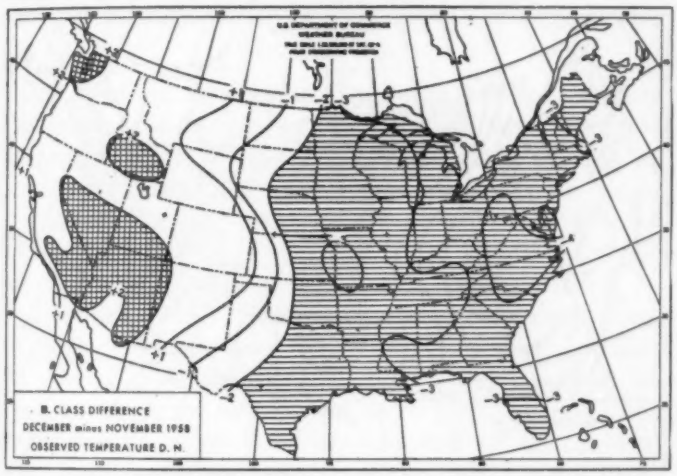

FIGURE 2.—(A) Difference (in tens of feet) between the mean monthly 700-mb. height departures from normal of November and December 1958. Greatest changes occurred over the Baltic Sea, near England, and north of Alaska. Middle-latitude changes in the Western Hemisphere amplified November systems. (B) The number of classes the surface temperature anomaly changed from November to December 1958. Warming in the West accompanied stronger cooling in the East.

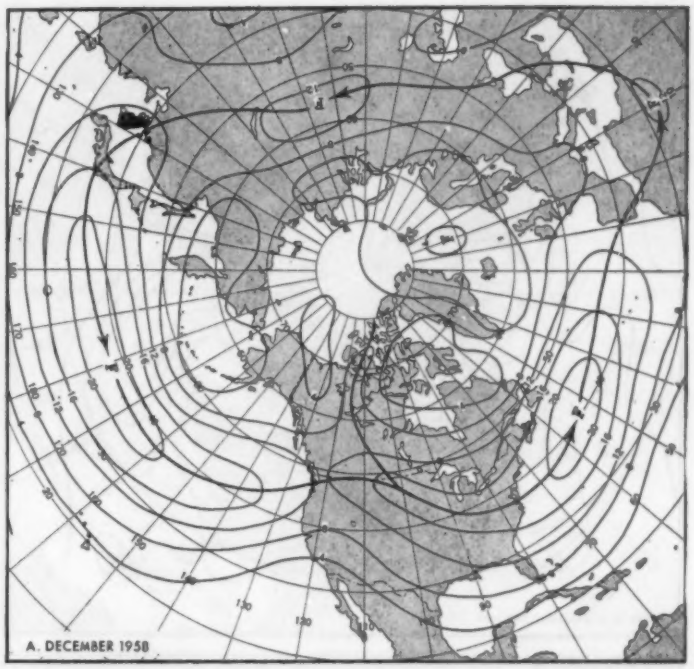

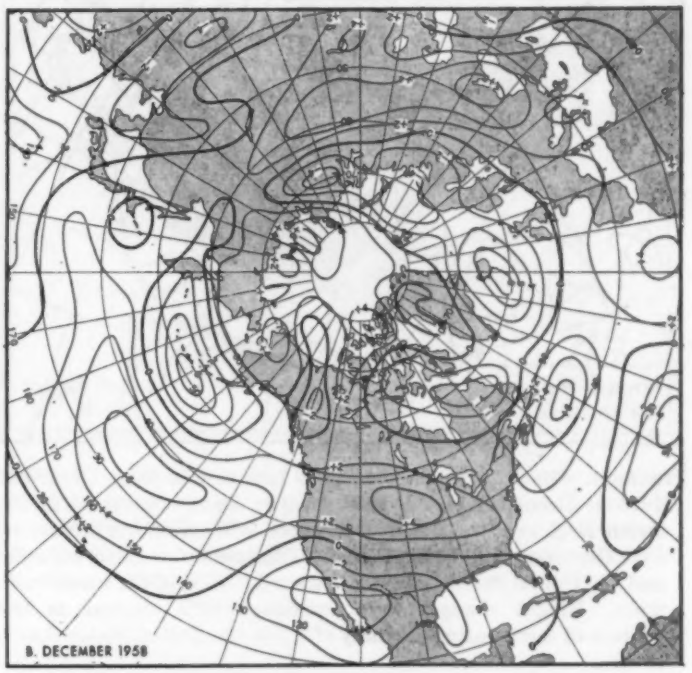

FIGURE 3.—(A) Mean isotachs (in meters per second) of 700-mb. wind speed during December 1958. Solid arrows indicate axes of maximum wind speed. Fastest winds occurred over the oceans at middle latitudes. (B) Departure from normal of mean 700-mb. wind speed. Greatest positive departures were found over the middle-latitude oceans, from the Black Sea to western Siberia, and over the Northern Plains of the United States. Strong negative areas associated with blocking appeared near Iceland, the Aleutians, and eastern Canada.

height anomaly centers over the Western Hemisphere. Centers over and adjacent to North America were strong and relatively stationary during the first half-month, weaker and more transitory during the second. Figure 4A, a comparison of half-month means, brings to light the changes which modified earlier 700-mb. height and anomaly flow over much of the United States. There was tremendous alteration (−800 ft.) of the pattern over the Arctic Basin in the area occupied by the Arctic High. At the same time the wave in the eastern Pacific and North America lost some amplitude and (more important with respect to United States weather) moved eastward. Blocking became more pronounced over Greenland as the month progressed, and the Atlantic mean ridge was flattened.

Temperature anomalies in the United States reacted sharply as circulation characteristics favoring the warm-West-cold-East regime gave way to higher index condi-

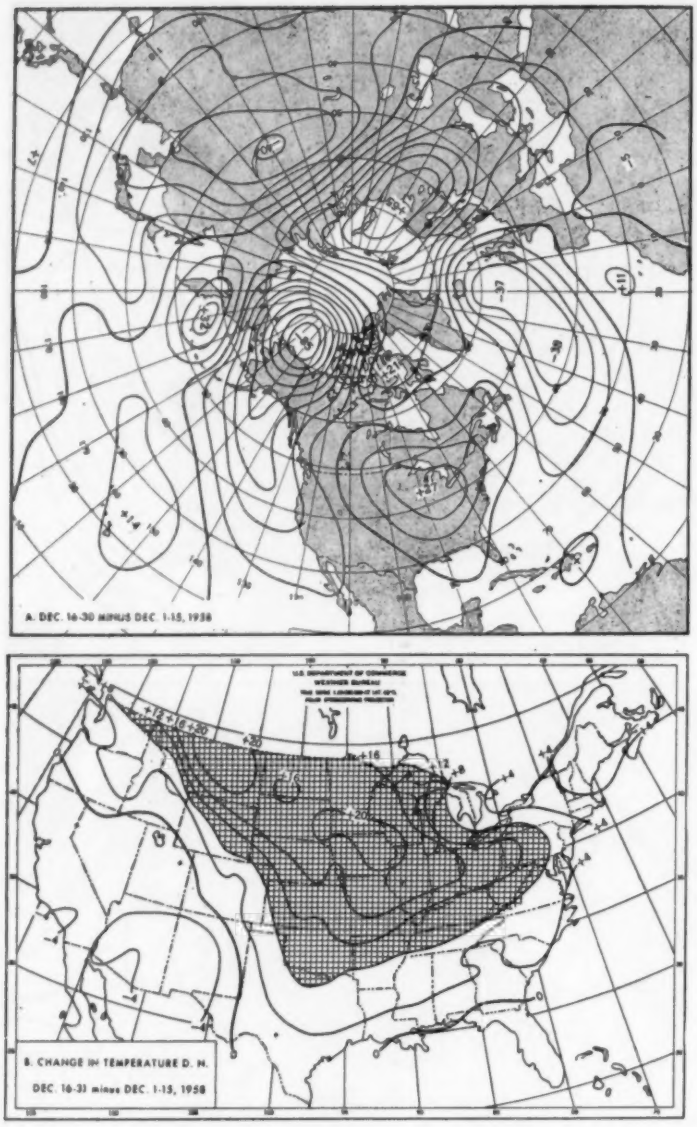

FIGURE 4.—700-mb. height change in tens of feet from December 1–15 to December 16–30, 1958. Large changes occurred in the Arctic High over the Beaufort Sea area, while blocking intensified over Greenland and Baffin Island. Changes in the eastern Pacific and the United States reflected eastward motion of the mean wave train. Height changes were associated with changes in the pattern of temperature anomaly (° F.) in the United States shown in (B).

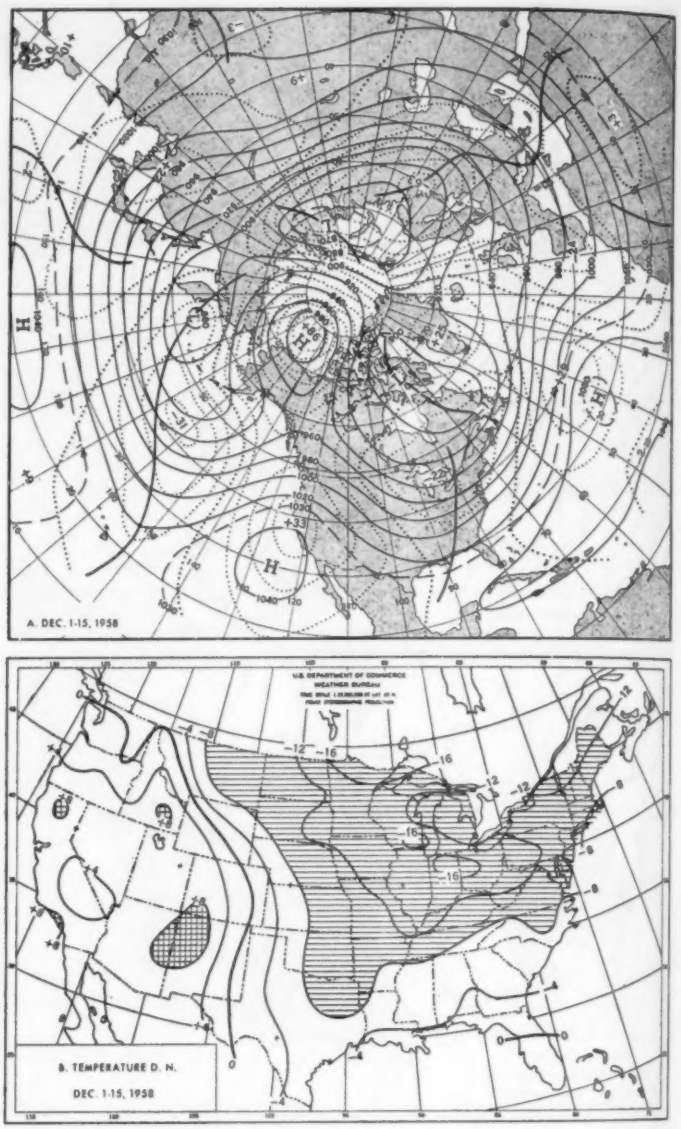

FIGURE 5.—(A) Fifteen-day mean 700-mb. height contours (solid) and departures from normal (dotted), both in tens of feet, for December 1–15, 1958. The Arctic High, the strong ridge over western North America, and the deep trough in the East helped to deploy cold Canadian air into the United States. (B) Mean United States temperature anomalies for December 1–15 (° F.).

tions. Part B of figure 4 shows the magnitude and extent of differences between temperature anomalies of the two half-months. There was close agreement between changes in surface temperature and 700-mb. height, especially where 700-mb. changes opposed earlier anomalous flow from the north in the area from Montana to Iowa. An interesting double maximum in this warmer area may have been related to foehn warming just east of the Divide. On the other hand, foehn warming diminished over parts of the Southwest, where cooler anomalies accompanied generally weaker anticyclonic circulation. Advective warming apparently counteracted the cooling influence of lowered 700-mb. height anomalies over the Pacific Northwest.

B. DECEMBER 1–15

A mean chart of the first fifteen days of December (fig. 5A) displays exaggerated (over mean December) versions of several features earlier described as differing most from November. The strongest system of this half-month was the Arctic High with an anomaly of +860 ft. at 700 mb. Positive anomalies projected strongly southward along a ridge over western North America and also toward Greenland. Mean troughs in the Pacific and the eastern United States were deep and the Atlantic ridge strong; the European ridge of November was no longer in evidence.

This half-month's pattern represented optimum condi-

tions for flooding central and eastern United States with cold air; namely, high 700-mb. heights over Alaska and the Yukon and strong northerly anomalous and actual flow from Canada into a deep mean trough over the eastern United States. Part B of figure 5 depicts the extent and intensity of cold east of the Divide, where only a part of Florida experienced average temperatures above normal for the period. As the avalanche of cold air traversed the steep incline of maximum winds from western Canada to the Middle Atlantic States, daily temperature records tumbled in Iowa, Ohio, New York, Rhode Island, and Virginia. The first polar outbreak followed the last storm of a series of rather weak Alberta waves which were speeding across the Great Lakes during the first few days of the month. The final storm deepened over the Lakes and decelerated while cold air became firmly entrenched east of the Divide and deterred later storms until mid-month.

Abnormal warmth prevailed west of the Divide beneath a strong mean ridge with onshore flow of warm Pacific air. New daily maximum temperature records were established in New Mexico, Arizona, Nevada, and California.

C. DECEMBER 16–31

Most Western Hemisphere systems reflected higher index characteristics during the second half-month (fig. 6). The Arctic High vanished and a weak mean trough extended northward across western Alaska. The ridge over western North America, the downstream United States trough, and the Atlantic ridge at middle latitudes were all flatter and located eastward from positions of the preceding period. While the mid-latitude wave from the Pacific through the United States retained greater than normal amplitude, conditions favoring transport of Canadian air into the States were greatly modified. 700-mb. height anomalies increased east of the Divide as the ridge moved eastward and the anomaly gradient decreased and became more westerly.

Warmest temperature anomalies (fig. 6B) occurred over central Montana, where fast westerlies increased the foehn warming often observed in that section of the country. Temperatures continued below normal over the Great Lakes and southeast of a line from the Ohio Valley to western Texas. This area remained under the influence of northerly flow and near to below normal 700-mb. heights.

A new series of rapidly moving Alberta waves (Chart X) was established at mid-month. Most of these were somewhat stronger than the early December storms. Rather weak outbreaks of Canadian air penetrated eastern sections of the country between Lows, except for the final surge which ended the series. The last storm was similar to the final storm of the earlier Alberta series. It was deeper than its predecessor and moved northeastward from the Great Lakes instead of continuing to the Atlantic Coast. The polar anticyclone behind the storm dominated the weather of the eastern United States for three days beginning Christmas Day. As the anticyclone moved into the Atlantic, a wave from the Gulf of Mexico

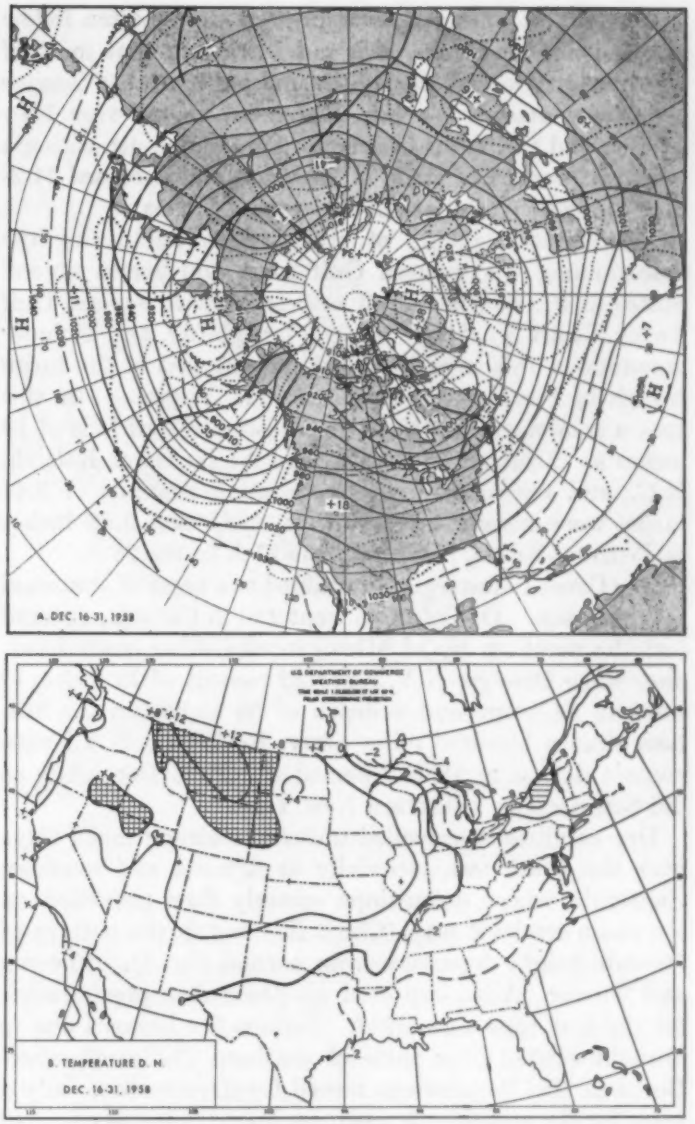

FIGURE 6.—(A) Sixteen-day mean 700-mb. height contours and departures from normal for December 16–31, 1958. Circulation over North America was flatter this half-month and temperature anomalies (B) considerably warmer than during the previous half-month shown in figure 5.

crossed Florida and moved inland from the South Atlantic coast before passing out to sea off the Virginia Capes. It was the first Gulf wave of several which crossed Florida during the month to re-enter the country. Copious precipitation accompanied the storm over the Carolinas and parts of Virginia.

4. PRECIPITATION

Precipitation exceeded normal in four general areas (Chart III–B), with greatest departures over the Pacific Northwest and the northern Divide. Large amounts west of the Divide (Chart II) can be attributed to the orographic lifting of fast westerlies, while a weak secondary storm track (Chart X) along the northern Divide helped to intensify lower-level upslope flow and precipitation east

of the Divide. Since these depressed storms often follow strong polar outbreaks, it is not surprising that most of this precipitation fell during the first half-month. Similar conditions attended a late December storm over New Mexico and the Texas-Oklahoma Panhandle, depositing a record 12 inches of snow in 24 hours and a record 14.2-inch December total at Albuquerque, N. Mex.

More than 2 inches of precipitation fell during the month along the western Gulf coast and across several States in the Southeast, all associated with several Gulf waves (Chart X) along the mean trough (fig. 1). Heavier amounts in this area exceeded normal east of the mean trough in Florida, the Carolinas, and Virginia. In this area a snowstorm on the 11th deposited record falls of 16 inches at Elizabeth City, N.C. and 9.1 inches at Raleigh, N.C., and record 24-hour precipitation amounts of 3.44 inches were measured at Asheville, N.C. and 3.48 inches at Winston-Salem, N.C. from the 27th to the 28th.

The Great Lakes region contained two areas of abnormal precipitation. One of them, centered in Canada, covered just the northern tip of Michigan; the other made headlines when Oswego, N.Y. reported records of 33 inches of snow in 24 hours and a depth of 56 inches on the 8th. Less than a hundred miles away, Rochester, N.Y., with records dating to 1835, reported its driest December, as did Schenectady in eastern New York.

Dry conditions prevailed under the strong mean ridge over the Southwest, especially in Arizona and southern California where down-slope easterly flow prevailed on the mean sea level map (Chart XI) and in the pattern of 700-mb. height departure from normal (fig. 1). Phoenix and Tucson, Ariz., reported no December precipitation for the first time since 1917. Serious fire hazards due to drought existed over parts of southern California where Burbank tied its previous record for dryness with only a trace for the month. A mean sea level High was centered near Salt Lake City, where the driest 8 consecutive months on record brought a total in that period of only 2.54 inches. The mean sea level ridge and the absence of storms from South Dakota to Virginia were indicative of anticyclonic conditions and dry weather from the Dakotas to the Ohio Valley. Lowest December totals on record were measured at Fargo, N. Dak. and Indianapolis, Ind., and totals were the second lowest on record at stations in Minnesota, Nebraska, and Wisconsin.

On the whole, December was a dry month over the United States, as one might expect from its circulation and temperature patterns and its higher than normal zonal index. However, this was not a typical high index pattern, as evidenced by the meridional orientation of the temperature anomalies. More important factors affecting precipitation were the anticyclonic nature of the circulation over much of the United States and the lack of low-level flow into the United States from either of two important sources of moisture, the Gulf of Mexico and the Atlantic Ocean. There were no intense large-scale storms in the United States and only one report of a severe local storm was noted, a tornado at Sarasota, Fla., on December 11.

REFERENCES

1. E. Paroczay, "The Weather and Circulation of November 1958—A Mid-month Reversal of Weather Regimes," *Monthly Weather Review*, vol. 86, No. 11, Nov. 1958, pp. 439–446.
2. W. H. Klein and J. S. Winston, "Geographical Frequency of Troughs and Ridges on Mean 700-mb. Charts," *Monthly Weather Review*, vol. 86, No. 9, Sept. 1958, pp. 344–358.
3. J. Namias, "The Annual Course of Month-to-Month Persistence in Climatic Anomalies," *Bulletin of the American Meteorological Society*, vol. 33, No. 7, Sept. 1952, pp. 279–285, and an unpublished extension through 1954.
4. U.S. Weather Bureau, *Historical Weather Maps, Northern Hemisphere, Sea Level*, January 1899–June 1939, Washington, D.C. 1943. (See December 1917).

NOTICE

This is the last issue of the *Monthly Weather Review* in which the following climatological charts will appear. They will continue to be printed in *Climatological Data, National Summary.*

U. S. GOVERNMENT PRINTING OFFICE: 1959

Chart I. A. Average Temperature (°F.) at Surface, December 1958.

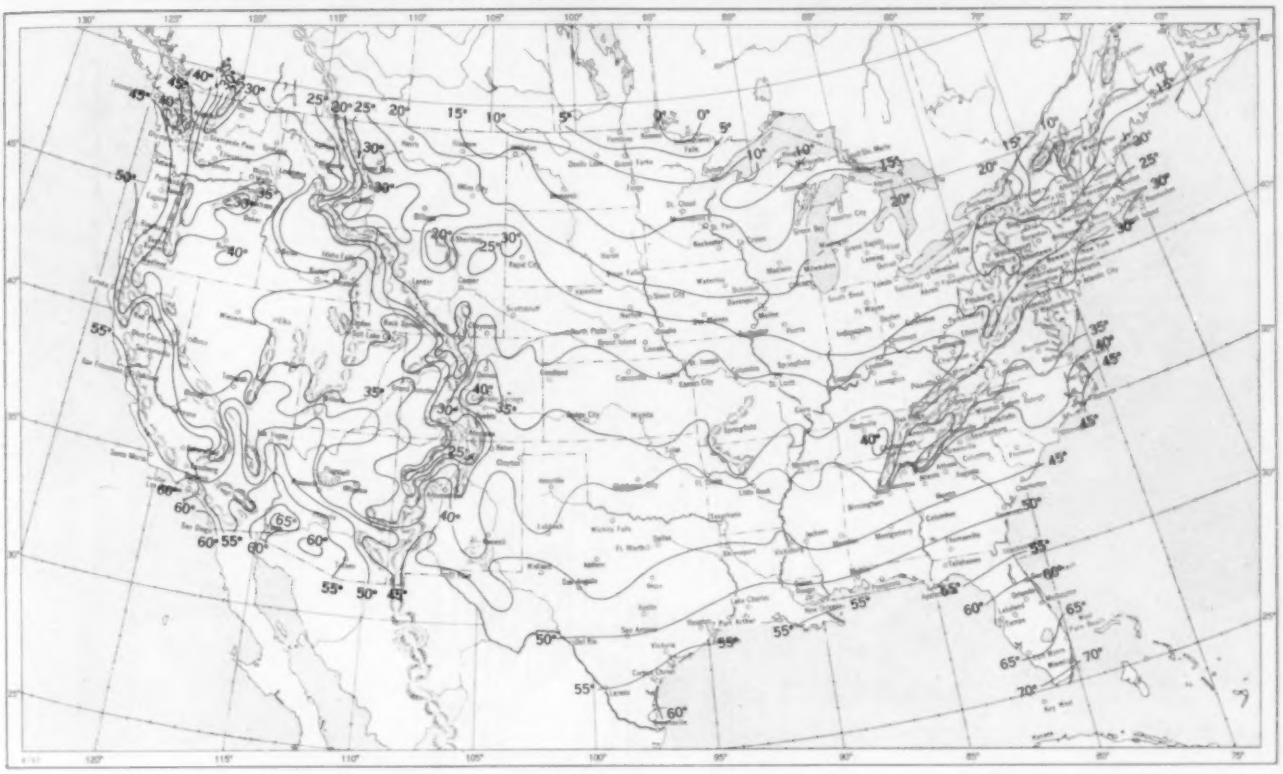

B. Departure of Average Temperature from Normal (°F.), December 1958.

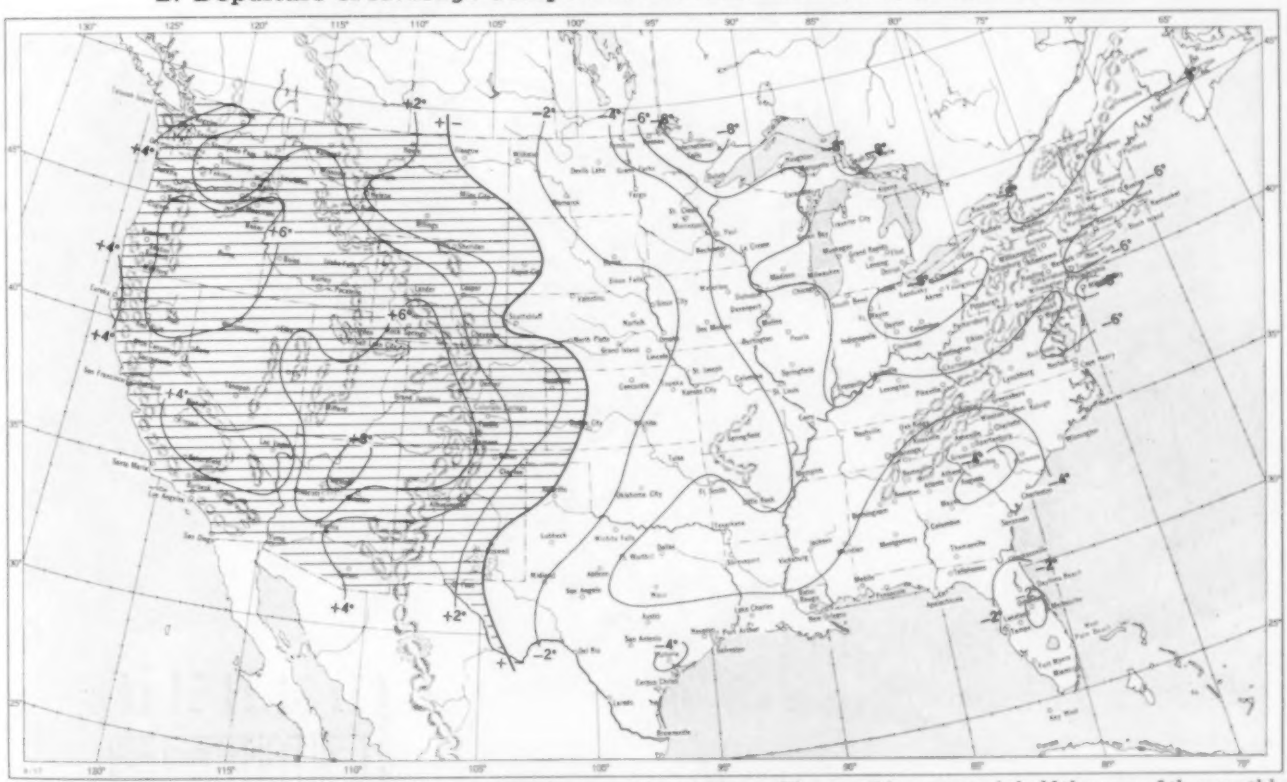

A. Based on reports from over 900 Weather Bureau and cooperative stations. The monthly average is half the sum of the monthly average maximum and monthly average minimum, which are the average of the daily maxima and daily minima, respectively.

B. Departures from normal are based on the 30-yr. normals (1921-50) for Weather Bureau stations and on means of 25 years or more (mostly 1931-55) for cooperative stations.

Chart II. Total Precipitation (Inches), December 1958.

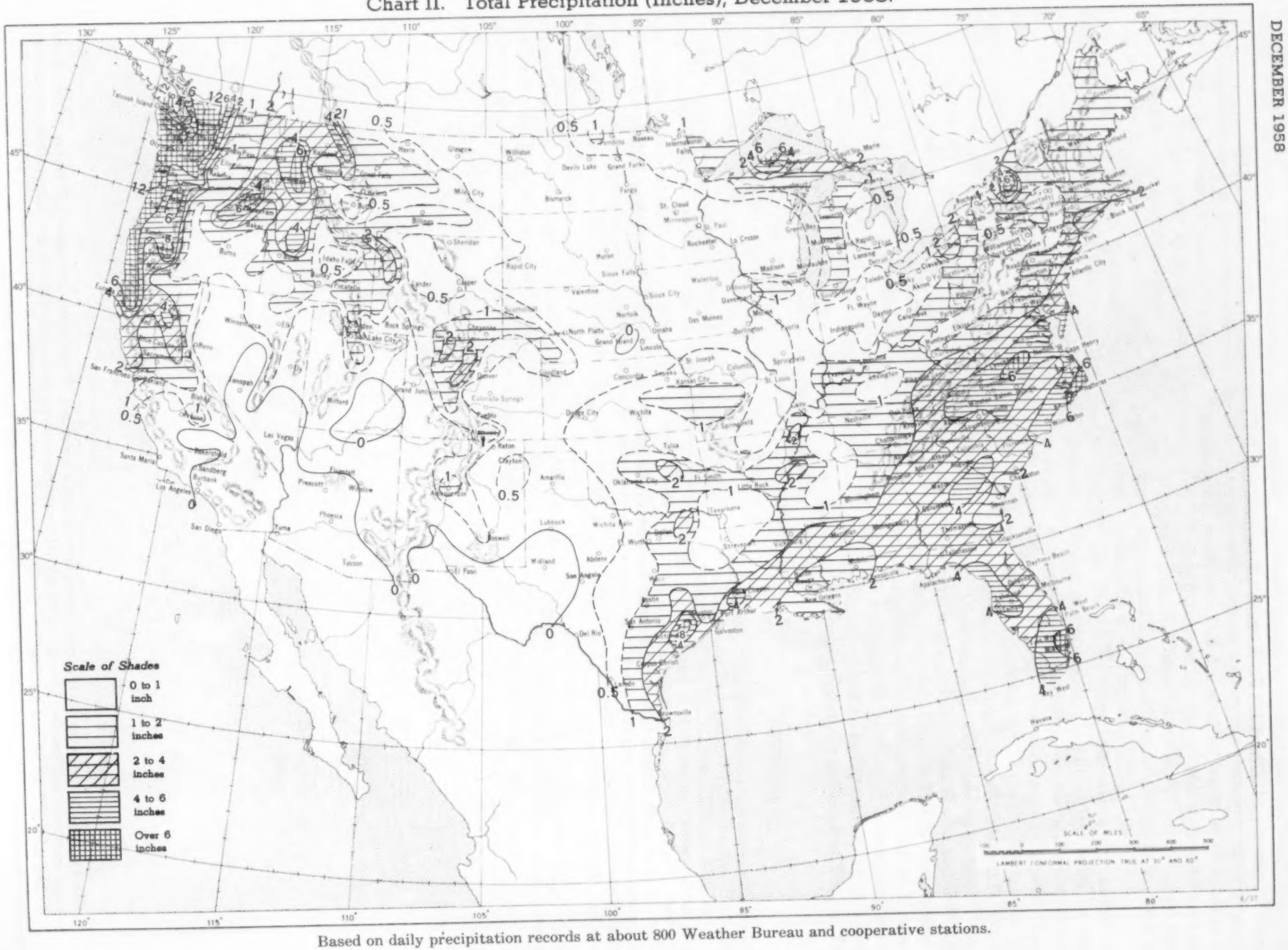

Based on daily precipitation records at about 800 Weather Bureau and cooperative stations.

Chart III. A. Departure of Precipitation from Normal (Inches), December 1958.

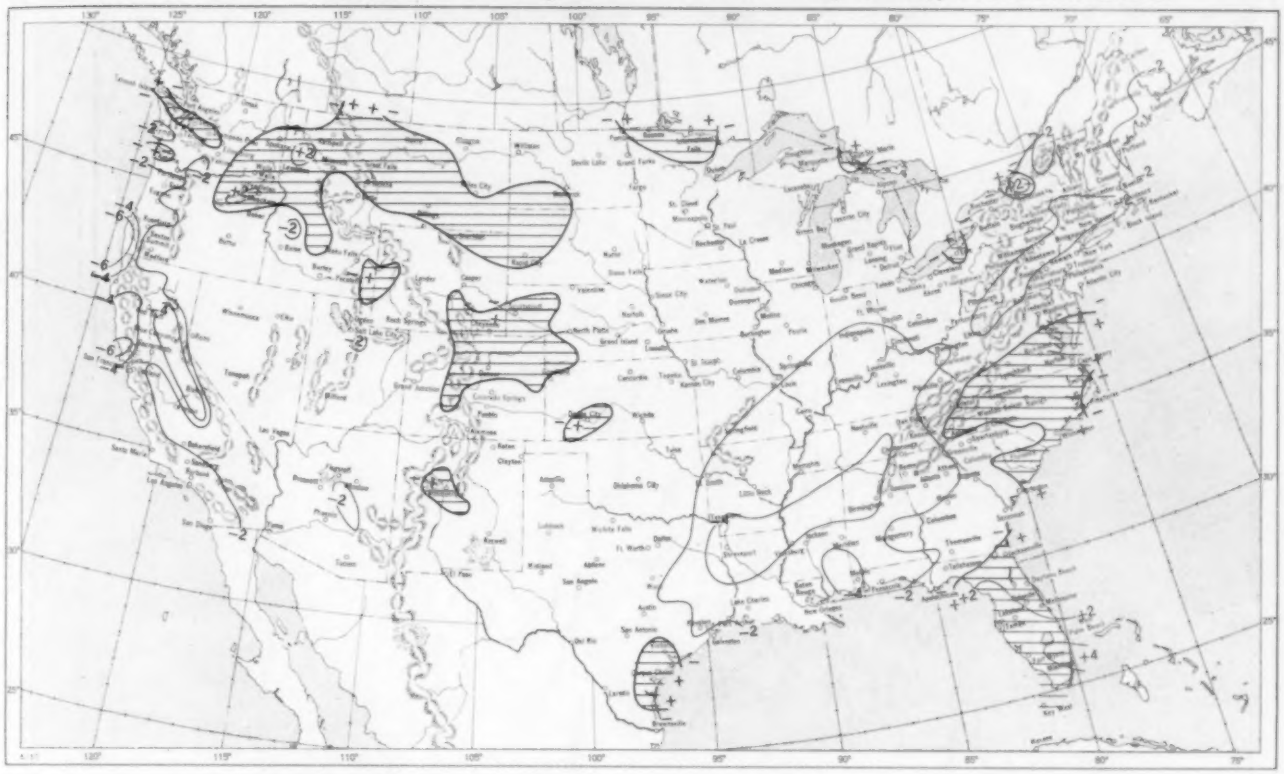

B. Percentage of Normal Precipitation, December 1958.

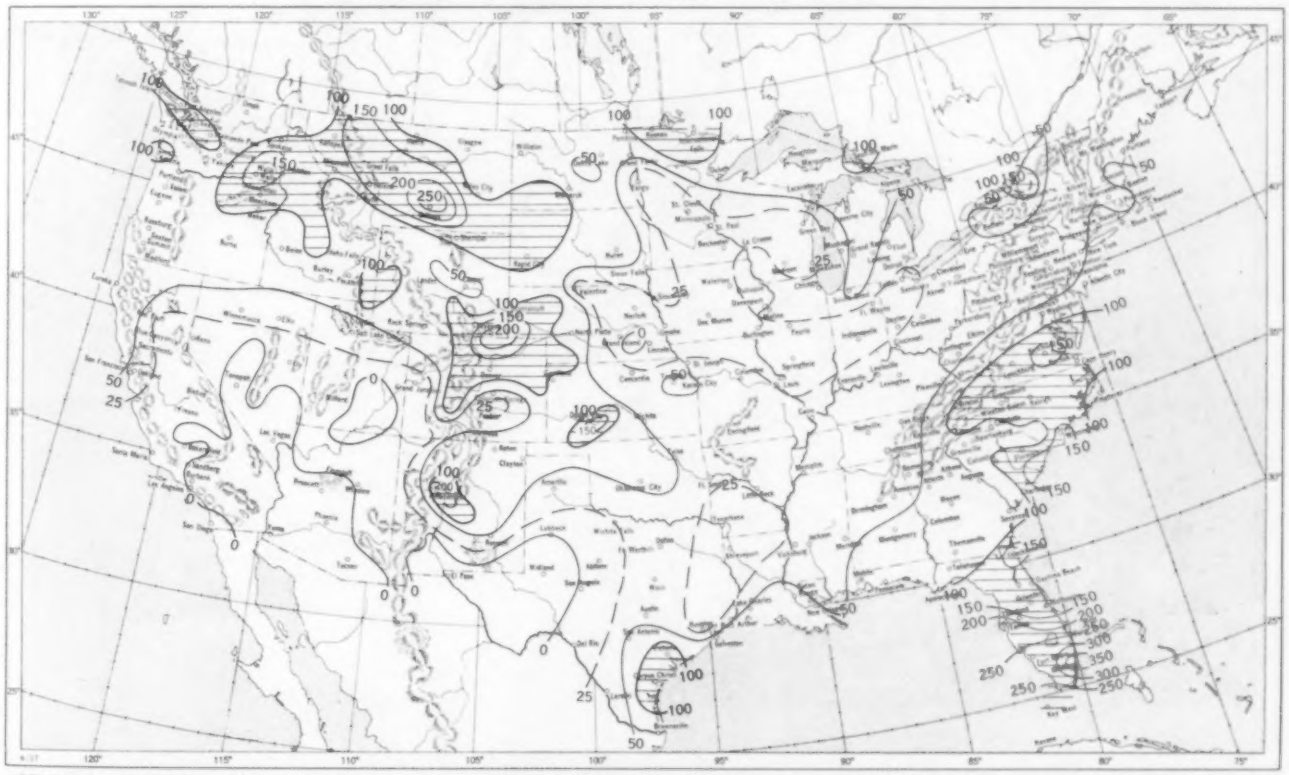

Normal monthly precipitation amounts are computed from the records for 1921-50 for Weather Bureau stations and from records of 25 years or more (mostly 1931-55) for cooperative stations.

Chart IV. Total Snowfall (Inches), December 1958.

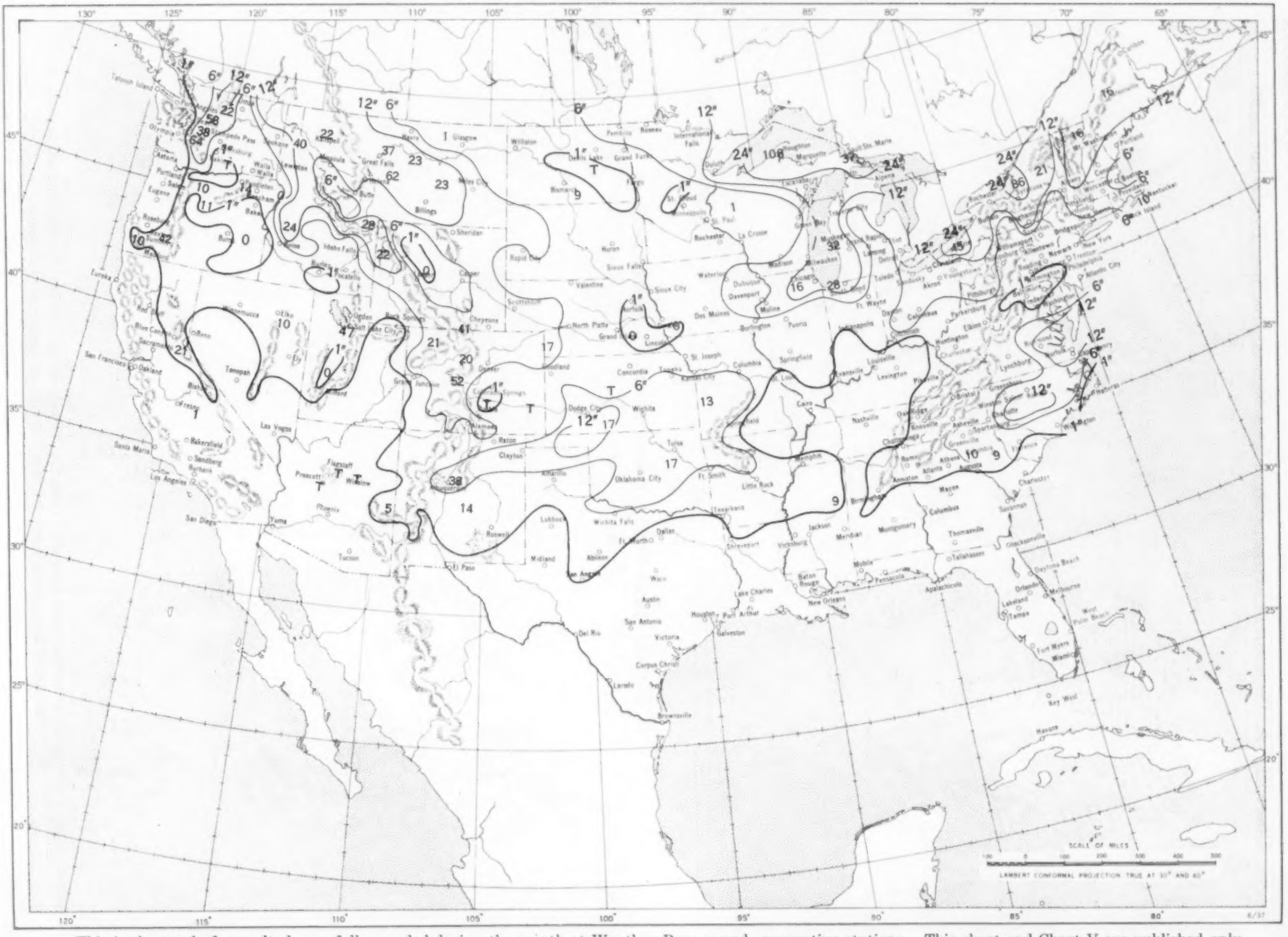

This is the total of unmelted snowfall recorded during the month at Weather Bureau and cooperative stations. This chart and Chart V are published only for the months of November through April although of course there is some snow at higher elevations, particularly in the far West, earlier and later in the year.

Chart V. A. Percentage of Normal Snowfall, December 1958.

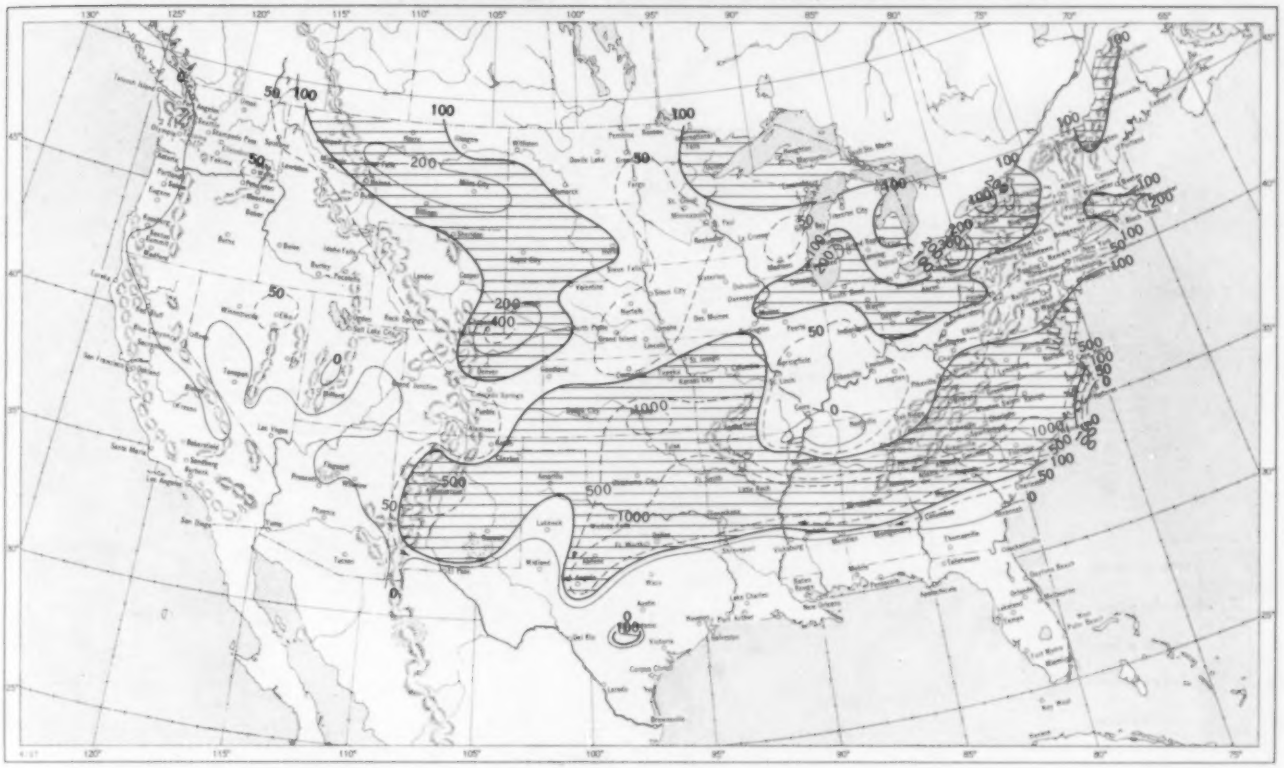

B. Depth of Snow on Ground (Inches), 7:00 a. m. E.S.T., December 29, 1958.

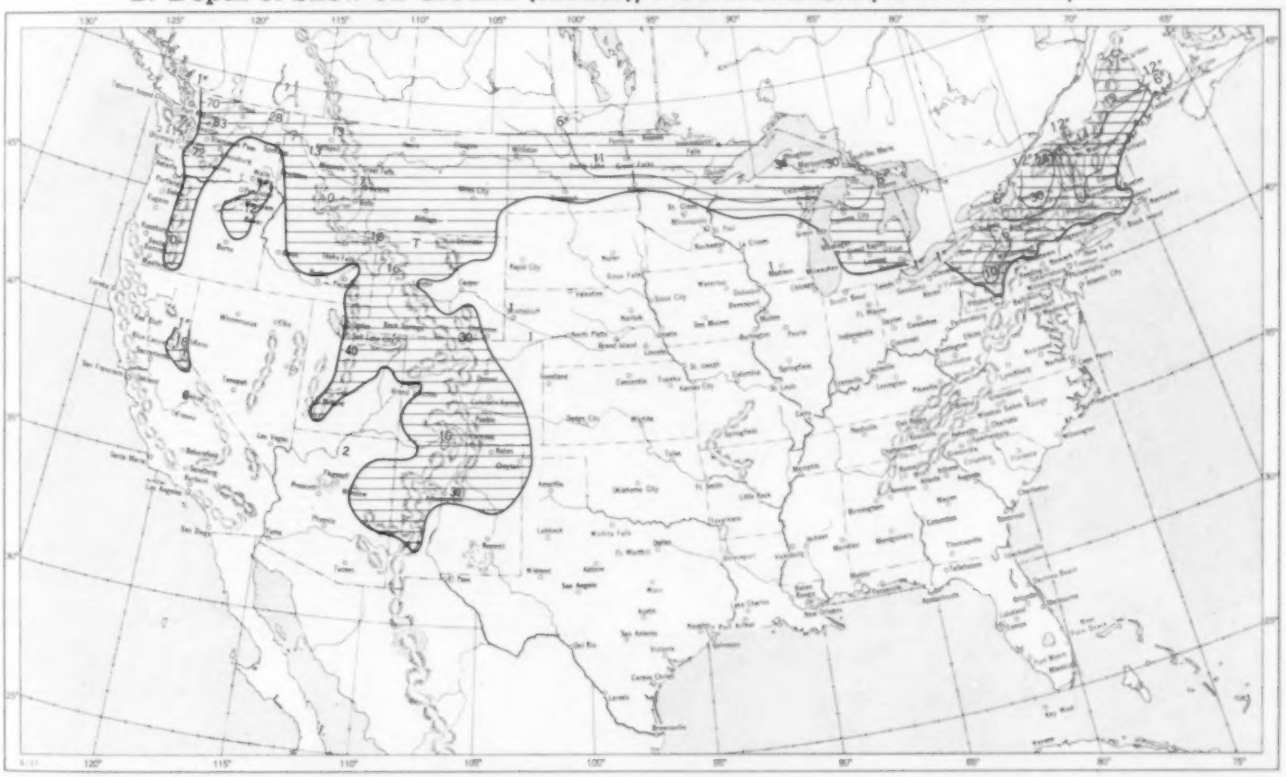

A. Amount of normal monthly snowfall is computed for Weather Bureau stations having at least 10 years of record.
B. Shows depth currently on ground at 7:00 a.m. E.S.T., of the Monday nearest the end of the month. It is based on reports from Weather Bureau and cooperative stations. Dashed line shows greatest southern extent of snowcover during month.

Chart VI. A. Percentage of Sky Cover Between Sunrise and Sunset, December 1958.

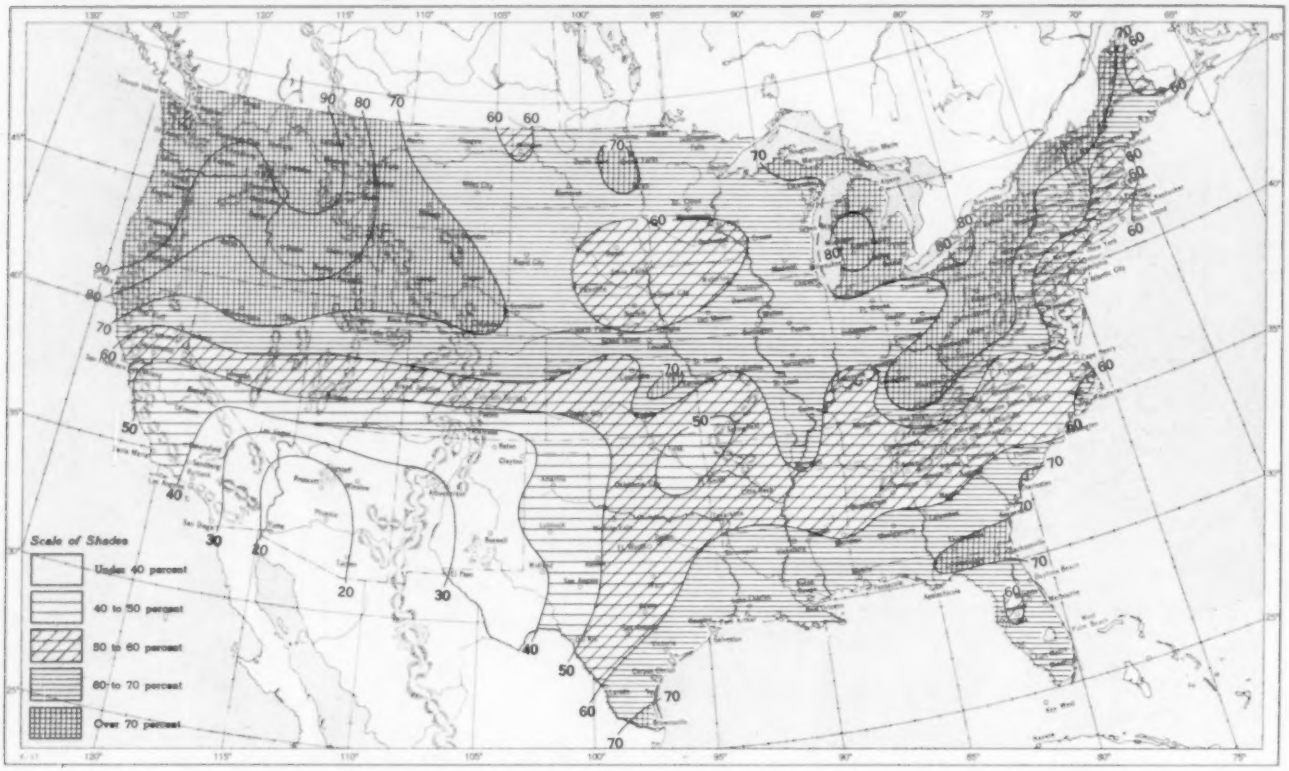

B. Percentage of Normal Sky Cover Between Sunrise and Sunset, December 1958.

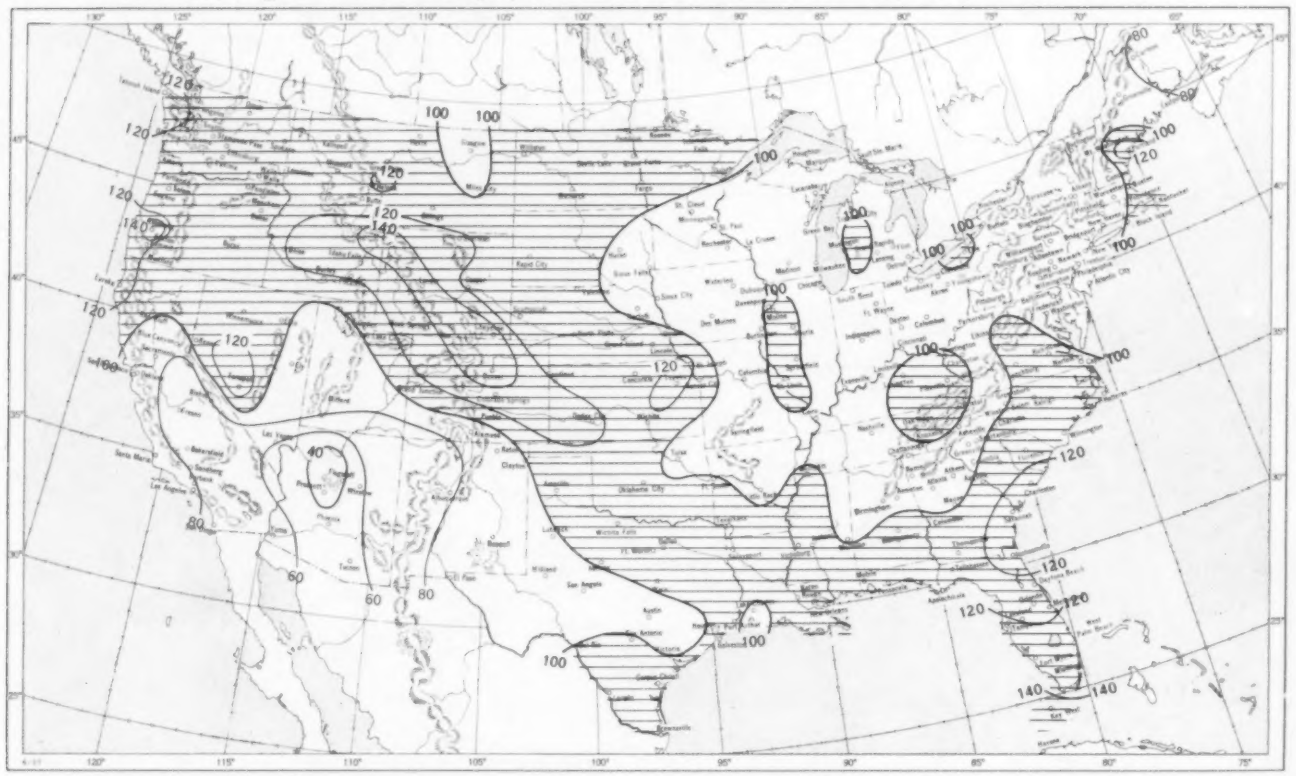

A. In addition to cloudiness, sky cover includes obscuration of the sky by fog, smoke, snow, etc. Chart based on visual observations made hourly at Weather Bureau stations and averaged over the month. B. Computations of normal amount of sky cover are made for stations having at least 10 years of record.

Chart VII. A. Percentage of Possible Sunshine, December 1958.

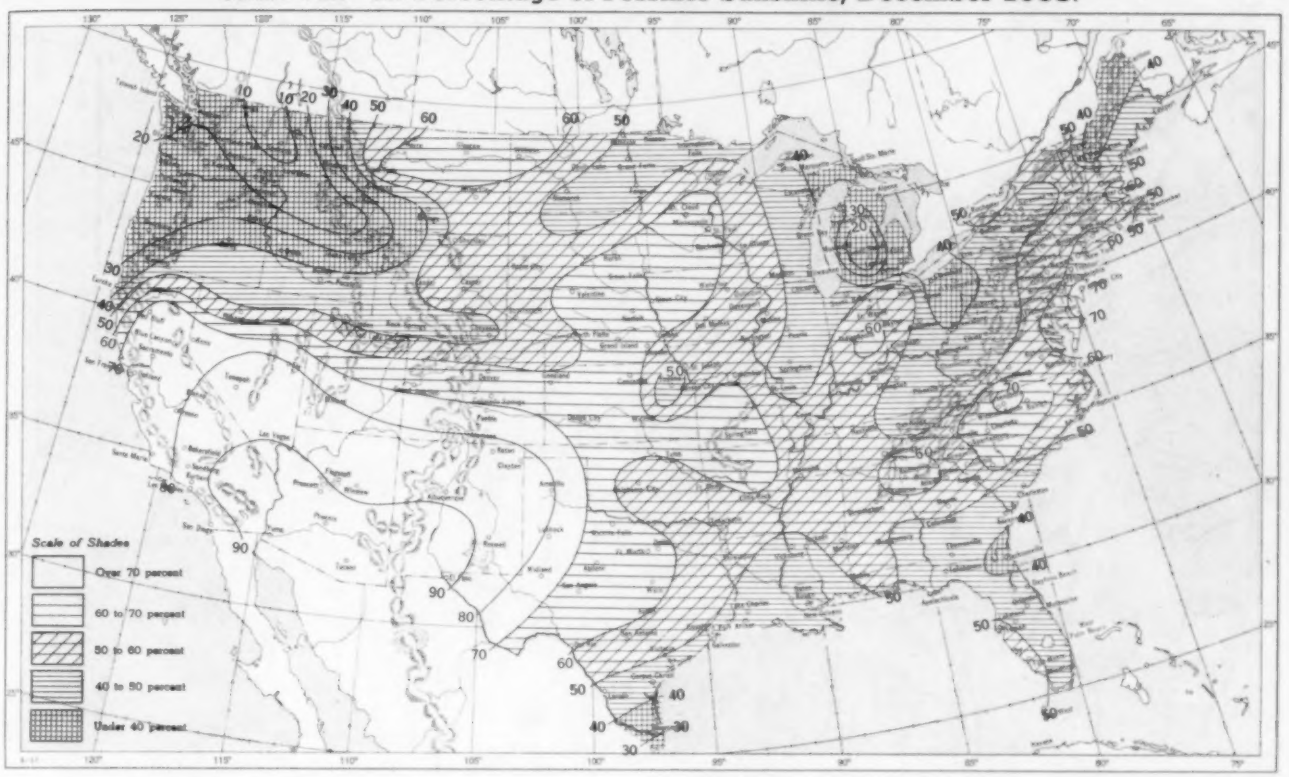

B. Percentage of Normal Sunshine, December 1958.

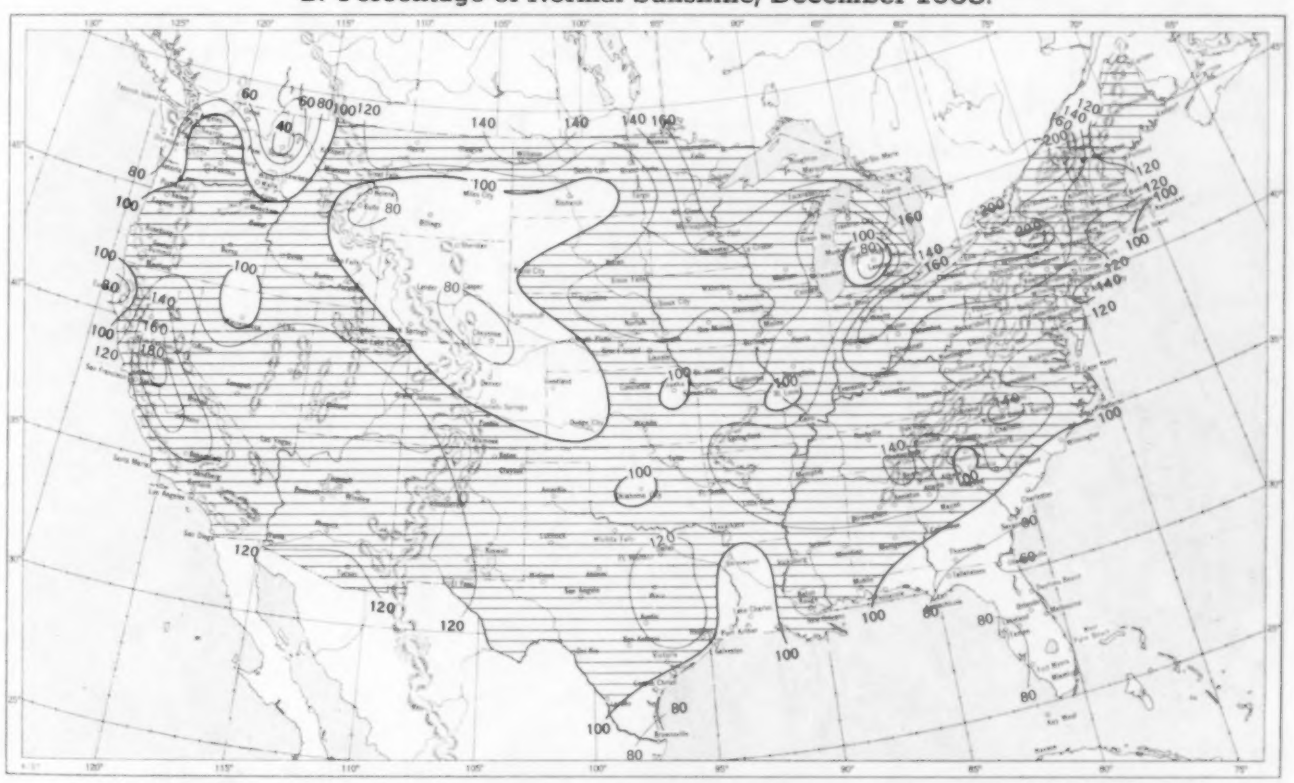

A. Computed from total number of hours of observed sunshine in relation to total number of possible hours of sunshine during month. B. Normals are computed for stations having at least 10 years of record.

Chart VIII. Average Daily Values of Solar Radiation, Direct + Diffuse, December 1958. Inset: Percentage of Mean Daily Solar Radiation, December 1958. (Mean based on period 1951-55.)

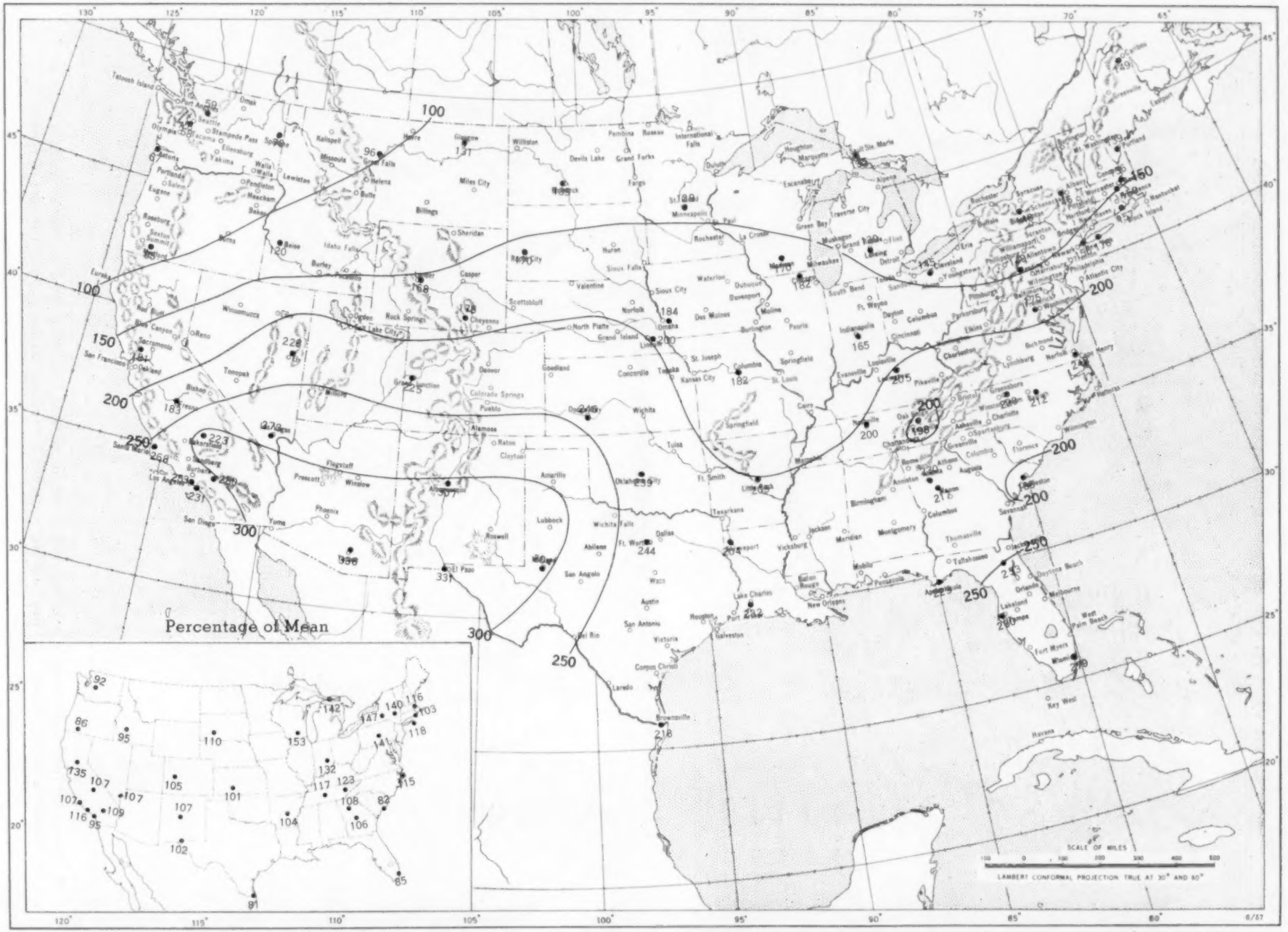

Chart shows mean daily solar radiation, direct + diffuse, received on a horizontal surface in langleys (1 langley = 1 gm. cal. cm. $^{-2}$). Basic data for isolines are shown on chart. Further estimates are obtained from supplementary data for which limits of accuracy are wider than for those data shown. The inset shows the percentage of the mean based on the period 1951-55.

Chart IX. Tracks of Centers of Anticyclones at Sea Level, December 1958.

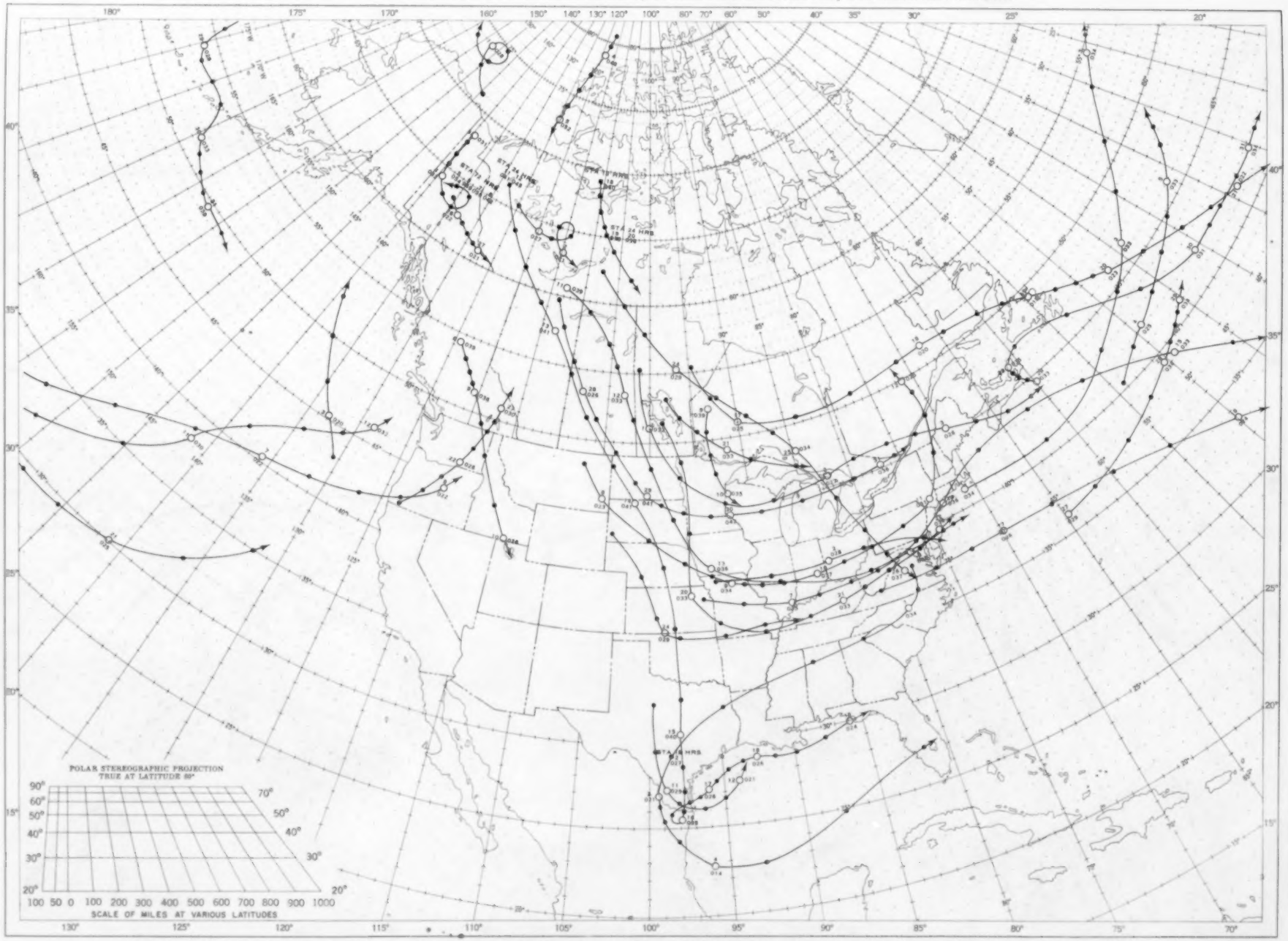

Circle indicates position of center at 7:00 a. m. E. S. T. Figure above circle indicates date, figure below, pressure to nearest millibar. Dots indicate intervening 6-hourly positions. Squares indicate position of stationary center for period shown. Dashed line in track indicates reformation at new position. Only those centers which could be identified for 24 hours or more are included.

Chart X. Tracks of Centers of Cyclones at Sea Level, December 1958.

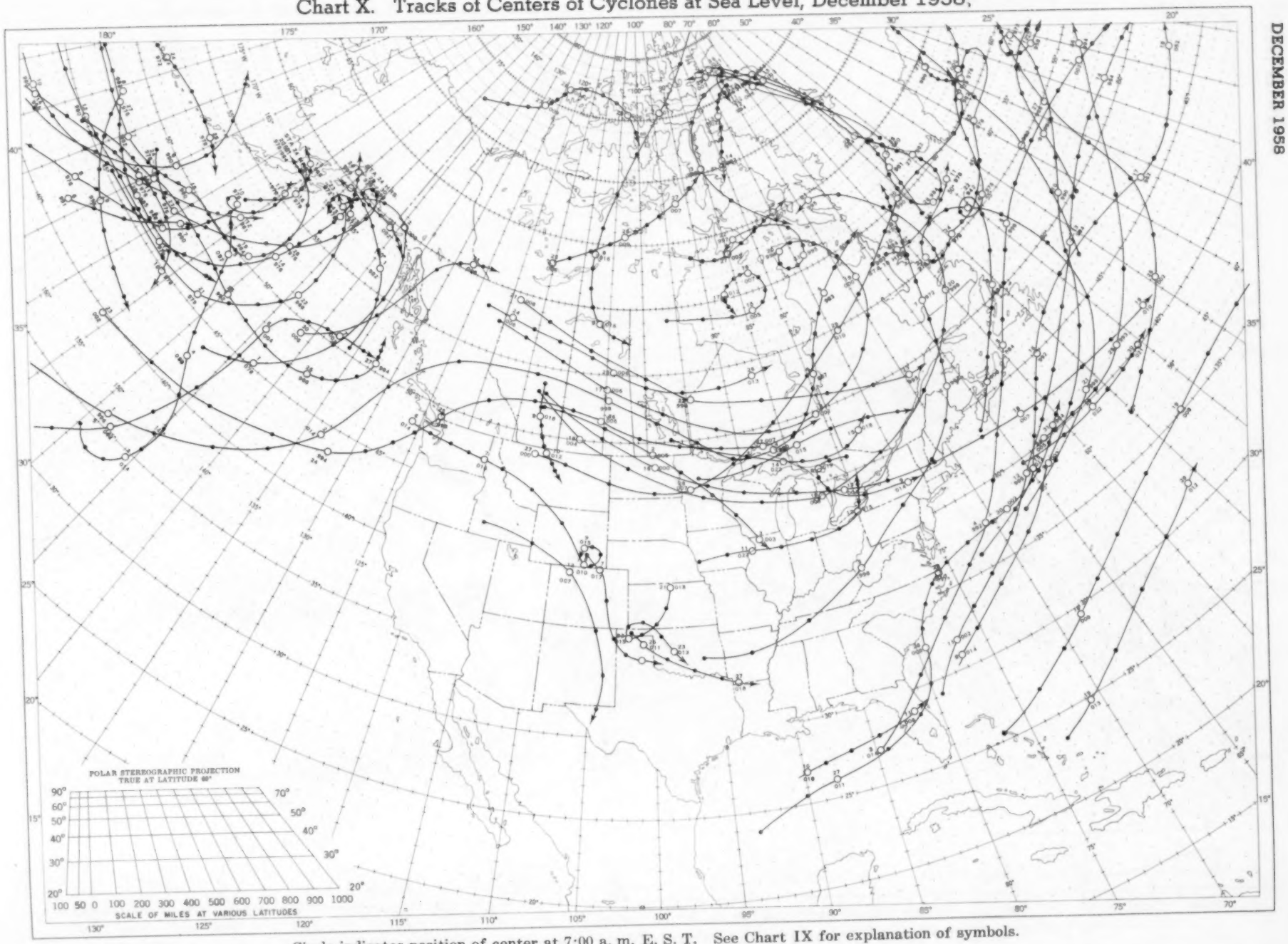

Circle indicates position of center at 7:00 a. m. E. S. T. See Chart IX for explanation of symbols.

Chart XI. Average Sea Level Pressure (mb.) and Surface Windroses, December 1958. Inset: Departure of Average Pressure (mb.) from Normal, December 1958.

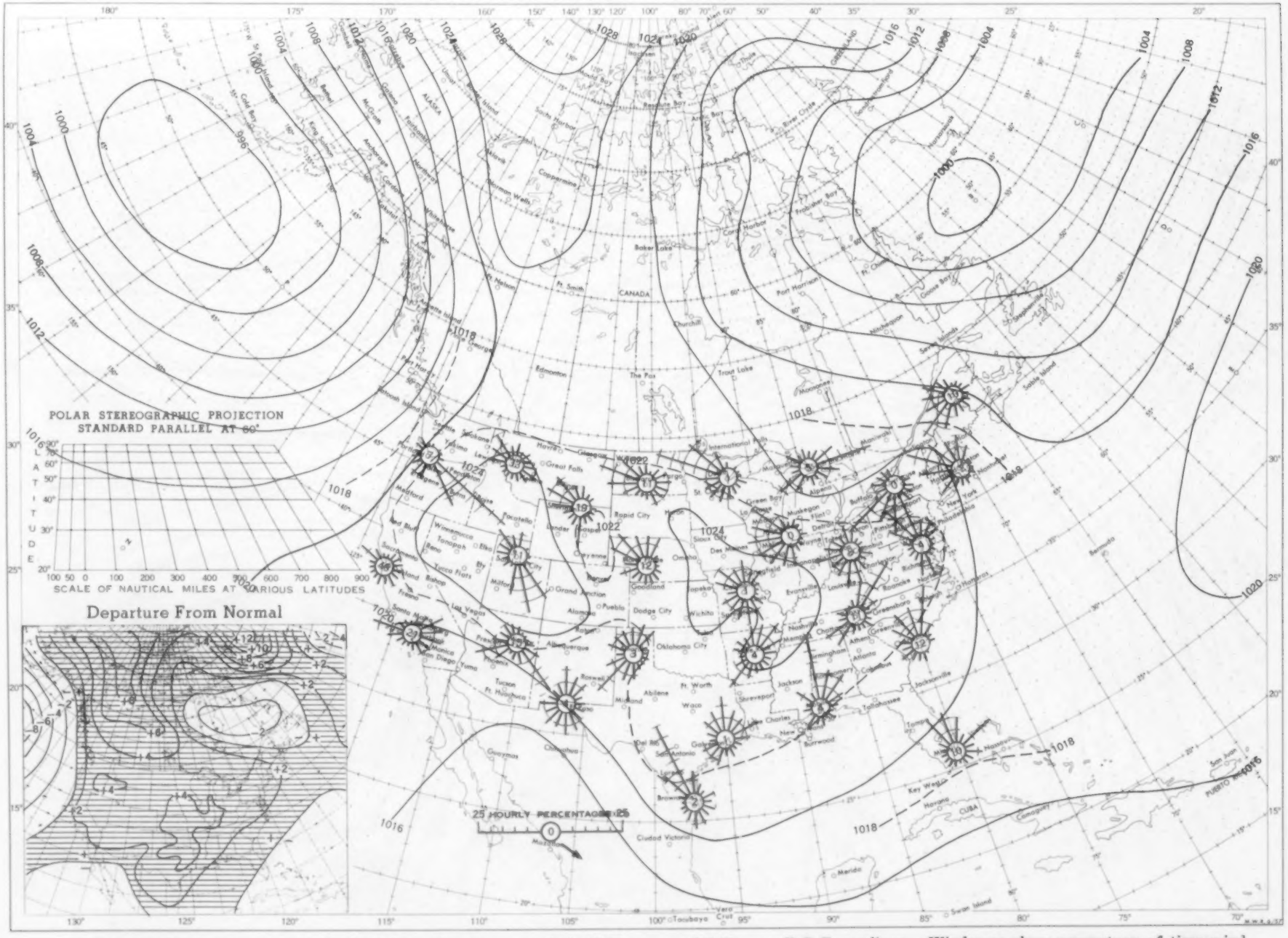

Average sea level pressures are obtained from the averages of the 7:00 a. m. and 7:00 p. m. E. S. T. readings. Windroses show percentage of time wind blew from 16 compass points or was calm during the month. Pressure normals are computed for stations having at least 10 years of record and for 10° intersections in a diamond grid based on readings from the Historical Weather Maps (1899-1939) for the 20 years of most complete data coverage prior to 1940.

Chart XII. 850-mb. Surface, 1200 GMT, December 1958. Average Height and Temperature, and Resultant Winds.

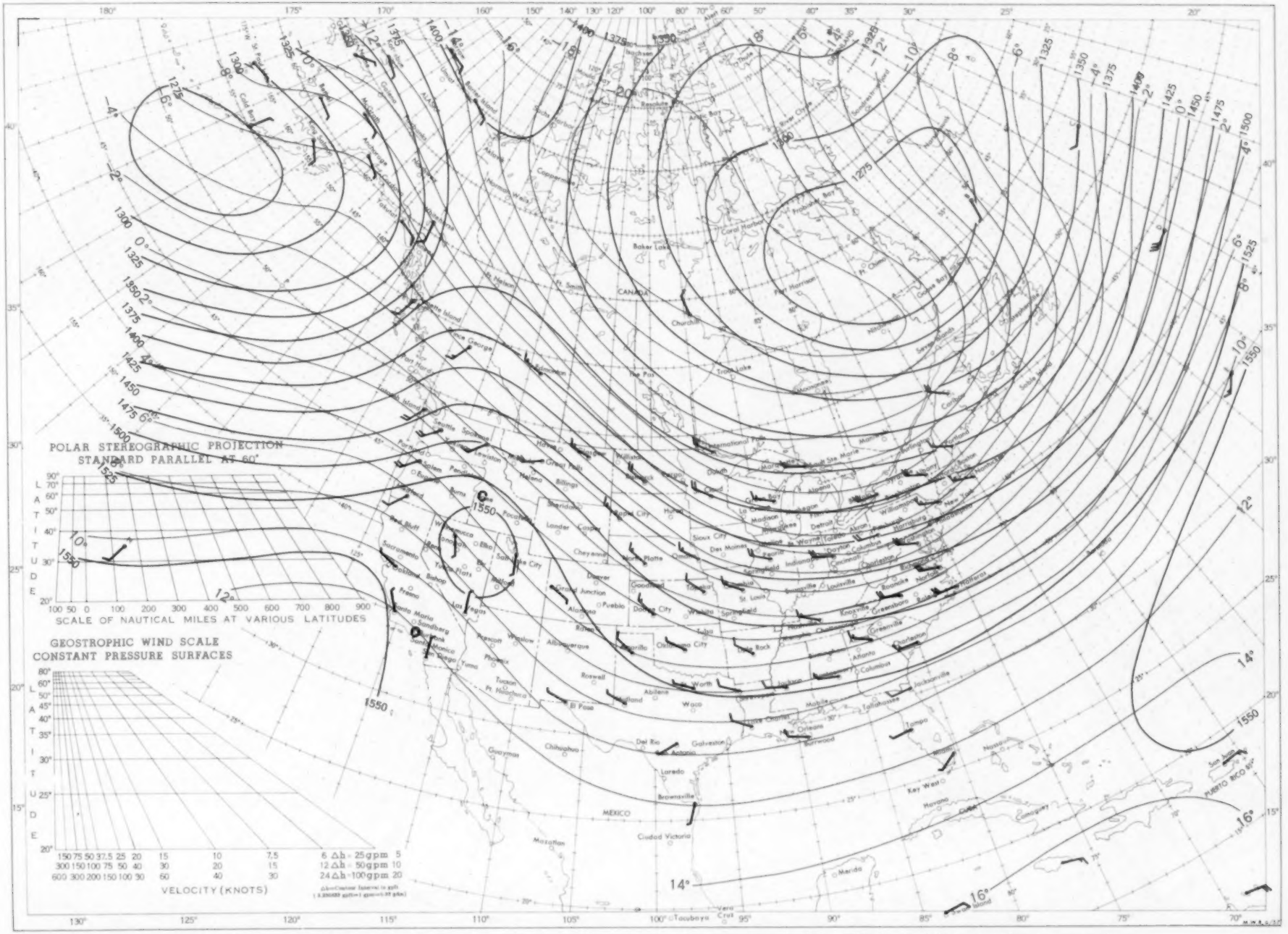

Height in geopotential meters (1 g.p.m. = 0.98 dynamic meters). Temperature in °C. Wind speed in knots; flag represents 50 knots, full feather 10 knots, and half feather 5 knots. All wind data are based on rawin observations.

Chart XIII. 700-mb. Surface, 1200 GMT, December 1958. **Average Height and Temperature, and Resultant Winds.**

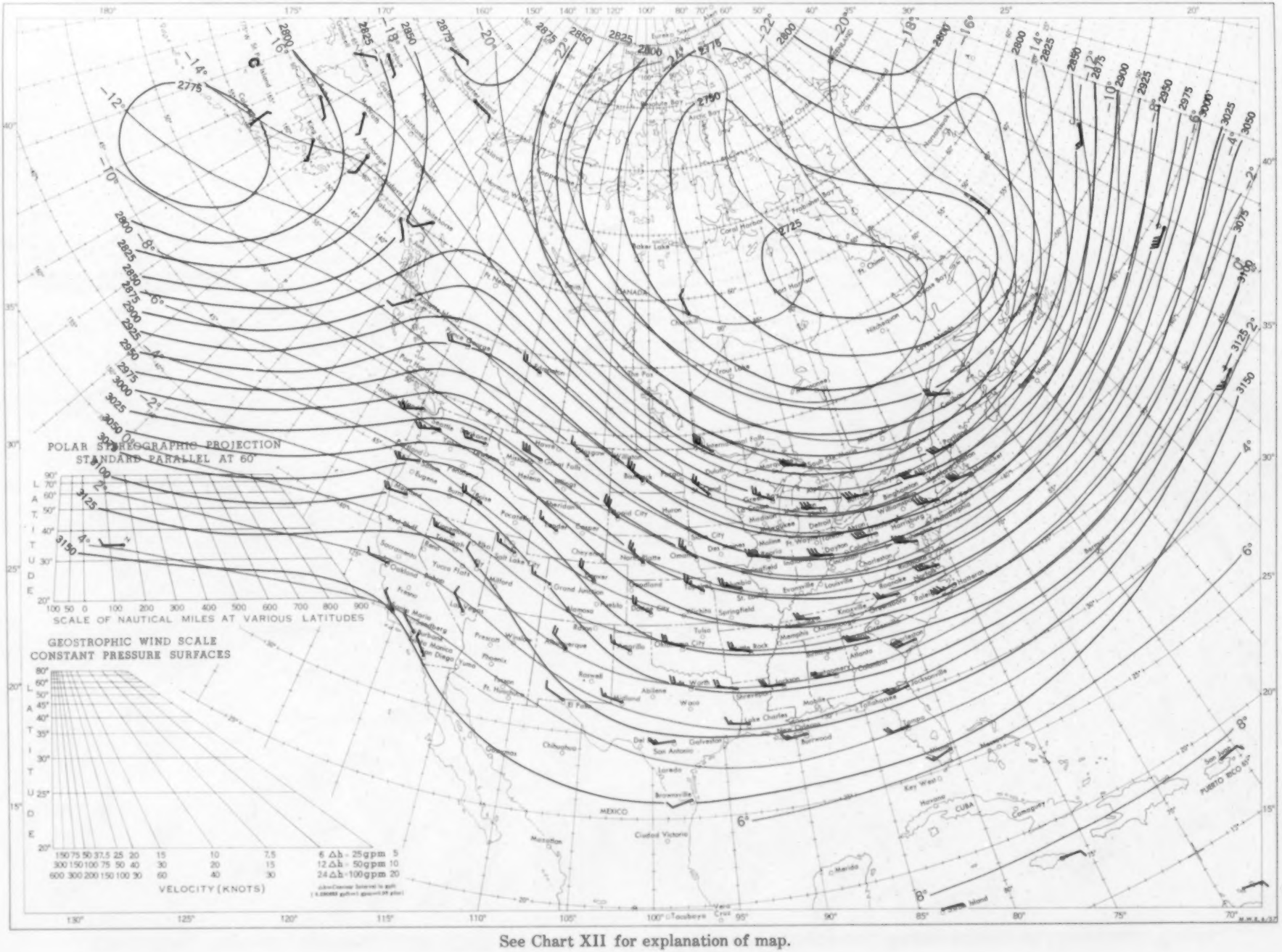

See Chart XII for explanation of map.

Chart XIV. 500-mb. Surface, 1200 GMT, December 1958. Average Height and Temperature, and Resultant Winds.

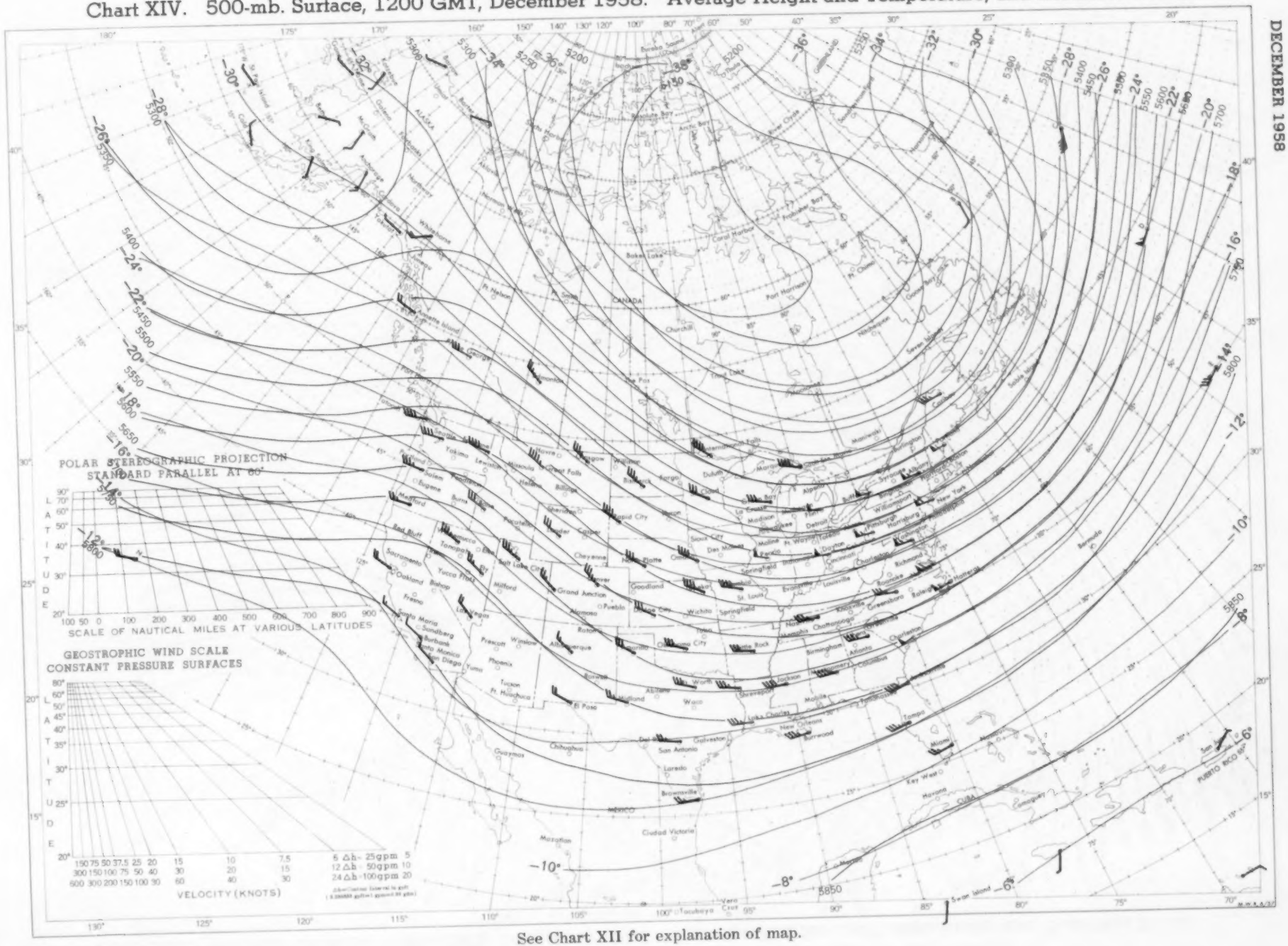

See Chart XII for explanation of map.

Chart XV. 300-mb. Surface, 1200 GMT, December 1958. Average Height and Temperature, and Resultant Winds.

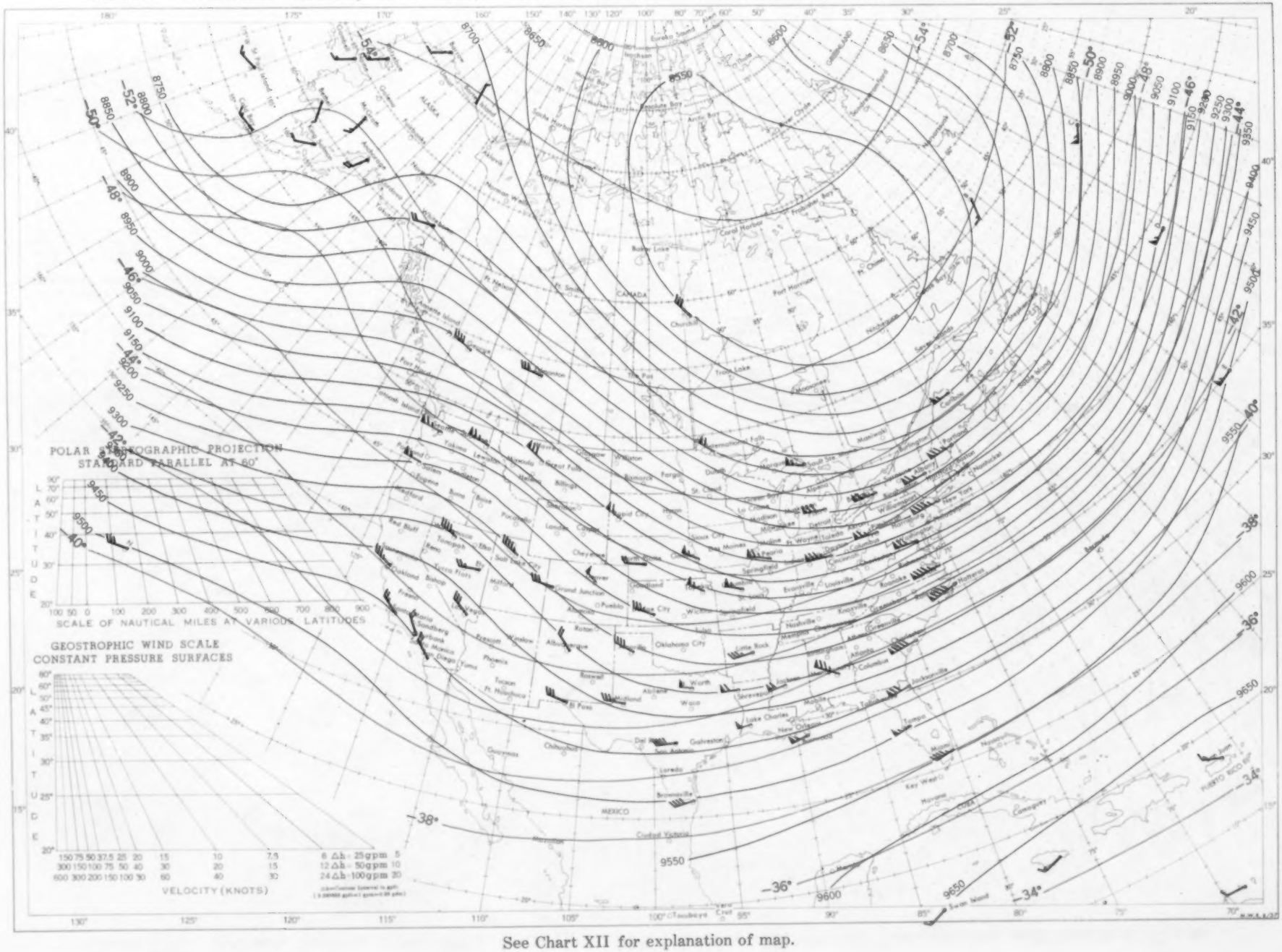

See Chart XII for explanation of map.

Chart XVI. 200-mb. Surface, 1200 GMT, December 1958. Average Height and Temperature, and Resultant Winds.

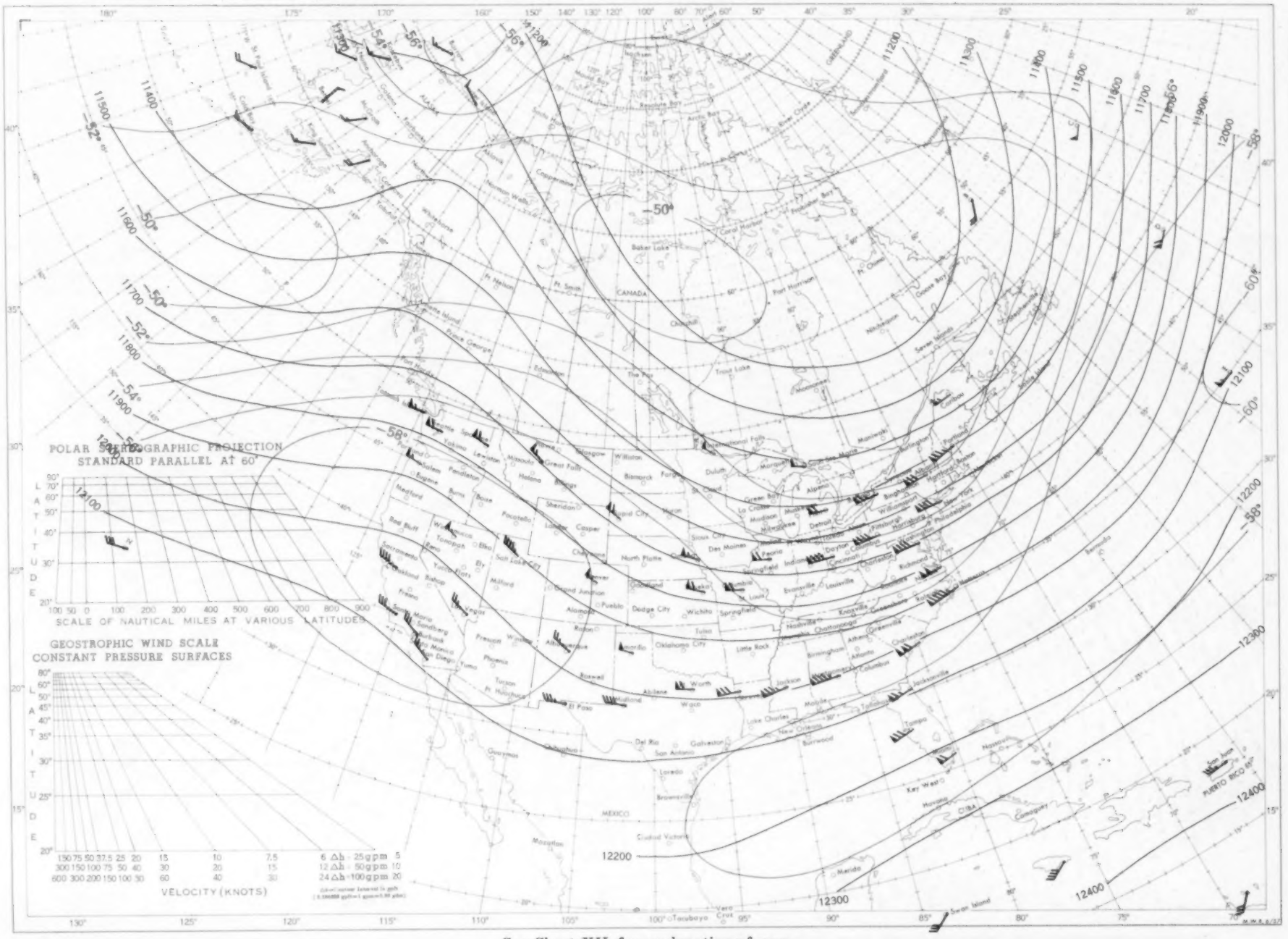

See Chart XII for explanation of map.

Chart XVII. 100-mb. Surface, 1200 GMT, December 1958. Average Height and Temperature, and Resultant Winds.

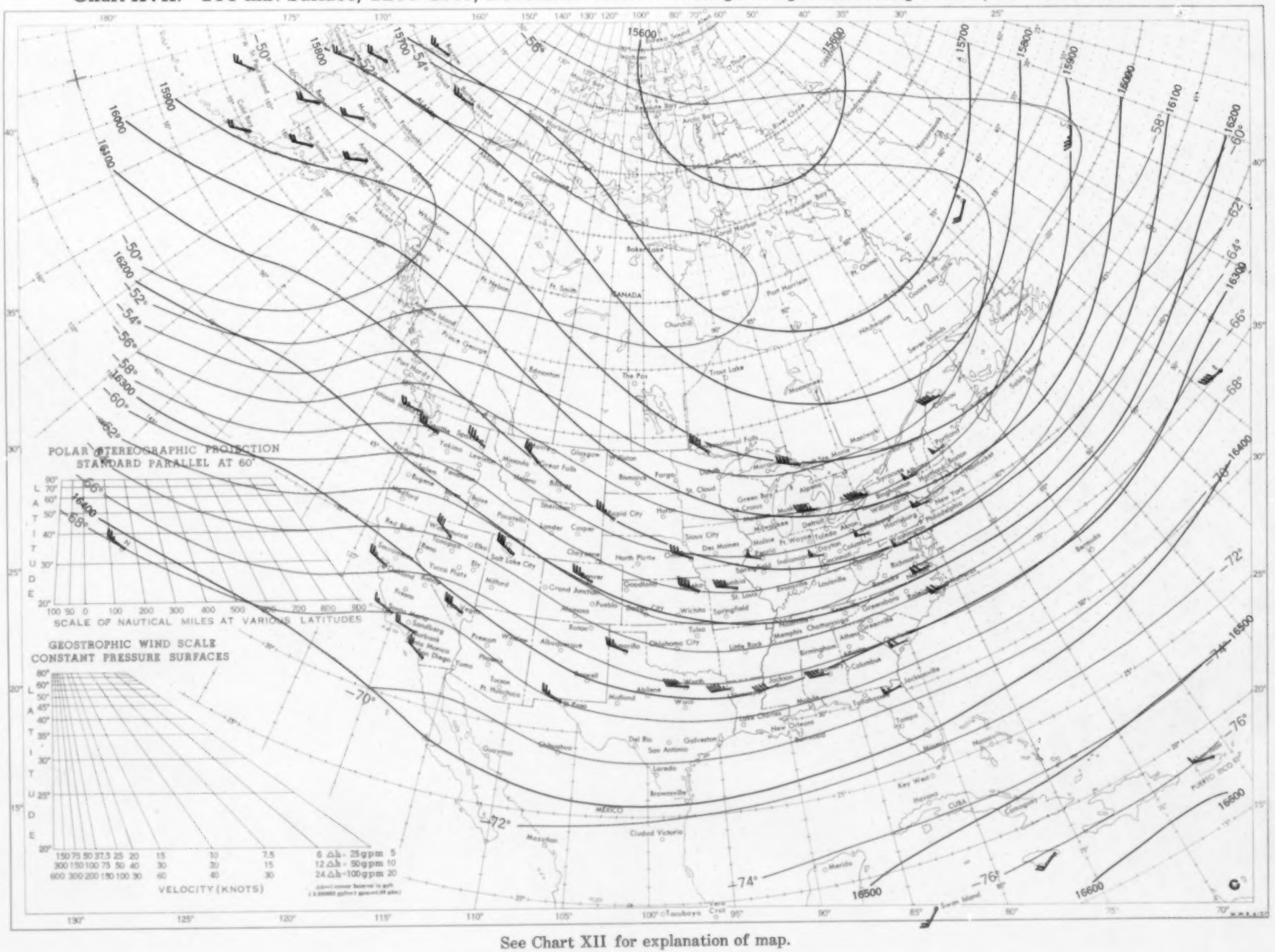

See Chart XII for explanation of map.

MONTHLY WEATHER REVIEW

VOLUME 86 NUMBER 12

DECEMBER 1958

CONTENTS

U.S. DEPARTMENT OF COMMERCE • WEATHER BUREAU

The Weather Bureau desires that the *Monthly Weather Review* serve as a medium of publication for original contributions within its field, but the publication of a contribution is not to be construed as official approval of the views expressed.

The issue for each month is published as promptly as monthly data can be assembled for preparation of the review of the weather of the month. In order to maintain the schedule with the Public Printer, no proofs will be sent to authors outside of Washington, D.C.

Use of funds for printing this publication approved by the Director of the Bureau of the Budget, January 16, 1958.

PUBLICATIONS OF THE U.S. WEATHER BUREAU

As the national meteorological service for the United States, the Weather Bureau issues several periodicals, serials, and miscellaneous publications on weather, climate, and meteorological science as required to carry out its public service functions. The principal periodicals and serials are described on this page and on the inside of the back cover. A more complete listing of Weather Bureau publications is available upon request to Chief, U.S. Weather Bureau, Washington 25, D.C.

Orders for publications should be addressed to the Superintendent of Documents, Government Printing Office, Washington 25, D.C.

MONTHLY WEATHER REVIEW

First published in 1872, the *Monthly Weather Review* serves as a medium of publication for technical contributions in the field of meteorology, principally in the branches of synoptic and applied meteorology. In addition each issue contains an article descriptive of the atmospheric circulation during the month over the Northern Hemisphere with particular reference to the effect on weather in the United States. A second article deals with some noteworthy feature of the month's weather. Illustrated. Annual subscription: $4.00; additional for foreign mailing, $1.25; 40¢ per copy. Subscription to the *Review* does not include the *Supplements* which have been issued irregularly and are for sale separately.

WEEKLY WEATHER AND CROP BULLETIN

Issued on Tuesday of each week. A summary of the weather of the week and its effect on crops and farm activities over the entire country is presented, with short reports from individual States supplemented by maps of average temperature and total precipitation for the week and for the month. In the winter months a snow depth chart is included along with a table of ice conditions on rivers and lakes. Descriptions of, and data on, current unusual conditions, such as drought, floods, blizzards, etc., are offered, often with charts. Short articles on the application of weather data to agricultural and industrial pursuits are included. Annual subscription: $3.00; additional for foreign mailing, $1.00; 10¢ per copy. For period December through March, $1.00; additional for foreign mailing, 50¢.

CLIMATOLOGICAL DATA—NATIONAL SUMMARY

This monthly publication contains climatological data such as pressure, temperature, winds, rainfall, snowfall, severe storms, floods, etc., for the United States as a whole. A short article describing the weather of the month over the United States, tables of the observational data, and a description of flood conditions are supplemented by 17 charts. An annual issue summarizes weather conditions in the United States for the year. Annual subscription: $4.00; additional for foreign mailing, $1.50; 30¢ per monthly issue; 50¢ for annual issue alone. (More detailed local data are provided in the Climatological Data (by sections) for 45 sections representing each State or a group of States and Hawaii, Alaska, and the West Indies. Annual subscription, $2.50; additional for foreign mailing, $1.00; 20¢ per monthly issue.)

LOCAL CLIMATOLOGICAL DATA

Issued monthly for cities in which Weather Bureau stations are located, this publication consists of a single sheet listing the daily observational data for the station. When records are obtainable from both city and airport offices, both sets of data are included. Most stations issue a supplement to cover hourly observations, and an annual issue containing a description of the average climate, with tables of data for the current and past years. Subscription price, $1.50 per year including supplement and annual where issued, $1.00 additional for foreign mailing; 15¢ each issue (including supplement), 15¢ for annual.

(Continued on inside back cover)

PUBLICATIONS OF THE U.S. WEATHER BUREAU

(Continued from inside front cover)

MARINERS WEATHER LOG

A new bi-monthly publication containing meteorological information for the maritime industry, including weather and shipping on the Great Lakes as well as oceanic areas. Each issue usually contains two major articles and several smaller contributions of current maritime interest. Recent ocean weather is described and a table of selected ship gale observations is included. Annual subscription, $1.00; additional for foreign mailing, 25¢; 20¢ per copy.

SUMMARY OF HOURLY OBSERVATIONS

Now issued for 114 stations which take 24 surface observations daily, these data cover a 5-year period, usually 1950–55. Price, 10 cents each.

DAILY RIVER STAGES

Annual publication of daily river stages for about 625 stations on the principal rivers of the United States, with added data on elevation, drainage area, flood stage, and extreme stages for each station. Prices vary.

DAILY WEATHER MAP

Printed and distributed daily from Washington, D.C. This map consists of a 24″ x 19″ sheet on which is printed a large map of the United States showing the surface weather conditions as of 1:00 a. m., EST, and 2 small maps of North America, one showing the surface analysis at the 1:00 p. m., EST, the other the 500-mb. analysis at the 6:00 p. m., EST, previous to the large map. Precipitation areas and amounts and high and low temperatures for the 24 hours previous to the large map are also given. Occasionally short descriptive articles on some phase of applied meteorology or the Bureau's work are printed on the map back. Annual subscription: $7.20; 60¢ per month.

AVERAGE MONTHLY WEATHER RÉSUMÉ AND OUTLOOK

A semimonthly publication presenting for the coming 30 days by means of charts the expected patterns of average temperature and precipitation over the United States and the average atmospheric circulation patterns for the same 30-day period. Also given are corresponding charts for the past 30-day period showing the observed averages. A brief description of expected conditions is included. These charts are best suited for use where a general picture of future conditions over a wide area is needed. They should be used in conjunction with the short-term forecasts issued by the nearest Weather Bureau Office. Annual subscription: $4.80; $2.40 for 6 months (minimum subscription accepted).

RESEARCH PAPERS

The research paper series and the technical paper series described below are issued at irregular intervals as the material becomes available. Each Research Paper is a report of original research in which at least part of the answer to a specific meteorological problem has been worked out and is presented as a contribution to knowledge of the weather. Forty have so far been issued covering such subjects as precipitation forecasting for the TVA basin, the artificial production of precipitation, the application of the hydraulic analogy to atmospheric flow problems, etc. Prices vary.

TECHNICAL PAPERS

This series contains compilations of meteorological and climatological data on such topics as temperatures in the upper air, daily total solar and sky radiation, thunderstorm days in the United States, normal maps for the Northern Hemisphere, etc. Thirty-three have been issued so far. Prices vary.